# Dissertation

# Biomechanical properties of Gastrocnemius muscle and Achilles tendon


submitted by

**Andreas Habersack, BSc MSc**


for the Academic Degree of

**Doctor of Medical Science**

**(Dr. scient. med.)**

at the

**Medical University of Graz**


**Department of Orthopaedics and Trauma**


under the Supervision of

**Priv.-Doz. Dr.med. Martin Svehlik PhD**

2024

## Statutory Declaration

I hereby declare that this thesis is my own original work and that I have fully acknowledged by name all of those individuals and organisations that have contributed to the research for this thesis. Due acknowledgement has been made in the text to all other material used. Throughout this thesis and in all related publications I followed the “Guidelines of the Medical University of Graz on Good Scientific Practice”.

15.05.2024, Graz

## Disclosure

The main parts of this thesis have been published in:

(1) Habersack A, Zussner T, Thaller S, Tilp M, Svehlik M, Kruse A. Validity and reliability of a novel 3D ultrasound approach to assess static lengths and the lengthening behavior of the gastrocnemius medialis muscle and the Achilles tendon in vivo. Knee Surg Sports Traumatol Arthrosc 2022; 30(12):4203–13.
doi: 10.1007/s00167-022-07076-2

(2) Habersack A, Svehlik M, Guggenberger B, Tilp M, Kruse A. Gastrocnemius medialis and Achilles tendon properties do not differ between children with unilateral or bilateral spastic cerebral palsy. J Biomech 2024; 166:112041.
doi: 10.1016/j.jbiomech.2024.112041



The following co-authors have contributed to the original research presented as part of this thesis:

Bernhard Guggenberger, Medical University of Graz, Department of Orthopaedics and Trauma; Institute of Physiotherapy, JOANNEUM University of Applied Science

Annika Kruse, University of Graz, Institute of human movement sciences, sport and health

Sigrid Thaller, University of Graz, Institute of human movement sciences, sport and health

Markus Tilp, University of Graz, Institute of human movement sciences, sport and health

Martin Svehlik, Medical University of Graz, Department of Orthopaedics and Trauma

Thomas Zussner, University of Graz, Institute of Psychology

All co-authors explicitly agreed to the use and reproduction of the published und non-published data, text excerpts, figures and tables. Written statements are submitted together with the thesis.

All the data has been collected exclusively by the author of this thesis, Annika Kruse and Thomas Zussner. These co-authors have agreed to the inclusion of their collected data in this dissertation and permitted to reproduce figures, tables and text excerpts from two mentioned publications and non-published material. No data of any other co-author was used.

During the preparation of this thesis “ChatGPT 3.5” and “DeepL Write” were used in order to improve grammar, readability and writing style of the texts.

## Acknowledgements

I would like to express my gratitude to the Austrian Academy of Sciences for granting me the DOC Fellowship and funding my research.

As a doctoral student, I was financially supported by the Medical University of Graz through the doctoral school “Bone, Muscle, and Joint“ and the Department of Orthopaedics and Trauma.

## Expression of thanks

In addition, I would also like to express my gratitude to all those who supported me in the completion of this dissertation.

I would like to express my gratitude to my main supervisors, Priv.-Doz. Dr.med. Martin Svhelik, PhD and Univ.-Prof. Dr. Markus Tilp, for their invaluable guidance and support throughout my academic journey. Their ideas and constructive feedback have significantly contributed to the completion of this doctoral thesis and my overall academic progress. I am truly grateful for the opportunity to work with such knowledgeable and supportive mentors.

I would like to express my gratitude to my supervisors, Ass.-Prof. Priv.-Doz. Dr. med. Tanja Kraus and Ass.-Prof. Hans Kainz, PhD, for their consistent advice and support.

I would also like to thank my colleague Ass.-Prof. Dr. Annika Kruse, for her mentorship and care from the very beginning. Her excellent cooperation, support, helpfulness, and organisation in the context of our studies made this dissertation possible in the first place. She made me realise how important it is to question things critically and what it means to work in science in general. In recent years, I have often reached my limits and without her encouragement and support, I would never have got this far. I very much hope that our paths will cross again.

In this context, I would like to express my gratitude to all family members and study participants for their cooperation and participation in my research, which laid the foundation for this dissertation.

I am grateful to my colleagues at the Institute of Human Movement Sciences, Sport and Health who have accompanied me in recent years and further served as subjects for my investigations and test measurements.

The past few years have demanded a significant amount of my time, time that was then missed spending with important people in my life. I would like to express my gratitude to my friends and family, especially my parents Maria and Mag. Helmut Habersack, for their unwavering support throughout this journey. Completing my doctorate has been one of the most challenging but crucial decisions I have made. Although the future is uncertain, I find comfort in the unwavering support of my family and friends. Their guidance will help me overcome any challenges that lie ahead.

# Table of Contents

## Abbreviations

| | |
|---|---|
| BSCP: | Bilateral spastic cerebral palsy |
| CI: | Confidence interval |
| CP: | Cerebral palsy |
| CS: | Compressed sensing |
| CSA: | Cross-sectional area |
| CT: | Computed tomography |
| CV: | Coefficient of variation |
| DTI: | Diffusion tensor imaging |
| EFOV: | Extended field of view imaging |
| EMG: | Electromyographic/electromyography |
| FoV: | Field of view |
| GM: | Gastrocnemius medialis |
| GMFCS: | Gross Motor Function Classification System |
| GL: | Gastrocnemius lateralis |
| ICC: | Intraclass correlation coefficient |
| ICF: | International Classification of Functioning, Disability and Health |
| IMVC: | Isometric maximum voluntary contraction |
| MDC: | Minimal detectable change |
| MITK: | Medical Imaging Interaction Toolkit |
| MRI: | Magnetic resonance imaging |
| MTJ: | Muscle tendon junction |
| MTU: | Muscle tendon unit |

| | |
|---|---|
| PCSA: | Physiological cross-sectional area |
| R: | Pearson's correlation coefficient |
| RF: | Radiofrequency |
| RoM: | Range of Motion |
| SCALE: | Selective Control Assessment of the Lower Extremity |
| SCP: | Spastic cerebral palsy |
| SD: | Standard deviation |
| SEM: | Standard error of measurement |
| SNR: | Signal to noise ratio |
| TA: | Tibialis anterior |
| TD: | Typically developing |
| US: | Ultrasound |
| USCP: | Unilateral spastic cerebral palsy |
| US-PaP: | Ultrasound probe as a spatial pointer |
| 3DfUS: | Three-dimensional freehand ultrasound |
| 2D: | Two-dimensional |
| 3D: | Three-dimensional |

## Zusammenfassung

Spastische Zerebralparese ist eine häufige neurologische Entwicklungsstörung bei Kindern, die in unilaterale und bilaterale Subtypen unterteilt werden kann. Die meisten Studien, welche die Muskel-Sehnen Eigenschaften der unteren Extremitäten bei Personen mit spastischer Zerebralparese untersucht haben, unterscheiden jedoch nicht zwischen den genannten Subtypen. Die spastische Muskelmorphologie ist jedoch ein wichtiger Faktor für die Muskelfunktion. Unterschiede in der Muskel-Sehnen Pathologie können verschiedene Behandlungsstrategien erfordern. Ein Ziel der Dissertation war es daher, die Muskel-Sehnen Eigenschaften zwischen Kindern mit einseitiger oder beidseitiger spastischer Zerebralparese zu untersuchen. Um mögliche Unterschiede auf Muskel-Sehnen Ebene beurteilen zu können, ist der Einsatz valider und reliabler Messmethoden von entscheidender Bedeutung. Daher wurde in einer zuvor durchgeführten Studie ein 3D-Ultraschallansatz zur Beurteilung der Länge des Muskelbauches des Gastrocnemius medialis, dessen Muskel-Sehnen Einheit und der Achillessehne entwickelt. Dieser Ansatz wurde in Hinblick auf zwei wesentliche Aspekte bewertet: erstens, die Validität im Vergleich zur Magnetresonanztomographie, und zweitens, die Reliabilität für statische und dynamische Längenmessungen.

Um die Validität und Reliabilität des neuartigen 3D-Ultraschallansatzes bewerten zu können, wurden zwei Ultraschallmessungen und eine Magnetresonanztomographie-Untersuchung durchgeführt. Durch die Kombination von 2D-Ultraschall und 3D-Bewegungserfassung wurden die Gewebelängen an einer bestimmten Sprunggelenksposition ermittelt und mit den Magnetresonanztomographie-Messungen verglichen. Außerdem wurde die Intra- und Interrater-Reliabilität mittels Variationskoeffizienten, Standardmessfehlern, minimal nachweisbaren Änderungen und Intraklassenkorrelationskoeffizienten für die statischen und dynamischen Längenmessungen bestimmt. Um weiters die Muskel-Sehnen Eigenschaften in den Subtypen der spastischen Zerebralparese zu beurteilen, wurden insgesamt 33 Kinder (15 mit einseitiger und 18 mit beidseitiger spastischer Zerebralparese) in die Studie inkludiert. Der Bewegungsumfang des Sprunggelenks, die isometrische Muskelkraft und die morphologischen Muskel-Sehnen Eigenschaften der Muskel-Sehnen Einheit des Gastrocnemius medialis (z. B. Muskelvolumen, Gewebelängen und Ausdehnungsverhalten) wurden mit isokinetischer Dynamometrie, Ultraschall und 3D-Bewegungserfassung bewertet. Unabhängige t-Tests oder Mann-Whitney-U-Tests wurden verwendet, um Gruppen-unterschiede zu testen ($\alpha = 0,05$).

Der 3D-Ultraschall-Ansatz zeigte um ca. 1,1% kürzere Gewebelängen im Vergleich zur Magnetresonanztomographie-Messung. Darüber hinaus zeigte die Messmethodik eine ausgezeichnete Intra- und Interrater-Reliabilität mit hohen Intraklassenkorrelations-

koeffizienten (≥ 0,94), kleinen Standardmessfehlern (≤ 1,3 mm) und guten minimal nachweisbaren Änderungen (≤ 3,6 mm).

Im Rahmen des Vergleiches zwischen Kinder mit einseitiger oder beidseitiger spastischer Zerebralparese wurden unter Verwendung der validierten Messmethode und zusätzlichen Messtechniken keine signifikanten Unterschiede in den untersuchten Muskel-Sehnen Eigenschaften sowie weiteren funktionellen Parametern festgestellt ($p > 0,05$, $d < 0,57$).

Der vorgestellte 3D-Ultraschallansatz erwies sich als valide und reliabel für die Beurteilung der statischen Längen der Muskel-Sehnen Einheit des Gastrocnemius medialis, des Muskelbauchs und der Achillessehne sowie deren Ausdehnungsverhalten. Die Ergebnisse bestätigen das Potenzial der Messmethodik als nützliches Instrument zur Untersuchung statischer und dynamischer Muskel-Sehnen Eigenschaften. Zusätzlich zeigen die Ergebnisse, dass die funktionellen sowie auch die morphologischen Eigenschaften des Gastrocnemius mediales bei Kindern mit einseitiger oder beidseitiger spastischer Zerebralparese ähnlich entwickelt sind. Daher deuten die Studienergebnisse auch darauf hin, Studiendesigns in Zukunft nicht ändern zu müssen, um zwischen Personen mit einseitiger oder beidseitiger spastischer Zerebralparese zu unterscheiden. Basierend auf den Studienergebnissen ist es möglicherweise auch nicht notwendig, die Behandlung der Muskel-Sehnen Pathologie zwischen der einseitigen oder beidseitigen spastischen Zerebralparese zu ändern.

## Abstract

Spastic cerebral palsy, which can be divided into unilateral and bilateral subtypes, is a common neurodevelopmental disorder in childhood. However, the majority of studies that have examined the muscle-tendon properties of the lower limb muscles in individuals with spastic cerebral palsy have not distinguished between the two subtypes. One of the most significant factors influencing the functionality of spastic muscles is their morphological characteristics. Therefore, different muscle-tendon pathologies may require different treatment strategies. Accordingly, one aim of this thesis was to conduct a comparative analysis of the muscle and tendon characteristics of children with unilateral or bilateral spastic cerebral palsy. The use of valid and reliable measurement methods is critical in assessing potential differences at the musculotendinous level. Therefore, in a study performed beforehand, a 3D ultrasound approach was developed for the assessment of the gastrocnemius medialis muscle belly, muscle-tendon unit, and Achilles tendon lengths. This approach was evaluated with regard to two key aspects: firstly, its validity in comparison to magnetic resonance imaging, and secondly, its reliability for static and dynamic length measurements.

In order to evaluate the reliability and validity of the 3D ultrasound approach, two ultrasound assessment sessions and one magnetic resonance imaging examination were conducted. The tissue lengths were assessed at a fixed ankle joint position by combining 3D motion capture techniques, 2D ultrasound and vector algebra. Subsequently, the aforementioned measurements were then compared to those obtained from magnetic resonance imaging. The intra- and inter-rater reliability of the static and dynamic length assessment was evaluated using various statistical parameters including standard errors of measurement, coefficients of variation, intraclass correlation coefficients, and minimal detectable changes. A total of 33 ambulatory children were included to assess the muscle-tendon properties of the spastic cerebral palsy subtypes. Of these, 15 had unilateral and 18 had bilateral spastic cerebral palsy. Isometric muscle strength, ankle joint range of motion, and muscle-tendon properties of the gastrocnemius medialis muscle-tendon unit (e.g., muscle volume, tissue lengths and lengthening behaviour) were assessed using isokinetic dynamometry, 3D motion capture, and ultrasound, respectively. Independent t-tests or Mann-Whitney-U-tests were used to test for group differences with a level of significance set at $\alpha = 0.05$.

A comparison of the 3D ultrasound approach with magnetic resonance imaging revealed a slight underestimation of tissue lengths, with a difference of approximately 1.1%. Moreover, the approach demonstrated excellent intra- as well as inter-rater reliability, as indicated by high intraclass correlation coefficients (≥ 0.94), small standard errors of measurement (≤ 1.3 mm), and good values for minimal detectable change (≤ 3.6 mm). No significant differences were

observed in any of the assessed parameters between children with unilateral or bilateral spastic cerebral palsy ($p > 0.05$, $d < 0.57$).

The proposed 3D ultrasound approach was found to be reliable and valid for the assessment of the gastrocnemius medialis muscle belly, muscle-tendon unit, and Achilles tendon lengths, as well as the lengthening behaviour of these tissues. It has been demonstrated that the approach can serve as a valuable measurement technique for examining both static and dynamic muscle-tendon characteristics. The functional and morphological properties of the gastrocnemius medialis muscle-tendon unit seem to be similarly developed in children with unilateral or bilateral spastic cerebral palsy. Therefore, the findings do not indicate a need for modification of study designs in the future to differentiate between individuals with unilateral or bilateral spastic cerebral palsy. Furthermore, the results of this study indicate that modifying the treatment of muscle-tendon pathology may not be necessary in individuals of unilateral or bilateral spastic cerebral palsy involvement.

# 1. Introduction

## 1.1. Anatomy and biomechanics of lower limb muscles

Muscle-tendon units (MTU) are composed of two essential parts of the musculoskeletal system: an active component that produces force (i.e., the muscle) and a passive structure that is capable of absorbing, storing and releasing energy (i.e., the tendon) (3). The ankle plantar flexor MTU is composed of three muscles, which are also known as the triceps surae: the medial and lateral heads of the gastrocnemius and soleus muscle (4). The gastrocnemius and soleus muscles are composed of muscle fibres and are encased by connective tissue, the epimysium, which is further connected to the Achilles tendon (5). The Achilles tendon connects the triceps surae to the calcaneus bone, enabling force transmission and joint movement (5). Skeletal muscles are composed of fascicles of muscle fibres (6). Each individual muscle fibre is composed of parallel myofibrils (Figure 1) (7).

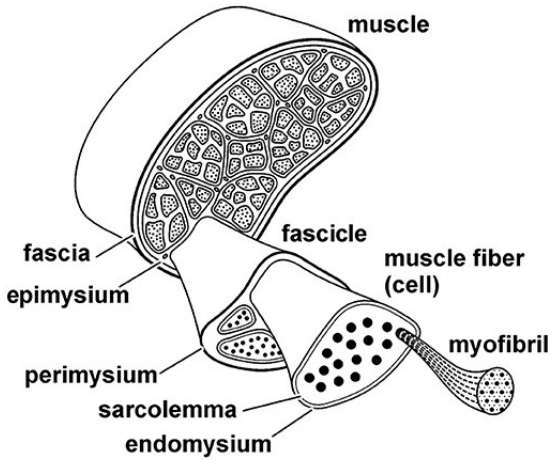


**Figure 1**: Schematic structure of a skeletal muscle. The muscle is composed of fascicles of muscle fibres, which consist of myofibrils, which in turn consist of sarcomeres, the smallest unit of muscle tissue. Figure reproduced from (8). © 2021 Howard and Herzog. The figure was published in an open-access article distributed under the terms of the Creative Commons Attribution License (CC BY 4.0, https://creativecommons.org/licenses/by/4.0/). The use, distribution or reproduction in other forums is permitted, provided the original author(s) and the copyright owner(s) are credited and that the original publication in this journal is cited, in accordance with accepted academic practice, which is the case in this thesis.

Each myofibril consists of sarcomeres connected in series, which is the smallest functional unit of the muscle tissue (7). The sarcomeres contain the main contractile filaments actin and myosin, which are responsible for contraction and shortening of the muscle (7).

The characteristics of muscle, such as muscle volume, fascicle length, muscle belly length, and thickness play a crucial role in determining function such as force generation, the maximum shortening velocity, muscle excursion, and the force transmission to the tendon (9). One factor determining the muscle function is the length of a muscle (10). The length of a muscle influences the distance over which a fibre can shorten, resulting in a variability of muscle strength at different muscle lengths (10). The strength capability depends on the actin and myosin filament interactions and their overlay (Figure 2) (10, 11). When sarcomeres are shortened, any further shortening is opposed mechanically, which restricts the production of force (10). This region is referred to as the ascending limb of the sarcomere length–tension curve (Figure 2) (10). At the optimal sarcomere length, which is defined as a length of 2.1 to 2.2 μm, there is the greatest actin and myosin overlap, which allows the muscle to produce the greatest force, termed the force plateau (10). However, when the sarcomere is overstretched, there is a reduction in the overlap between the filaments, which consequently reduces the force-producing capacity of the muscle (10). This region is designated as the descending limb (10). Conversely, there is an increase in the passive forces, which is due to the resistance to stretch that is caused by passive elastic properties (10).

With each muscle fibre connected in parallel, the maximum force of the contraction increases (6, 12). Conversely, the further a muscle fibre can shorten is determined by the number of sarcomeres connected in series (6, 12). Another factor determining the function is the volume of the calf muscles, which is notably the primary factor of plantar flexion torque (13, 14). A muscle with a greater thickness and an increased physical cross-sectional area (PCSA) and muscle fibre diameter is capable of generating a greater force (6, 15). The maximum contraction velocity of a muscle depends proportionally on the length of its constituent fibres (15). This evidence indicates that the greater the number of sarcomeres arranged in series, the faster the muscle can contract (15).

Muscles with high pennation angles, large PCSA, and short fibres are capable of generating large forces (15). For example, the gastrocnemius muscles are both pennate, which means they have more parallel muscle fibres and can generate greater maximum force than fusiform muscles (16). Another example of muscles with high PCSA and short fibres is the soleus muscle, which is well-suited for generating high forces with small excursion, playing an important role in postural stabilization and gait (15).

Conversely, relatively long fibres and intermediate to low PCSA are more suitable for large excursions and generating relatively low forces (e.g., hamstrings) (15).

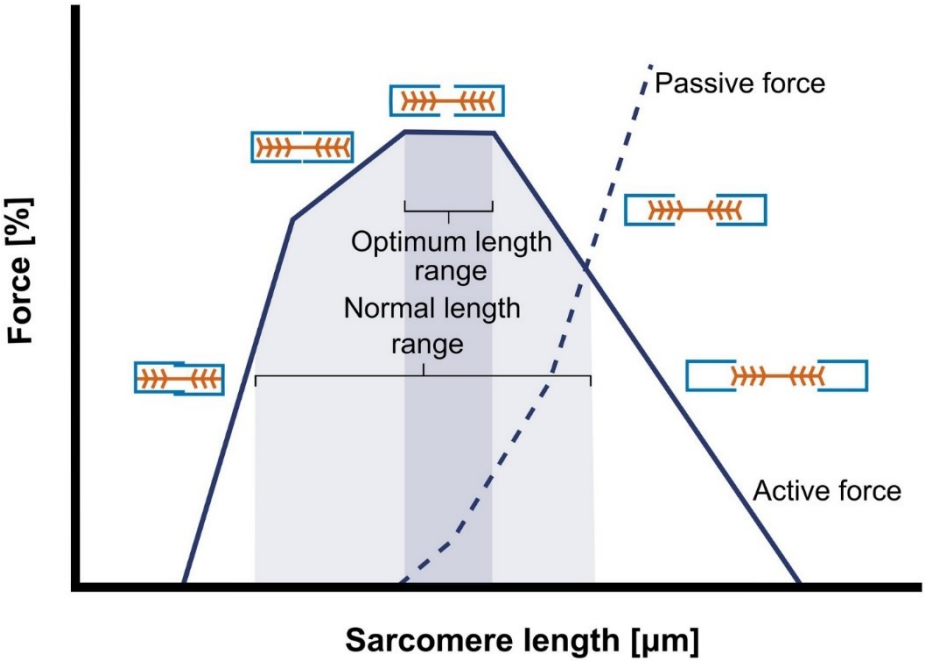


**Figure 2:** Schematic illustration of the sarcomere length-force curve. When sarcomeres are shortened, any further shortening is opposed mechanically, which restricts force production as designated by the ascending limb curve (10). At the optimal sarcomere length there is the greatest actin and myosin overlap, which allows the muscle to produce the greatest force (10). When sarcomeres are stretched, the overlap between the filaments is reduced, which consequently reduces the active force-producing capacity, while increasing the passive forces, as designated by the descending limb (10). Figure reproduced from (17). 

The gastrocnemius MTU is biarticular, spanning both the knee and ankle joints, which allows the gastrocnemius to perform the flexion of the knee and foot (18) playing a crucial role in forward propulsion during gait and other activities of daily living (7). In typically developing (TD) individuals the forward progression of the tibia as the ankle dorsiflexes is controlled by an eccentric contraction of the soleus muscle during the stance phase of walking, which results in a lengthening of the MTU (19, 20). Subsequently, as the ankle joint reaches its maximum dorsiflexion during terminal stance, a concentric contraction of the plantar flexors initiates plantar flexion motion, which serves as the primary power source for propelling the body forward (19, 20). Furthermore, considering the interaction between the active component of

the MTU (i.e., muscle) and the passive component (i.e., tendon) of the plantar flexors contributes to a more comprehensive understanding of muscle-tendon interaction (19). During normal walking, the gastrocnemius and soleus muscles contract to maintain a relatively constant length in mid and terminal stance (19, 21–24). Meanwhile, the Achilles tendon (AT), which is more compliant, functions as a spring to absorb and store energy as the tibia moves forward and the ankle dorsiflexes (19, 21–24). This stored energy is subsequently released during pre-swing and push-off when the MTU shortens (19, 21–24).

## 1.2. Assessment of morphological plantar flexor muscle-tendon properties

The MTUs are highly plastic and adapt in response to a variety of stimuli, including mechanical loading, diseases, bone growth and disorders (1). Information about changes in tendon and muscle belly lengths due to treatment is important when developing efficient therapies and training interventions (e.g., orthotic treatment and stretching interventions) (1). In recent decades, the knowledge about the adaptations and behaviour of MTUs has broadened, mainly due to advancements in ultrasonographic devices and other measurement techniques (e.g., three-dimensional (3D) motion capture, magnetic resonance imaging (MRI), musculoskeletal simulations). Every technique has its own unique range of application and therefore advantages and disadvantages. Furthermore, some of the measurement techniques can also be effectively used together, complementing each other to ensure accurate results (1, 25–28). Besides ultrasound (US), other imaging modalities, such as MRI and computed tomography (CT), are commonly used for imaging soft tissue (29). Both MRI and CT have advantages over US due to their ability to visualize deeper muscles, particularly in cases of deep soft tissue structures for MRI and bones for CT (29, 30).

### 1.2.1. Magnetic resonance imaging

Magnetic resonance imaging is a non-invasive imaging modality that uses electromagnetic radiation to produce detailed images of internal tissue (31). Magnetic resonance imaging depends on detecting small magnetization of the atomic nuclei for image formation, with hydrogen being the most commonly used nucleus in clinical imaging (32). However, this small magnetization cannot be directly measured as it is in the same longitudinal direction as the much stronger applied external magnetic field (31–35). The magnetization can, however, be indirectly measured by application of a radiofrequency (RF) excitation pulse that imparts energy into the system (31–35). When the RF pulse is switched off, the atomic nuclei relax

over time and revert to their default lower energy state by re-emitting specific frequencies of electromagnetic waves, which are measured by RF coils (31–35). These relaxation times show how quickly protons in tissues return to their normal alignment after being excited by the RF pulse (31–35). As different tissues such as fat or muscle have different relaxation times, MRI provides data on tissue biochemistry and structure, allowing a wide range of clinical applications, including neurological, musculoskeletal, and vascular applications (31–35). In terms of capturing muscle characteristics, MRI is often used to measure muscle volume, cross-sectional area (CSA), and can also be used to measure lengths of the tendon and muscle belly in vivo (36). Furthermore, by weighting the different relaxation times, it provides information about fatty infiltration of muscle and intermuscular adipose tissue (36). The detection of muscle characteristics at the fascicle level, which are not visible on regular weighted MRI scans (e.g., T1 or T2), is made possible by the use of diffusion tensor imaging (DTI), which is sensitive to changes in tissue microstructure and capable of quantifying the 3D visualisation of the architectural and morphological muscle architecture (37–50). DTI fibre tractography enables accurate reconstruction of 3D muscle architecture, allowing for assessing muscle properties such as PCSA, fibre length, and pennation angle (47). Due to its not ionizing radiation, it is considered as one of the most powerful and flexible medical imaging tools (31–35). However, it is important to consider that MRI is expensive and time-consuming when compared with US (51–53). Additionally, it may require sedation in certain population groups, particularly young children, due to the need for absolute stillness during the examination to avoid movement artifacts (54). Furthermore, MRI is not suitable for studying tissue movement and dynamic lengthening behaviour (1). In summary, despite of its wide range of clinical applications (31–35), MRI is often inadequate for capturing muscle characteristics in young populations and individuals with neurological disorders such as cerebral palsy (CP) (1).

### 1.2.2. Computed tomography imaging

Besides MRI, CT scan is another diagnostic technique that is widely used in the medical field to generate detailed cross-sectional images of the body. Unlike traditional X-rays, which provide two-dimensional (2D) images, CT scans use a rotating X-ray machine and sophisticated computer technology to generate 3D images of internal structures by capturing multiple X-ray images from various angles around the body and integrating them to create a comprehensive depiction (55, 56). CT imaging is particularly effective at visualizing bones, organs, soft tissues, and blood vessels with exceptional clarity (57). Due to its acquisition speed and precision, CT scans facilitate the detection of various medical conditions, making

CT scans pivotal in diagnosing a wide range of health issues from identifying tumours and fractures to assessing the severity of internal injuries following trauma (57). Therefore, CT scans play critical roles in both diagnosis and treatment planning (55). However, CT has a major disadvantage as it exposes the patient to ionizing radiation (55–57). Therefore, this technique should be limited to necessary examinations only, making it unsuitable for repeated follow-up checks during interventions, particularly in children.

### 1.2.3. Ultrasound imaging

Because of the mentioned disadvantages of MRI and CT, US is often the method of choice when it comes to investigations at muscle-tendon level (2). Ultrasound imaging has several advantages when compared to MRI or CT: in addition to its wide availability, cost-efficiency, and quicker examinations (51–53), US has a better patient tolerability (51, 53, 58) and can be conducted in absence of any ionizing radiation (59). Furthermore, US provides a higher intrinsic spatial resolution (51, 52), resulting in a resolution up to 0.1 mm (29), which is higher than the resolution than can be achieved with, for example, a 3-Tesla MRI (29, 60), enabling the assessment of architectural muscle properties (e.g., fascicle length, pennation angle, etc.). Ultrasound also provides benefits such as non-invasiveness and the ability to easily compare structures between opposing sides (61). In US measurements, a transducer emits pulses of high-frequency sound waves in the tissues and detects their reflections (29). Generating an image from the returning echoes depends on a computerised analysis of their temporal and acoustic attributes (29). The position of the pixels in the resulting US image is determined by the duration between the transmission and reception of the US pulse, while the luminosity of the pixel corresponds to the magnitude of the received sound wave (29, 62, 63). Sound wave reflection occurs when an emitted US beam interacts with tissue that has distinct acoustical properties, which is called acoustical impedance (29, 62, 63). Acoustical impedance is determined by the combined factors of sound velocity passing through the tissue and its density (29, 62, 63). Biological tissues are primarily composed of water and fat, which both efficiently transmit sound waves and exhibit a minimal difference in acoustical impedance (29). However, when encountering a boundary between different tissues, such as muscle tissue and fascia, the sound wave experiences partial reflection, with some of the sound being transmitted to deeper layers (29). The acoustical impedance contrasts particularly between bone and air as the bone has a sound velocity of approximately 300 m/s, while air has a sound velocity of approximately 4000 m/s (29, 63). In comparison, muscle tissue has a sound velocity of roughly 1580 m/s (29, 63). As a result, emitting sound waves through muscle to bone or air leads to

significant reflection, which appears as a bright spot on the US image, as most of the emitted sound waves get reflected on the mentioned transition (63). The structures beneath such transitions cannot be visualized, which makes it difficult to investigate underlying tissue (63). In addition to visualization issues, US gel application and the correct placement, orientation, and application of pressure of the US probe are essential for image quality (59). Therefore, the skills of the operator are crucial for accurate results (59). Compared to the benefits described for primary localized and superficial muscle and tendon examinations, measuring the extended length of larger anatomical structures, such as the entire MTU of the lower leg and associated components, presents a challenge with conventional 2D B-mode US due to the limitations in accurately depicting large structures in a single image (64). This aspect highlights the challenge of precise measurements, emphasizing the necessity for alternative imaging methods (64). Therefore, in addition to the architectural muscle and tendon properties (e.g., fascicle length, pennation angle, muscle thickness, etc.), several methods have been developed to assess the morphological properties, in particular the lengths of the gastrocnemius medialis (GM) muscle and the AT, which will be described in the following sections.

#### 1.2.3.1. Extended field-of-view imaging

The lengths of muscles and tendons can be assessed using extended field of view (EFOV) imaging, which is also referred to as panoramic US. Weng et al. (65) developed an EFOV US scanning technique for panoramic imaging without having a position sensor indicating its potential for enhanced diagnostic capabilities. This technique produces large resolution-preserved composite images up to 60 cm (65). EFOV US uses standard 2D B-Mode US imaging to create a panoramic view. The US system captures an extended image by moving the US probe along a predefined direction across the area of interest while aligning the images using image registration methods and fusion techniques (65–71). Recent research has focused on the length assessment of the AT and muscle structures (64, 72–77). Each study contributes uniquely to the field, with a shared focus on reliability, validity, and clinical applicability. For instance, Brouwer et al. (72) investigated the reliability of EFOV imaging and skin marking measurements for AT length. Their results showed good to excellent test-retest and inter-tester reliability for both measurements (Intraclass correlation coefficient (ICC) ≥ 0.82), with skin markings demonstrating better agreement and reliability compared to EFOV imaging (72). Silbernagel et al. (75) examined the reliability and validity of EFOV US imaging for assessing the length of the AT in cadavers. Their results showed good correlation

(ICC ≥ 0.744) with cadaveric measurements and low value for the standard error of measurement (SEM) (≤ 0.64 cm). Ying et al. (64) compared the reliability and accuracy of EFOV and dual-image US measurement techniques for measuring distances. They found that EFOV US showed slightly higher accuracy and reliability (Pearson's correlation coefficient (r) ≥ 0.997 for EFOV vs. r ≥ 0.948 for dual image US) in assessing distance measurements in tissue phantoms when compared with dual-image US, although both techniques exhibited high accuracy and reliability (64). In comparison to the studies conducted by Ying et al. (64) and Silbernagel et al. (75), Ryan et al. (74) concentrated on assessing the test-retest reliability and values for the AT length using EFOV imaging on human subjects. Their results indicated acceptable reliability with ICC and SEM values of 0.954 and 4.43 mm, respectively (74). The minimal detectable change (MDC) for the EFOV imaging of the AT length was found to be 12.27 mm (74). This value may be too high to be able to measure even small changes in the AT length. Another study by Franchi et al. (73) investigated the validity of panoramic US compared to MRI for evaluating hamstrings volume and CSA. Good agreement was found between US and MRI for the CSA and volume measurements (r ≥ 0.8) (73). The study also demonstrated that the experience of the examiner significantly influences the test results (r = 0.001 for the inexperienced rater vs. r = 0.50 for the experienced rater, respectively, for assessing the CSA of the Biceps femoris short head) (73).

Collectively, these studies enhance our comprehension and diagnostic capabilities of EFOV imaging in tendon assessment. Although the EFOV imaging enables to capture a larger region of interest (ROI) up to 60 cm (65), however, research on length assessment of the GM using EFOV imaging is limited. Additionally, EFOV imaging has several drawbacks, including the assumption that the detected US images lie within the same plane (67, 68) and ensuring the same speed and pressure during scanning (78). Although investigators can undergo training to manoeuvre the probe along a rigid and straight trajectory during data acquisition to stay in that same plane, this assumption may not always be met due to factors such as hand tremors, body curvature, any change in transducer orientation, position or pressure, and subject movement (68). In addition, the probe has to be moved slowly and steadily to ensure that there are enough overlapping regions for accurate rectification (68, 79, 80).

Furthermore, the EFOV imaging described in the studies can only be utilized in static positions and is not yet suitable for dynamic measurements. It necessitates absolute immobility during the scanning process, which poses challenges, particularly for certain populations, which may be difficult to achieve, especially among children and individuals with mobility issues or those who experience discomfort in maintaining static positions for extended periods. As a result, while the technique offers promising benefits in terms of accuracy and reliability, its applicability

may be limited in situations where dynamic measurements are essential for comprehensive assessment.

#### 1.2.3.2. Ultrasound tape measurements

Another approach to assess the lengths of the muscle and tendons is through the use of tape measurements, which can be combined with skin markings (25, 72, 81–85). For instance, Barber et al. (25) introduced an US tape method for assessing the length of the AT and the GM muscle reporting high reliability (ICC > 0.99). The approach involved fixing a measuring tape to an US probe at one end and positioning it over the insertion of the AT on the calcaneus at the opposite end (25). With the tape held taut at a consistent length, the transducer head was swept from medial to lateral over the medial femoral condyle to identify the most superficial part of the medial condyle and therefore also the muscle length (25). The muscle-tendon junction (MTJ) was scanned in the same manner as previously described in order to identify the AT length (25). During the post-processing, the length of the GM MTU and AT was determined (25).

Avoiding the sweeps, Kruse et al. (82) proposed a method by placing adhesive tape strips over the AT, MTJ of the GM, and the most superficial aspect of the medial femoral condyle. After the placement of the strips, a measuring tape was used to assess the distances between the calcaneus and each tape to obtain the muscle length, AT length and the GM MTU length (82). The anatomical landmarks of the medial condyle, MTJ and insertion can also be directly marked on the skin surface instead of using adhesive tape strips (84).

Several studies have measured only the length of the AT (72, 83, 85, 86). For example, by inserting a wire between the US transducer and the surface of the skin, the location of the MTJ and the insertion point at the calcaneus can be projected onto the skin surface (86). The point at which the US probe and the wire crossed was marked on the skin and then the distance between those landmarks was assessed with a tape measure (86). Their results indicated acceptable intra-rater reliability (ICC of 0.96, SEM of 3 mm and MDC of 10 mm) and inter-rater reliability (ICC of 0.97, SEM of 3 mm and MDC of 9 mm) (86). Although the mentioned studies contribute valuable information to the field of musculoskeletal assessments, they have several limitations. The tape measurements described in the studies can only be used in static positions and are therefore not suitable for dynamic measurements. Additionally, measuring the distance with a tape measure on the skin surface simplifies the muscle and tendon length in 2D space, as it only measures the projection of the tissue length on the skin. In summary, the tape measure limitations highlight the need for more dynamic measurement techniques that accurately capture the complex 3D structure of muscles and tendons.

#### 1.2.3.3. Combination of ultrasound and 3D motion capture

Other more complex approaches for assessing the length of the GM MTU and its components have been developed by combing B-mode US imaging with 3D motion capture technology (e.g., (3, 26, 78, 87–91)). As mentioned before, US transducers have limited dimensions, which makes it impossible to visualize an entire MTU in one image (3). To overcome this limitation, a 3D freehand US (3DfUS) technique has been developed (91, 92). This technique combines the picture or video information, respectively, of an US system with the position information of a rigid marker cluster mounted to the US probe captured by a 3D motion tracking system, allowing for the acquisition of larger anatomical volumes (3, 91, 92). The postprocessed 3D reconstruction visualizes the entire MTU, enabling the extraction of muscle and tendon lengths, as well as other information pertinent to clinical practice, including fascicle lengths, muscle volume, and echo intensity (3, 91, 92). In addition, the 3DfUS offers shorter acquisition times compared to MRI (3). While the 3DfUS approach delivers significantly improved muscle and tendon diagnostic capabilities in research and clinic, it has limitations similar to EFOV imaging. The 3DfUS can only be used in static positions, requiring absolute immobility during the scanning process, which can be challenging for certain populations (3). Additionally, applying no pressure to the skin during scanning may be difficult for inexperienced raters and its post-processing procedure can be long lasting (3).

The use of US probes as spatial pointers (US-PaP) offers an alternative approach to assess the length of the GM muscle belly and AT (3, 26). This method involves visualizing landmarks in two dimensions and recording the location of the transducer by a 3D motion capture system (3, 26). Compared to 3DfUS, US-PaP provides a more efficient and less time-consuming acquisition and post processing procedure (3, 26). When compared with the 3DfUS technique, the US-PaP performs the visualization and information extraction in single images rather than a dataset (3, 26). This technique has also been used in 3D gait analysis to enhance the precision of participant-specific modelling and reduce processing time by calculating linear distances between landmarks (3, 93). Although the US-PaP technique overcomes the limitation of long-lasting acquisitions and post-processing times, it still does not enable dynamic length measurements to assess the lengthening behaviour of the MTU and its components during movements such as ankle dorsiflexion.

Table 1 provides a summarizing overview of the advantages and disadvantages of each mentioned imaging method, with a particular focus on their strengths and limitations for assessing muscle and tendon properties.

**Table 1:** Advantages and disadvantages of each imaging method, providing an overview of their strengths and limitations for assessing muscle and tendon properties.

| Imaging Method | Advantages | Disadvantages |
|---|---|---|
| CT | - Generates detailed 3D images of internal structures.<br>- Effective for diagnosing fractures, tumours, and internal injuries. | - Exposes patients to ionizing radiation.<br>- Unsuitable for repeated follow-up checks, especially in children. |
| MRI | - Provides detailed images without ionizing radiation.<br>- Wide range of clinical applications.<br>- Measures muscle volume, cross-sectional area, and length. | - Expensive and time-consuming.<br>- May require sedation.<br>- Unsuitable for studying tissue movement.<br>- Requires absolute immobility during scanning. |
| Standard 2D US | - Widely available and cost-efficient<br>- Provides high spatial resolution.<br>- Allows for easy comparison. | - Limited in depicting large structures in one image.<br>- Not suitable for dynamic measurements. |
| EFOV | - Captures larger regions of interest.<br>- Enhances diagnostic capabilities. | - Assumes images lie within the same plane.<br>- Requires absolute immobility during scanning.<br>- Not suitable for dynamic measurements. |
| US tape measurements | - Simple and low-cost. | - Limited to static positions.<br>- Simplifies measurements in 2D space. |
| Combination of US and 3D motion capture | - Provides comprehensive visualization of muscle properties (e.g., volume, muscle belly length, thickness, fascicle length). | - Requires immobility during scanning.<br>- Lengthy acquisition and post-processing.<br>- Does not enable dynamic measurements. |

CT: computed tomography; 2D: two-dimensional; 3D: three-dimensional; MRI: magnetic resonance imaging; US: ultrasound; EFOV: extended field of view imaging.

## 1.3. Cerebral Palsy

### 1.3.1. Incidence of cerebral palsy

Cerebral palsy is a common neurodevelopmental disability in childhood, with an incidence of 1 to 4 per 1000 live births (94–96), whereby it affects ~1.5 per 1000 births in high-income regions of Europe, Australia, and Japan (97) and above 3 in Sadjadpour, Bangladesh, Moldova, Taiwan and Egypt (97, 98).

Although the prevalence of CP is evenly distributed worldwide, some studies have reported a sustained decline in the birth prevalence of CP in high-income countries such as Europe, Australia, and Japan (97, 99–102). In contrast, increasing rates of CP have been reported in regions of low- and middle-income countries (98, 103). The decrease in high-income countries is being attributed to a range of improvements in public health, perinatal and maternal care, while the rise in prevalence in middle- and low-income countries is partially explained by a decrease in infant mortality rate (104) and improved case registration (96).

### 1.3.2. Aetiology and pathogenesis of cerebral palsy

As mentioned before, CP refers to a range of disabilities resulting from non-progressive lesions in the developing brain, causing impairments in posture, motor ability, and control (97, 105, 106). Risk factors for CP can be identified across different life stages, including preconception, prenatal, perinatal, and early infancy periods up to the age of 2 years (97, 106). Cerebral palsy arises from destructive processes that damage healthy brain tissue in approximately 90% of cases, rather than originating from abnormalities in brain development (107, 108). These factors include genetic variations, preterm delivery, intrauterine growth restriction, infections, hypoxic-ischemic events, cerebrovascular incidents during pregnancy and infancy, as well as accidental and non-accidental brain injuries (97, 106). Preterm birth is currently recognised as the primary risk factor for CP (107). The causes of CP during the prenatal period primarily involve maternal and pregnancy-specific issues, such as systemic maternal infections, inflammation, or trauma affecting either the mother or the foetus (107). Regarding spastic diplegia, this condition is typically associated with periventricular white matter loss and is correlated with foetal growth retardation at term and preterm birth (107). Similarly, spastic quadriplegia is often associated with premature birth, with neuroimaging demonstrating severe multicystic cortical encephalomalacia and periventricular leukomalacia (109). Spastic hemiplegia usually occurs due to an ischemic stroke during pregnancy or shortly after birth (107). However, it can also affect premature babies with unilateral porencephalic cavities (107).

While CP is typically attributed to non-progressive disruptions in the developing infant or foetal brain, there is evidence of a functional decline, particularly during adolescence growth spurts (110). Factors contributing to this decline in function and mobility include increasing musculoskeletal issues and alterations in the ratio between strength and body mass (111). Studies on the natural progression of CP have indicated that children without intervention experience a decline in several critical clinical gait parameters, including decreases in hip abduction and ankle flexion range of motion (RoM), timing of toe-off, cadence, and walking

velocity (112, 113). Additionally, muscle weakness and negative changes in the ratio between body mass and strength during adolescence contribute to the progressive decline in mobility with age (114).

### 1.3.3. Classification of cerebral palsy

Cerebral palsy is the predominant cause of motor disorders during childhood (115). Cerebral palsy is a multifaceted condition that affects not only muscle function but also encompasses all levels of the International Classification of Functioning, Disability, and Health (ICF) (107). Its presentation varies in terms of lesion timing, clinical manifestations, affected site, and severity of impairments (116). The motor impairments associated with CP can encompass abnormal muscle tone (e.g., spasticity and dystonia), muscle contractures, abnormal bone growth (e.g., deformities, dislocation or subluxation), balance issues, and diminished selective motor control (105, 116). Typically, classifications of CP are based on the type of motor impairment (e.g., spastic, athetoid, ataxic or mixed forms) as well as the involvement of the extremities (e.g., unilateral or bilateral) (105, 116).

#### 1.3.3.1. Topographical classifications

Individuals with CP can be categorized based on the extent of involvement, which may be hemiparetic/unilateral or bilateral, depending on whether one body half or both body halves are affected, respectively (107). Within unilateral CP, individuals may exhibit monoplegia, where only one limb is affected, or hemiplegia, where one body side is affected (107). Hemiplegia typically manifests with greater involvement of the upper limb compared to the lower limb (107). Conversely, bilateral CP encompasses diplegia, triplegia, and quadriplegia (107). Diplegia involves impairment in all limbs, with the lower limbs being significantly more impaired than the upper limbs (107). Triplegia typically presents with unilateral upper limb involvement, accompanied by bilateral (asymmetrical) lower limb involvement (107). The severity of the latter is typically greater on the same side as the upper limb impairment (107). Quadriplegia involves the trunk and all four limbs, with synonymous terms including tetraplegia or 'whole-body involvement' (107).

#### 1.3.3.2. Classification based on muscle tone

Another commonly used classification system for CP is based on motor disorders and tone, which categorizes affected individuals into three main subtypes: spastic, dyskinetic, or ataxic CP (107, 117–119). Spastic CP (SCP) is the most prevalent subtype, impacting

approximately 88% of all children with CP (118). Spasticity, the defining feature of SCP, refers to a clinical phenomenon characterized by an excessive muscle response to rapid stretching (107), presenting as velocity-dependent resistance to passive movement (119–121). In the majority of individuals, spasticity is observed to predominantly affect the lower limbs in children with bilateral involvement, while in those with unilateral involvement, it is observed to affect the upper limbs (119, 122). Mostly two-joint muscles are affected (119, 122). Commonly involved lower limb muscles include the hamstrings, adductors, gastrocnemius and soleus, rectus femoris, and psoas, while in the upper limb, spasticity is often observed in the shoulder external rotators, elbow pronators, and wrist and finger flexors (119, 123).

It is postulated that spasticity may disrupt muscle control, increase energy expenditure during movement, and impede normal muscle lengthening during growth, thereby contributing to the progression of secondary muscle contractures and skeletal deformities (119, 124, 125).

The severity of spasticity in children with CP is closely associated with their functional performance in activities of daily living such as gait, feeding, hygiene, dressing, and motor skill acquisition (126, 127).

Dyskinetic CP is present in approximately 6-14% of all individuals with CP and includes various movement disorders, mainly dystonia and athetosis (128). The condition is characterized by uncontrolled, erratic, and sluggish movements in the hands, feet, arms, or legs (117, 129). Dystonia is a condition that causes abnormal muscle tone and results in distorted voluntary and involuntary movements (98, 108, 130, 131). Athetosis, on the other hand, is characterized by involuntary movements of the face, neck, and distal extremities that change direction frequently (98, 108, 130, 131).

Ataxic CP is present in approximately 5% of all individuals with CP (132). Children with ataxic CP experience reduced coordination, which affects their balance, depth perception, and ability to perform controlled and goal-directed movements (133–135). The individuals exhibit an unsteady and stomping gait, which causes difficulties in motor tasks or performing precise actions such as walking, writing or buttoning a shirt (117, 129).

Due to the common occurrence of multiple movement disorders in many children, singular classification may lack precision or reliability with the classification typically being based on the dominant disorder (136).

#### 1.3.3.3. GMFCS classification

The Gross Motor Function Classification System (GMFCS) provides a classification system that is based on the motor ability of individuals with CP and has become the gold standard in classifying children with CP according to their motor abilities (11, 137). The GMFCS has five

levels, each described by specific descriptors that define motor abilities (137). Approximately 60% of children with CP belong to the GMFCS levels I and II and are ambulatory (11, 138). Another 11% use walking aids and belong to the GMFCS level III, while 29% are predominantly dependent on wheelchairs and belong to the GMFCS levels IV and V (11, 138).

**GMFCS level I**

Children and adolescents classified as level I can walk independently at school, outdoors, and at home (98, 137). Level I includes tasks such as climbing stairs without using a railing and performing more challenging skills like jumping and running (98, 137). However, their balance, speed and coordination are limited compared to TD peers (98, 137).

**GMFCS level II**

Compared to level I, children classified as GMFCS level II are able to walk independently in most settings, but may require assistance when climbing stairs by holding onto a railing (98, 137). For longer distances, children may need assistive devices such as hand-held mobility devices or physical assistance (98, 137). Children frequently encounter difficulties when required to walk longer distances and to navigate uneven terrain, and their ability to perform gross motor skills, such as running and jumping, is often constrained (98, 137).

**GMFCS level III**

When classified as level III, children typically require the use of a hand-held mobility device to walk within indoor environments and a wheelchair for longer distances (98, 137). They also require additional assistance to climb stairs, in addition to holding onto a railing (98, 137).

**GMFCS level IV**

When classified as level IV, children and adolescents require a powered mobility device or physical assistance in most indoor and outdoor settings (98, 137). It is possible that they may be able to walk short distances with the assistance of another person and require a manual or powered wheelchair for longer distances, such as at school and outdoors (98, 137).

**GMFCS level V**

Children classified as level V require transportation in a manual wheelchair in all settings (98, 137). In terms of motor function, they are limited in controlling their head and trunk against gravity and can perform only simple arm movements (98, 137).

### 1.3.4. Functional deviations in children with cerebral palsy

Although all individuals with CP experience difficulties with movement, balance, and posture control, the diverse aetiology results in distinct functional deviations in individuals with unilateral compared to bilateral SCP (2). It is worth noting that children with unilateral SCP tend to be taller and heavier than their bilaterally affected peers (2, 139). Moreover, children with unilateral SCP typically follow growth trajectories similar to those of TD children (2, 139, 140). In the absence of comorbidities and cognitive impairments, they often present only mild functional impairments (107, 109, 141). In contrast, bilateral CP is frequently accompanied by more significant impairments of cognition and function (2, 141). There is a notable distinction between individuals with spastic diplegia and quadriplegia with the latter group exhibiting more severe limitations, deficits, and associated conditions (98, 109). Furthermore, studies indicate that adults with CP experience a 25% decrease in mobility (142). Those adults with bilateral involvement are at a greater risk of experiencing a reduction in mobility than those with unilateral involvement (142).

In individuals with unilateral involvement, there is a tendency to walk with an internally rotated limb, fully extended knees, and an internally rotated foot position (143, 144). This gait is accompanied by a deformity of the ankle, which is characterised by a varus alignment of the joint (143, 144). In contrast, children with bilateral CP frequently exhibit a crouched posture (144), characterised by adduction and internal rotation of the thighs, as well as flexion of the knees (143, 145). These postural abnormalities result in the development of functional genu valgus (143, 145). Furthermore, a greater prevalence of varus foot deformities was observed in individuals with unilateral CP, while those with bilateral CP exhibited a higher incidence of valgus deformities (90% and 64%, respectively) (146). In addition, children with unilateral CP exhibited greater capacity for strength production than their bilaterally affected peers (147).

These findings provide evidence that individuals with unilateral CP and those with bilateral CP demonstrate differences in their lower extremity function, joint function and overall motor function (2). The changes in turn seem to result in deviating movement patterns and strategies, which likely lead to a different use and impact on the underlying movement generating tissues, i.e., muscles and tendons (2).

### 1.3.5. Mechano-morphological properties of the spastic gastrocnemius medialis muscle-tendon unit

In pathological conditions such as CP, musculoskeletal characteristics are often significantly impaired when compared with TD peers, affecting both functionality and mobility (148). Muscle volume, which is positively correlated with maximal isometric strength (14, 149), is significantly reduced in individuals with CP by approximately 47% when compared to TD peers (11). This reduction is most pronounced in overall function and increased GMFCS levels (11, 150, 151). Although individuals with CP tend to be smaller and lighter than TD peers, the smaller muscle volume is not attributed to their smaller statures (11, 152). Furthermore, the extent of muscle volume deficits varies among different muscle groups, with the more distal ones (such as the soleus) being more commonly and severely affected (11, 152).

Ultrasound studies have shown that children with CP have reduced muscle belly length on the paretic side and in the non-affected leg in individuals with hemiplegia (11, 153). In addition, children with CP demonstrated reduced muscle thickness and CSA, as well as longer AT when compared to TD individuals (11, 152, 154).

The reports about differences in fascicle length between children with CP and TD are diverse. The observed differences in muscle fascicle lengths range from no difference (19, 154, 155) up to a 25% reduction in individuals with CP (11, 156, 157). Similarly, studies have shown inconclusive results regarding differences in pennation angles (11), with some reporting increased (157–159), decreased (160), or no significantly different (154, 156, 161–163) pennation angles when compared with TD children. The length of sarcomeres in lower limb muscles were observed to be longer than those of TD peers (11, 164–166). This indicates that the muscles in CP are functioning on the descending limb of the length-force curve (Figure 2), which has significant implications for explanation of the loss of muscle strength in individuals with CP (10).

The mentioned differences primarily arise from studies that incorporated both subjects exhibiting bilateral SCP and those displaying unilateral SCP (2). However, there is a scarcity of literature that compares the properties of spastic muscles between individuals with bilateral SCP and those with unilateral SCP (2, 167, 168). Although there is no difference in GM muscle volume between the groups, children with unilateral CP showed a significantly reduced GM muscle growth rate compared to both children with bilateral CP and their TD peers (2, 167). The observed trend indicates a progressive disparity in lower leg muscle volume among distinct CP cohorts as children progress through puberty and adulthood (2, 167). In a cohort of very young children, with an average age of 27 months post-partum, Willersley-Olsen et al. (168) observed no significant age-related disparities in passive and reflex stiffness, muscle

volume, or RoM between children with unilateral or bilateral CP (2). The studies by Barber et al. (167) and Willersley-Olsen et al. (168) only investigated the volume of the muscle in young children with bilateral CP or unilateral CP (2). Nevertheless, in addition to the potential variability observed at the muscle level, the differences in AT properties between these groups could significantly impact treatment strategies such as surgical lengthening or serial casting (2).

## 1.4. Summary of research deficits and knowledge gaps and rationale/aims of the dissertation

The doctoral thesis comprises two published studies aimed at addressing significant research gaps and knowledge deficiencies in methodological approaches, as presented in Study 1 (1), and advancing biomechanical understanding of muscle-tendon properties in children and adolescents with SCP, as elucidated in Study 2 (2). The research and knowledge deficiencies, along with the respective aims and hypotheses of the proposed studies, are presented in chapters 1.4.1 and 1.4.2.

### 1.4.1. Study 1: Assessment of morphological properties of the Gastrocnemius muscle-tendon-unit

Assessing individual muscle belly and tendon lengths is valuable for detecting muscle belly contracture (25) and enhancing our comprehension of structural adaptations (1, 82). Furthermore, the acquisition of data pertaining to alterations in muscle belly and tendon lengths resulting from treatments such as orthotics or stretching is of paramount importance for the development of efficacious therapies (1). Ultrasound is often preferred for evaluating muscle and tendon properties due to its advantages over other methods such as MRI (1, 51–53, 58). Measuring the length of an entire MTU of the lower leg accurately presents challenges with traditional 2D US techniques (1). Therefore, several US methods have been developed to overcome this limitation (1). For example, studies evaluating the GM muscle belly, GM MTU, or AT have been conducted using various methods (1), including 1) a combination of B-mode US with 3D motion capture (26, 27, 78, 87, 88), along with 3DfUS techniques (89–92); 2) US with tape measurements (2, 25, 72, 81–86); and 3) the use of EFOV imaging or panoramic US (72–76, 169). Although many approaches have been considered as accurate and reliable for length assessments, their validation against gold standards such as MRI or tissue dissections has been infrequently performed (75, 86, 91). Furthermore, several drawbacks are associated with these approaches. For instance, approaches that combine US and motion

capture rely on the assumption that the marker placed at the MTJ is aligned with the marker placed at the medial femoral epicondyle (88). However, fulfilling this prerequisite may not always be possible due to subject-related restrictions, such as short legs in children, or setup-related restrictions, such as the appropriate camera placement and required positioning of the subject to ensure marker visibility, especially during dynamic measurements. Furthermore, when conducting 3DfUS assessments, it is necessary for subjects to remain still throughout the examination (1). This can be particularly challenging when examining large muscles or specific population groups, such as children (1). Although approaches that combine US and tape measures or skin markings may be useful for assessing tissue lengths at rest or specific static positions, they may not be suitable for evaluating tissue behaviour during dynamic tasks. Achieving reliable results with panoramic US requires a certain level of experience and practice, making it unsuitable for novice sonographers or researchers. It is worth noting that muscle and tendon lengths were often calculated in 2D, which is a simplified representation of biological tissue properties (1).

To overcome these limitations mentioned above, as part of this thesis, an easily applicable 3D US approach was developed (1). This method enables the measurement of the static lengths and the lengthening behaviour of the GM muscle belly, GM MTU, and AT in 3D space by combing 3D motion capture, 2D US imaging, and vector algebra (1). The aim of this investigation was to assess the validity and both intra- and inter-rater reliability of this approach (1). The hypothesis was that the approach would demonstrate high reliability and adequate accuracy in measuring the static and dynamics lengths of the muscle and tendon (1).

### 1.4.2. Study 2: Functional and mechano-morphological properties of the spastic muscle in individuals with unilateral or bilateral cerebral palsy

Studies have shown that individuals with CP present impaired muscle growth and altered structural, mechanical, and morphological properties of the tendon and muscle when compared to TD individuals (e.g., (2, 82, 170–175)). These findings are mainly based on studies that included both individuals with unilateral or bilateral SCP (2). It is possible that differences between the two groups exist at the muscle-tendon level due to their differences in aetiology as well as bony and functional deviations (2). However, there is limited literature comparing spastic muscle properties between individuals with bilateral SCP and individuals with unilateral SCP (2, 167, 168). Barber et al. (167) stated that children with unilateral CP had a significantly lower rate of GM muscle growth compared to both children with bilateral CP and their TD peers (2). The observed difference in GM muscle growth rate during early childhood

is likely to result in a significant divergence in calf muscle volume between the different CP groups during adolescence and adulthood (2, 167). However, a study by Willersley-Olsen et al. (168) did not observe any significant differences, which are related to age, in RoM, reflex and passive stiffness, and muscle volume between the two CP subtypes. Additionally, Barber et al. (167) and Willersley-Olsen et al. (168) only investigated the muscle volume in young children with unilateral CP or bilateral CP (2). Moreover, aside from potential variations at the muscle level, differences in AT properties between the groups could significantly impact treatment approaches (2). Consequently, further research is necessary to enhance our comprehension of muscle-tendon pathology in individuals with bilateral or unilateral SCP including parameters such as muscle architecture and strength, as well as AT morphology (2). In general, it is hypothesized that there are discrepancies in muscle strength and morphological muscle-tendon properties between groups due to the observed discrepancies in functional and skeletal impairments (2). If this hypothesis is correct, it would suggest that future treatments may need to be tailored to the specific CP subtype (2, 14, 176). This is due to the fact that any discrepancies in the muscle structure itself, as indicated by factors such as volume and fascicle length, may have an effect on the functionality of the joint and, consequently, potentially lead to an increased risk of surgical complications (2, 14, 176).

Therefore, the primary aim of the second study of this thesis was to compare the mechano-morphological characteristics of the GM MTU and its constituent parts, as well as the ankle joint function and isometric muscle strength between children with bilateral SCP and those with unilateral SCP (2).

# 2. Methods

## 2.1. Study 1: 3D Ultrasound validation and reliability study

### 2.1.1. Participants

Sample size determination was based on ICC estimates (1) as described by Walter et al. (177). Aiming for an ICC of 0.9, 80% power, with a minimum acceptable ICC of 0.7 and a significance level of 5%, the calculation of the sample size indicated a need for 18 subjects or legs (1). To counteract potential dropouts, 16 healthy subjects (32 legs) were ultimately included (1), in line with the methodology used in previous studies (25, 74, 178). However, data of one participant was omitted from the reliability evaluation due to incorrect recording of the US data (1). Therefore, 15 datasets were used for the reliability analyses, which resulted in a total of 30 legs, as both legs of the subjects were examined (1). Moreover, 9 datasets (18 legs) were used for the validity evaluation (1). The flow chart and the characteristics of the participants are displayed in Figure 3 and Table 2, respectively. None of the participants had a documented history of injury and surgery on the lower extremities in the last year or current pain, restrictions, or problems in the lower extremities (1). In addition, all participants demonstrated the ability to accept and adhere to verbal instructions (1).

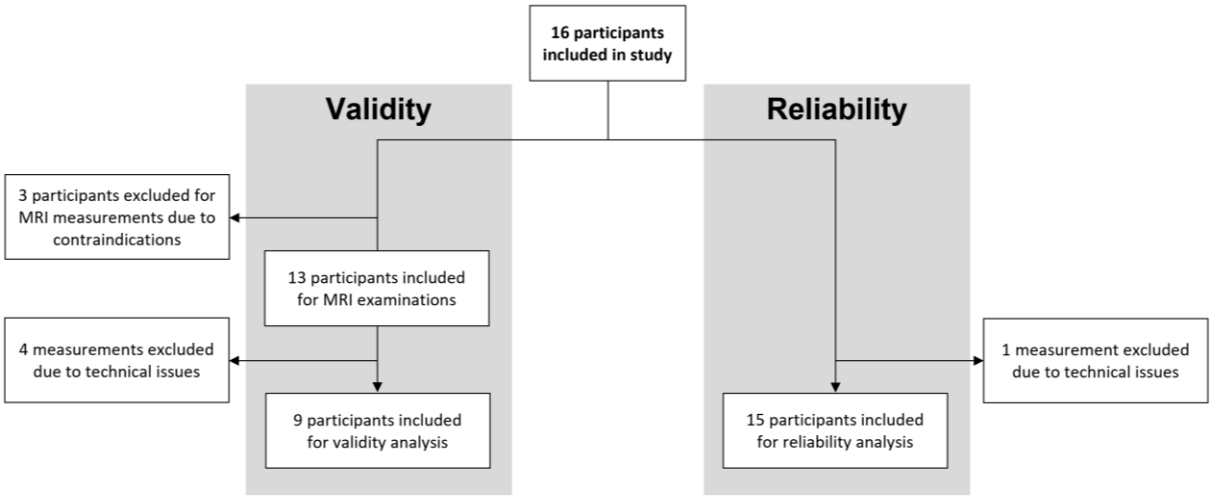


**Figure 3.** Flowchart of the participants. This figure was created by the author of this thesis.

The Ethics Committee of the University of Graz, Austria, has given positive ethical approval for this study (registration number: 39/20/63 ex 2020/21) (1). Every participant included in the study received prior information about its purpose, the procedure, and safety guidelines related to MRI and gave written informed consent (1).

**Table 2.** The characteristics of the participants (mean ± standard deviation (SD)). Table and adapted caption reproduced from (1) with permission of the publisher (Springer Nature).

| Sex | Number | Age (years) | | Body mass (kg) | | Body height (cm) | | BMI | |
|---|---|---|---|---|---|---|---|---|---|
| | | Mean | SD | Mean | SD | Mean | SD | Mean | SD |
| F | 7 | 32.43 | 10.15 | 67 | 13.20 | 170.14 | 4.56 | 23.12 | 4.48 |
| M | 9 | 34.78 | 7.22 | 77.67 | 8.60 | 185.11 | 4.44 | 22.70 | 2.77 |

F, female; M, male; BMI, Body-Mass-Index

### 2.1.2. Experimental design

To assess the reliability and validity of this approach, two sessions of US assessments and one MRI measurement were carried out (1). The data of the first US measurement session were compared with the results obtained from the MRI scanning, which took place approximately 24.4 ± 8.1 hours after the initial US assessment (1). The reliability of the data was determined by analysing the results of the initial and subsequent US measurement sessions, with a time gap of 2.1 ± 0.6 days between the two sessions (1). Throughout the entire study, participants abstained from any intense physical activity (1).

### 2.1.3. Validity Assessment

The validity of the innovative 3D US methodology was evaluated by comparing the lengths of the GM muscle belly, GM MTU, and AT in static position obtained by the proposed US method (see section 2.1.4 for a detailed description) with those obtained using MRI (1).

Magnetic resonance imaging data was evaluated at the MRI-Lab at the University of Graz by a 3.0 Tesla Magnetom Vida system with syngo MR XA20A (Siemens Medical Systems, Erlangen, Germany) (1). This evaluation was performed using a combination of the following coils: posterior part of 20-channel Head/Neck, 32-channel Spine, 18-channel Body and 18-channel Body Long (1). T1 measurements were assessed using a 3D-space sequence with compressed sensing (CS) obtained from the Numaris/X VA20A package. The sequence consisted of 228 sagittal slices (1 mm slice thickness), Field of View (FoV) read 544 mm, FoV phase 80.1%, TR 638 ms, TE 16 ms, base resolution 544 (acquisition matrix 436 x 544, 0.5 x 0.5 x 1 mm voxel size with interpolation), flip angle mode T1 Var, phase encoding direction AP, acceleration (CS, factor 7), standard fat water contrast with a measurement time of 5 min 28 s (1).

Prior to scanning, two markers filled with Radiance® (6 mm in diameter, MR-PinPoint®, No. 187, BeekleyMedical®) were precisely positioned with their centres aligned with the marks, which indicated the origin at the most superficial aspect of the medial condyle detectable at the knee hollow and the insertion of the GM MTU at the calcaneus (1). The landmarks were marked with a water-resistant pen beforehand during the first US measurement session, and corresponded to the position of the reflective markers during the US assessments, which were used to determine the 3D coordinate position of the landmarks by means of a 3D motion capture system (1). The participants were asked to lie on the examination bench in a supine position with slightly flexed knees (~20° flexion) to prevent pressure on the origin markers (1). Afterwards, two custom-made splints (Ortho-Aktiv; Graz, Austria) were applied to the ankle joints of the participant and fixed with straps to maintain the same predetermined ankle joint position during both the MRI and the US measurements sessions (1). By means of the custom-made splints, the ankle joints were kept at 90° (neutral position) and 80° for the right and left ankles, respectively, resulting in a 10° dorsiflexion for the left ankle joint (1).

A Head/Neck-20 coil was positioned over the feet encompassing the lower section of the measurement volume, while two Body-18 coils were utilized to cover the upper part (e.g., tibia/fibula and knee) in an overlapping setup (1). Additionally, the region from the feet to the mid-thigh area was covered using the Spine-32 coil to ensure optimal signal-to-noise ratio (SNR) volume coverage (1).

### 2.1.4. Reliability assessment

To examine the reliability within (intra-reliability) and between (inter-reliability) raters concerning both the static and dynamic length measurements, the US measurements were conducted according to a standardized protocol by two testers on two distinct days (1). Start order of both the investigators and the tested legs was randomized (www.randomizer.org) before enrolling the first participant (1). The participants were asked to lie down on an examination bench in a prone position (1). The static length measurements were carried out first (1). After finishing the static length measurements, the dynamic examinations were assessed (1). After the first investigator completed both the static and dynamic measurements, the second investigator conducted the same US assessments as described in the chapters 2.1.4.1 and 2.1.4.2. (1). To ensure and maintain objectivity, all markings of the first investigator were removed prior to the start of the examination of the second investigator (1). Figure 4 presents a schematic overview of both static and dynamic length measurements.

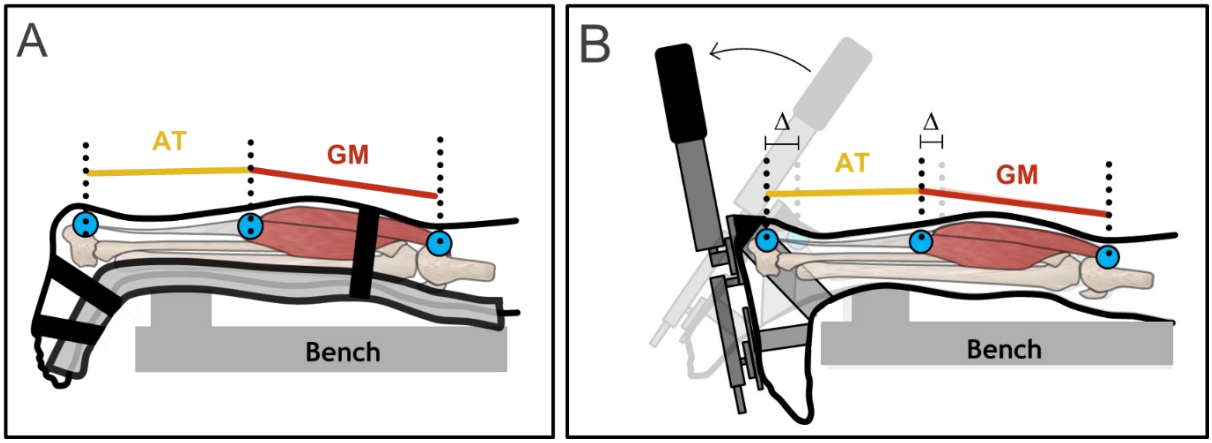


**Figure 4.** (A) Static length measurements of the GM muscle belly, MTU, and AT in vivo. (B) Dynamic length measurements of the GM tissues during passive ankle dorsiflexion movement in vivo. Figure and adapted caption reproduced with modifications from (2) with permission of the publisher (Elsevier).

#### 2.1.4.1. Static length assessment

After the participant was positioned on the examination bench, the anatomical landmarks of the insertion, MTJ, and origin of the GM MTU required for the US length assessments were detected by the use of a 5-cm linear array US probe (LA523, MyLab60; Esaote S.p.A., Genova, Italy) (1). The most superficial point of the medial epicondyle was defined as the origin of the GM detected at the popliteal fossa (1).

The insertion was identified as the most proximal attachment site of the AT at the calcaneus (Figure 5A) (1). The most superficial landmark of the medial condyle was located in the US images by determining the minimum vertical distance from the bony epicondyle to the skin surface ($l_{cond}$ in Figure 5C) (1). When the slice with the minimum distance was found, the slice was marked on the skin surface in both the transverse (Figure 5B) and longitudinal (Figure 5C) planes (1). Afterwards, the origin was obtained by crossing the two planes (see blue cross in Figure 5C) (1).

After locating the landmarks, the ankle joint on either the right or left side was stabilized at approximately 90° in neutral position or 80° (i.e., 10° dorsiflexion) with a custom-made splint (Figure 6A) (Ortho-Aktiv; Graz, Austria), respectively, depending on the randomization (1). A goniometer was used to control the angle of the ankle joint (Ka We V01, Medizintechnik) (1).

Passive spherical motion capture markers were attached to the skin collinear with the vertical axis over the origin and insertion (1). In addition, markers were also placed on the lateral and medial malleolus and lateral and medial condyles (Figure 6AB) (1).

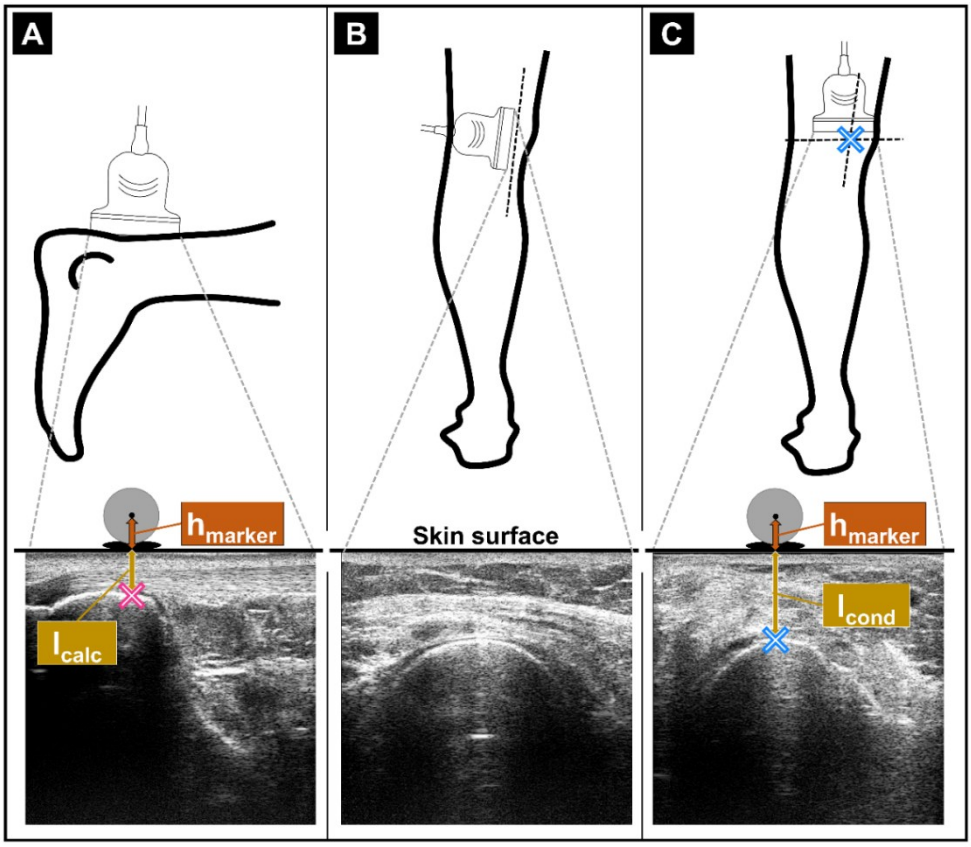


**Figure 5.** Determination of the anatomical landmarks: (A) Proximal AT attachment point at the calcaneus in longitudinal direction. (B & C) Most superficial point of the femoral epicondyle in longitudinal (B) and transverse (C) planes. Reflective markers were attached to the skin collinear with the vertical axis above the determined landmarks. The distances "$h_{marker}$ + $l_{cond}$" and "$h_{marker}$ + $l_{calc}$" were used to mathematically correct the reflective markers to the anatomical landmarks in vivo. $h_{marker,}$ distance from the centre of the marker to the skin surface; $l_{cond}$, distance from the skin surface to the proximal attachment point of the AT at the calcaneus; $l_{calc,}$ distance from the skin surface to the most superficial landmark of the medial condyle. Figure and adapted caption reproduced from (1) with permission of the publisher (Springer Nature).

The 3D coordinates of the reflective markers were captured by using an infrared 3D motion capture system (10 cameras, Miqus M3, Qualisys AB, Gothenburg, Sweden) (1). In addition to the reflective markers surface electromyographic (EMG) sensors were placed on the gastrocnemius lateralis (GL) (1). The skin surface was prepared and electrode (Blue Sensor N, Ambu A/S, Ballerup, Denmark) placement was performed according to the SENIAM guidelines (179) and verified using US (1).

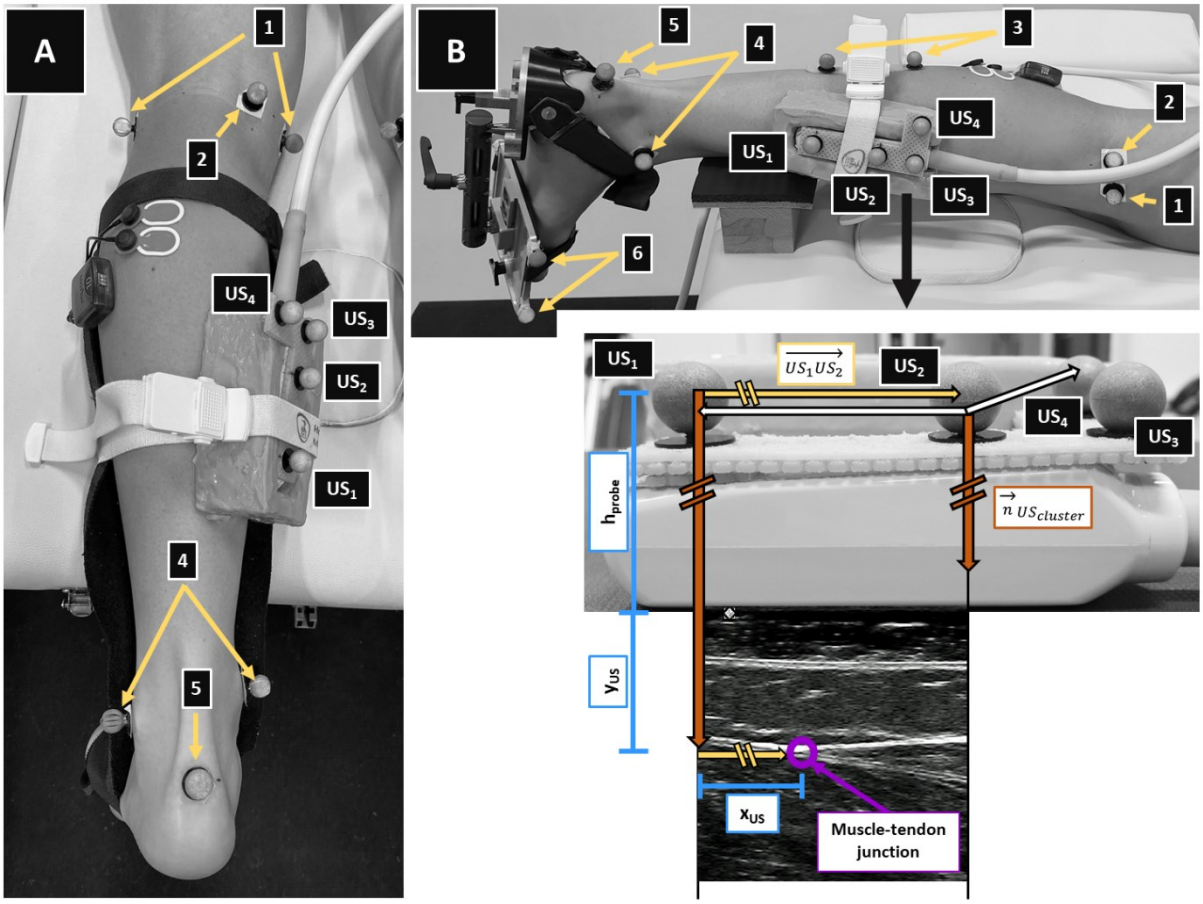


**Figure 6.** Measurement set-up for the static measurements (A) and dynamic measurements (B). Placement of reflective markers on specific landmarks, US transducer on the GM MTJ, and EMG sensors to assess the static lengths of the GM MTU, muscle belly, and AT tendon and the lengthening behaviour of these tissues, and muscle activity throughout dorsiflexion rotations, respectively. Marker placement locations: 1 = medial and lateral condyle; 2 = most superficial point of the medial condyle; 3 = four-marker cluster; 4 = medial and lateral malleolus; 5 = proximal insertion of the AT onto the calcaneus; 6 = four markers attached to footplate; $US_1$–$US_4$ = markers placed on the US probe. (B) shows the procedure used to calculate the location of the MTJ in vivo. Figure and adapted caption reproduced from (1) with permission of the publisher (Springer Nature).

EMG signals were checked visually for possible muscle co-activation to ensure that no voluntary muscle activation occurred during the passive measurements (1). To finalize the measurement setup, a 59 mm linear array US probe (LogicScan 128; Telemed, Vilnius, Lithuania) equipped with a rigid four marker cluster was fixated over the GM MTJ by use of a custom-made probe holder and straps (1). The four markers are mounted at the same height and form a plane perpendicular to the US image plane (see Figure 7).

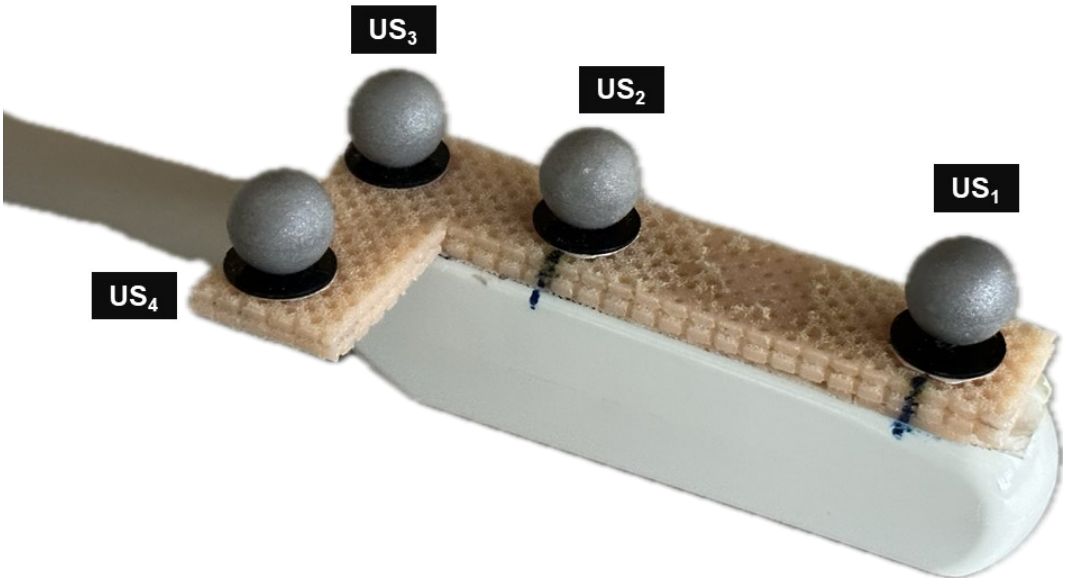


**Figure 7.** Ultrasound transducer with a rigid four marker cluster ($US_1$-$US_4$) representing a plane perpendicular to the US image plane. This figure was created by the author of this thesis.

The position of the linear US probe allowed for visualization of the most distal part of the GM muscle belly in the US images as visualised in Figure 8 (1).

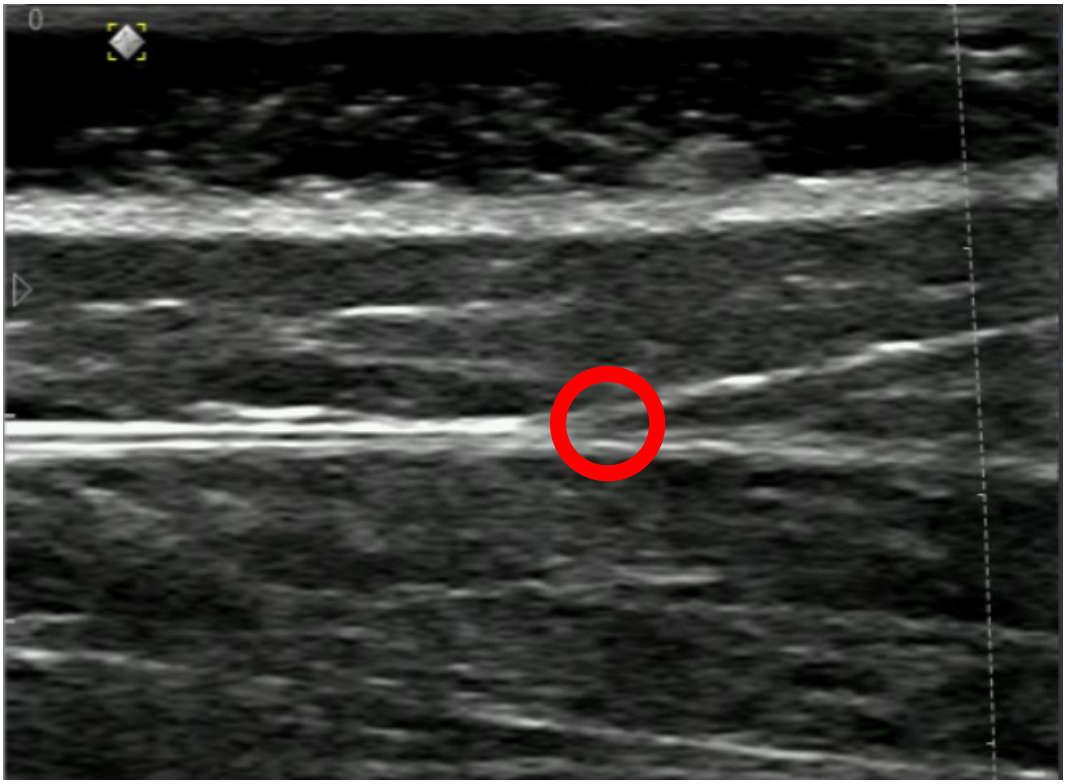

**Figure 8.** Visualization of the GM MTJ in an US image (red circle). This figure was created by the author of this thesis.

Both EMG data and 3D marker position as well as US videos were synchronized and recorded simultaneously at 100 Hz, 2000 Hz and 60Hz, respectively (1). Altogether two trials were captured (1). Afterwards, the US transducer and the splint were removed, and the measurement of the second leg was performed as previously described (1).

#### 2.1.4.2. Dynamic lengthening assessment

Upon completion of the static length measurement of both legs, an evaluation was conducted on the dynamic lengthening behaviour of the GM muscle belly, GM MTU, and AT of a single leg (1). The side of the leg was randomized beforehand (1). The participants kept lying in prone position on the examination bench (1). At first, the knee joint of the respective leg was positioned at approximately 20° of flexion using a specially designed cushion (refer to Figure 6B), allowing unrestricted sagittal plane movement at the ankle (1). A custom-made footplate has been fitted to the foot (see Figure 6B) and fixed with straps, which allows adjustments to stabilize the subtalar joint during sagittal movement of the ankle joint into dorsiflexion (1). To minimize the potential effect of foot deformation, the calcaneus was first put into neutral position within the frontal plane (1). The forefoot was slightly adducted and both the forefoot and midfoot were supinated until an adequate level of stability was attained (180).

Similar to the static length assessments (see description in chapter 2.1.4.1), the US transducer was positioned on the GM MTJ to record the movement of the MTJ (1). This ensured that the US videos captured the most distal segment of the GM muscle belly (1). Moreover, a torque wrench equipped with an inclinometer (180, 181) was attached to the footplate (Figure 6B) (1). Once the measurement setup was completed, the arm of the hand-held inclino-dynamometer was utilized to move the foot plate from maximum plantarflexion into maximum dorsal flexion within the sagittal plane, while simultaneously measuring the externally applied torque (1, 182). Furthermore, the shift of the GM MTJ was concurrently recorded throughout the rotation of the ankle joint (1). A total of two dorsiflexion rotations were executed (1). Upon completion of both the initial static and initial dynamic US measurement sessions, participants were instructed not to erase the markings indicating the locations of the origin (most superficial landmark of the medial epicondyle) and the tendinous insertion (1). These marks were subsequently utilized in the MRI assessments, contributing to the validation of previously described 3D US approach in the chapter 2.1.3.

### 2.1.5. Data analyses

Ultrasound examination

In the post-processing phase, the MTJ of the GM MTU was manually tracked every third frame in the US videos (1, 183). Custom software programmed in MATLAB (version 7.1, MathWorks Inc., 2005) was used to calculate tissue lengths and lengthening behaviour (1). To determine the lengths of the GM muscle belly, GM MTU, and AT as well as the lengthening behaviour of these tissues, the origin and heel markers (markers number 2 and 5 in Figure 6B, respectively) were mathematically corrected by vector algebra to calculate the positions of the anatomical landmarks in vivo in 3D rather than relying on the marker position on the skin surface (1). In examining the static trials, the origin marker, which was initially positioned collinearly with the vertical axis over the most superficial point of the medial condyle detectable at knee hollow, underwent correction along the vertical axis (z-axis) (1). The distance of the correction corresponded to the distance from the centre of the reflective marker to the most superficial landmark of the medial condyle visible in the US images ($h_{marker}$ + $l_{cond}$, see Figure 5C and Equation 1) (1).

**Equation 1.** Correction formula for the origin marker. $C_{Origin}$, corrected origin marker; $h_{marker}$, marker height, $l_{cond}$, distance from the skin surface to the most superficial landmark of the medial condyle; x,y,z, coordinates.

$$\begin{pmatrix} COrigin_x \\ COrigin_y \\ COrigin_z \end{pmatrix} = \begin{pmatrix} Origin_x \\ Origin_y \\ Origin_z \end{pmatrix} - \begin{pmatrix} 0 \\ 0 \\ h_{marker} + l_{cond} \end{pmatrix} \quad (1)$$

The heel marker was corrected accordingly ($h_{marker}$ + $l_{calc}$, see Figure 5A and Equation 2).

**Equation 2**. Correction formula for the heel marker in static trails. CHeel, corrected heel marker; $h_{marker}$, marker height, $l_{calc}$, distance from the skin surface to the most proximal attachment point of the AT at the calcaneus; x,y,z, coordinates.

$$\begin{pmatrix} CHeel_x \\ CHeel_y \\ CHeel_z \end{pmatrix} = \begin{pmatrix} Heel_x \\ Heel_y \\ Heel_z \end{pmatrix} - \begin{pmatrix} 0 \\ 0 \\ \mathrm{h_{marker}} + \mathrm{l_{calc}} \end{pmatrix} \quad (2)$$

The origin marker was corrected in the same manner for the dynamic trials as it was for the static trials (1). However, the marker on the heel was modified along the direction defined by the medially fixed footplate markers (Figure 6B) according to the distance from centre of the marker to the insertion at the calcaneus detectable in the US images (Equation 3) (1).

**Equation 3.** Correction formula for the heel marker in dynamic trails. $C_{Dyn}$Heel, Corrected heel marker; $h_{marker}$, marker height, $l_{calc}$, distance from the skin surface to the most proximal attachment point of the AT at the calcaneus; x,y,z, coordinates; $\overrightarrow{e_{FM_1FM_2}}$, unit vector from the medial posterior footplate marker to the medial anterior footplate marker.

$$\begin{pmatrix} C_{Dyn}Heel_x \\ C_{Dyn}Heel_y \\ C_{Dyn}Heel_z \end{pmatrix} = \begin{pmatrix} Heel_x \\ Heel_y \\ Heel_z \end{pmatrix} + (\mathrm{h_{marker}} + \mathrm{l_{calc}}) * \begin{pmatrix} \overrightarrow{e_{FM_1FM_{2_x}}} \\ \overrightarrow{e_{FM_1FM_{2_y}}} \\ \overrightarrow{e_{FM_1FM_{2_z}}} \end{pmatrix} \quad (3)$$

Finally, to determine the location of the MTJ in 3D, the normal vector $\overrightarrow{n_{UScluster}}$ and its unit vector $\overrightarrow{e_{n_{UScluster}}}$ of the cluster plane was determined by calculating the cross product of the vectors $\overrightarrow{US_2US_1}$ and $\overrightarrow{US_2US_4}$ (see Figure 6B and Equation 4). The vector represents the direction of the vertical axis in the US image.

**Equation 4.** Formula for calculating the normal vector ($n_{UScluster}$) of the cluster plane of the US transducer. $\mathrm{n_{UScluster}}$, normal vector of the US cluster plane; $\overrightarrow{US_2US_1}$, vector from the US marker $US_2$ to US marker $US_1$; $\overrightarrow{US_2US_4}$, vector from the US marker $US_2$ to US marker $US_4$; x,y,z, coordinates.

$$\begin{pmatrix} \mathrm{n_{UScluster_x}} \\ \mathrm{n_{UScluster_y}} \\ \mathrm{n_{UScluster_z}} \end{pmatrix} = \begin{pmatrix} \overrightarrow{US_2US_{1_x}} \\ \overrightarrow{US_2US_{1_y}} \\ \overrightarrow{US_2US_{1_z}} \end{pmatrix} \mathrm{x} \begin{pmatrix} \overrightarrow{US_2US_{4_x}} \\ \overrightarrow{US_2US_{4_y}} \\ \overrightarrow{US_2US_{4_z}} \end{pmatrix} \quad (4)$$

Furthermore, a second vector $\overrightarrow{US_1US_2}$ and its unit vector $\overrightarrow{e_{US_1US_2}}$ were calculated representing the horizontal direction of the US image. Subsequently, the MTJ position was then detected using the height of the US probe and marker ($h_{probe}$ + $h_{marker}$), the calculated vectors, and horizontal ($x_{US}$) and vertical ($y_{US}$) coordinates of the MTJ derived from the US tracking (see Figure 6B and Equation 5) (1).

**Equation 5.** Formula for calculating the position of the MTJ of the GM MTU. $US_1$, US marker 1; $h_{probe}$, height of the US transducer/probe; $h_{marker}$, marker height; horizontal ($x_{US}$) and vertical ($y_{US}$) coordinates of the MTJ derived from the US video tracking; $\overrightarrow{e_{n_{UScluster}}}$, unit normal vector of the four marker cluster plane representing the direction of the vertical axis in the US image; $\overrightarrow{e_{US_1US_2}}$, unit vector from marker $US_1$ to $US_2$ of the marker cluster mounted on the US probe representing the direction of the horizontal axis in the US image; x,y,z, coordinates.

$$\begin{pmatrix} \mathrm{MTJ_x} \\ \mathrm{MTJ_y} \\ \mathrm{MTJ_z} \end{pmatrix} = \begin{pmatrix} US_{1_x} \\ US_{1_y} \\ US_{1_z} \end{pmatrix} + (\mathrm{h_{probe}} + h_{marker} + y_{US)} * \begin{pmatrix} \overrightarrow{e_{n_{USclusterx}}} \\ \overrightarrow{e_{n_{USclustery}}} \\ \overrightarrow{e_{n_{USclusterz}}} \end{pmatrix} + (x_{US}) * \begin{pmatrix} \overrightarrow{e_{US_1US_{2x}}} \\ \overrightarrow{e_{US_1US_{2y}}} \\ \overrightarrow{e_{US_1US_{2z}}} \end{pmatrix} \quad (5)$$

After correcting the origin marker and heel marker and determining the MTJ in vivo, the length of the muscle belly was then calculated as the linear distance between the corrected origin $COrigin$ and the calculated MTJ (1). The length of the AT tendon was also calculated as the linear distance between the MTJ and the corrected heel marker position $CHeel$ for the static trials or $C_{Dyn}Heel$ for the dynamic trails by applying the Pythagorean theorem (Equation 6, Equation 7 and Equation 8 (1).

**Equation 6.** Formula for calculating the GM muscle belly length by applying the Pythagorean theorem. $COrigin$, corrected origin marker; $MTJ$; calculated MTJ in vivo; x,y,z, coordinates.

$$MuscleLength = \sqrt{(COrigin_x - MTJ_x)^2 + \left(COrigin_y - MTJ_y\right)^2 + (COrigin_z - MTJ_z)^2} \quad (6)$$

**Equation 7.** Formula for calculating the AT length for static trials by applying the Pythagorean theorem. $CHeel$, corrected heel marker; $MTJ$; calculated MTJ in vivo; x,y,z, coordinates.

$$TendonLength_{static} = \sqrt{(CHeel_x - MTJ_x)^2 + \left(CHeel_y - MTJ_y\right)^2 + (CHeel_z - MTJ_z)^2} \quad (7)$$

**Equation 8.** Formula for calculating the AT length for dynamic trials by applying the Pythagorean theorem. $C_{Dyn}Heel$, corrected heel marker; $MTJ$; calculated MTJ in vivo; x,y,z, coordinates.

$$TendonLength_{dyn} = \sqrt{\left(C_{Dyn}Heel_x - MTJ_x\right)^2 + \left(C_{Dyn}Heel_y - MTJ_y\right)^2 + \left(C_{Dyn}Heel_z - MTJ_z\right)^2} \quad (8)$$

The length of the GM MTU was calculated as the sum of both tendon and muscle length (1). To evaluate the lengthening behaviour, individual lengths of the GM MTU, AT tendon, and GM muscle belly were computed across the range from 0 Nm (representing the length in resting position) to the maximum applied common torque of 5.5 Nm for all participants (1).

MRI measurements

Since the maximum FoV for the used CS-space sequence is 550 mm and due to limitations in excitation, there is a significant decrease in SNR in frequency ranges at the edge of the FoV (1). Therefore, two T1-space assessments were carried out with overlapping FoVs, which were further composed to a single 3D volume, using the Numaris/X VA20A angio-compose algorithm with the Siemens View&Go software in the Siemens reference space (1).
The GM MTU origin was assessed by identifying the transverse and longitudinal slices with the largest marker diameter and marking the 3D position in the transverse plane (1). The medial epicondyle and its most superficial landmark were identified and marked in all three spatial planes by navigating through the coronal slices (Figure 9B) and the GM MTU insertion was then identified by determining the transverse and coronal slices with biggest marker diameter and referencing the 3D position in the coronal plane (1). The most proximal attachment point of the AT at the calcaneus was determined in the referenced transverse slices and marked in three spatial planes (Figure 9A) (1). In a third step the GM MTJ was located in the transverse plane and marked in 3D (1). Since the origin, insertion, and MTJ of the GM MTU were marked in three spatial planes, AT, GM muscle belly, and MTU length were directly assessed in a single 3D volume for both legs using the transverse slices, measuring between marker positions at a slice thickness of 1 mm (1).

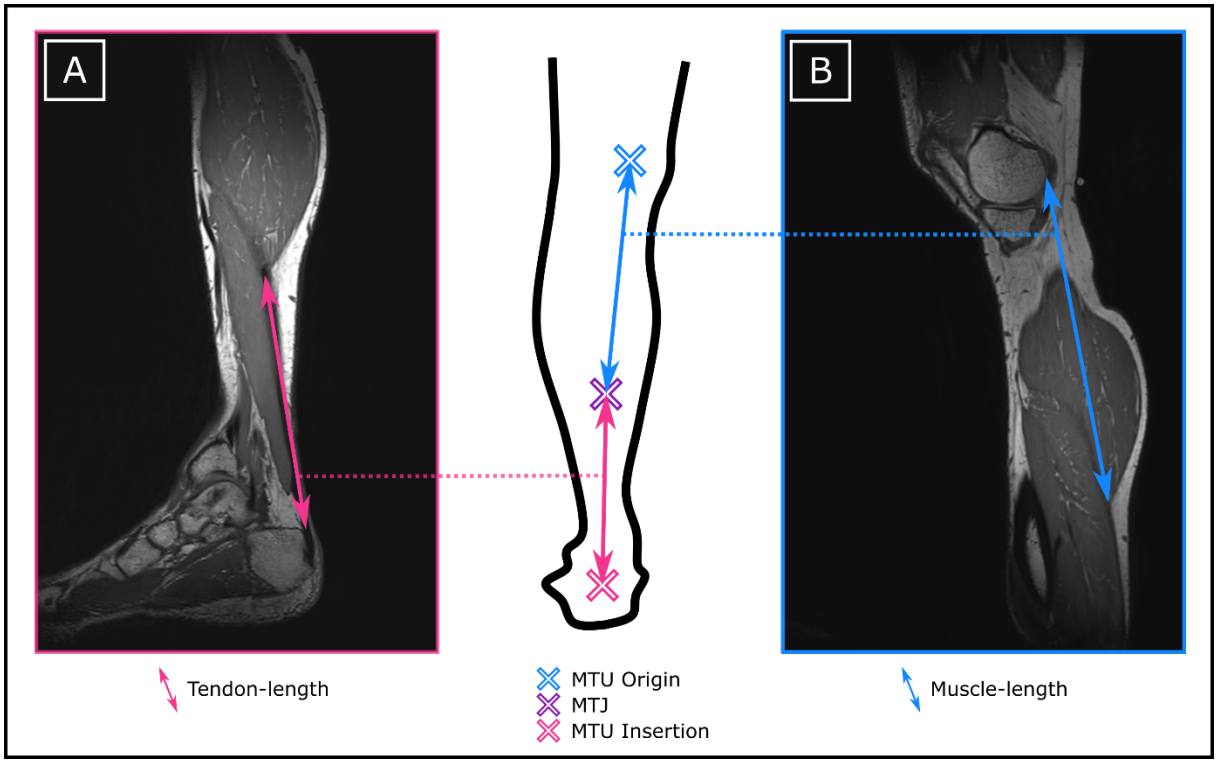


**Figure 9.** Direct 3D measurement of (A) AT length and (B) GM muscle belly length across three spatial planes in MRI (for a spatially simplified illustration in the sagittal plane). The GM MTU origin was determined by locating the most superficial landmark of the medial epicondyle. Insertion of the MTU was defined as most proximal aspect of the tendinous insertion at the calcaneus. Finally, the MTJ was determined as most distal point of the muscle belly. All three anatomical points were marked in three spatial planes. Permission obtained from the copyright holder (© Thomas Zussner) to reproduce this figure in this thesis.

### 2.1.6. Statistical analyses

Statistical analyses for this study were conducted using SPSS (version 22.0, SPSS Inc., Chicago, IL, USA), and the predetermined significance level was set at $\alpha = 0.05$ (1).

**Validity**

A dependent t-test was utilized to compare the initial US assessments taken by both investigators on the first day (1). The t-test indicated that there was no significant difference between the raters, and thus the mean of the US data from raters 1 and 2 was employed for further analysis (1). Bland-Altman plots were utilized to evaluate the absolute agreement between the MRI measurement and the proposed 3D US approach (1).

**Reliability**

For the reliability analyses, $ICC_{(2,2)}$ (95% confidence interval (CI)) and coefficients of variation (CV) were used (1, 74, 88, 178, 184, 185). Based on Koo and Li (184), ICC values < 0.5, between 0.5 - 0.75 and 0.75 - 0.9, and values > 0.90 indicate poor, moderate, good, and excellent reliability, respectively (1).

Moreover, the SEM was calculated to obtain the absolute reliability of the tissue length measurements (see Equation 9) (1, 186, 187).

**Equation 9.** Calculation of the standard error of measurement, where SD is the mean SD of the respective test–retest pair across the 15 participants (1, 186, 187).

$$\mathrm{SEM} = \mathrm{SD} \times \sqrt{1 - ICC_{(2,2)}} \tag{9}$$

The MDC with a 95% CI was then derived by Equation 10 (187).

**Equation 10.** Calculation of the minimal detectable change (1, 178, 187).

$$\mathrm{MDC}_{95} = 1.96 * \sqrt{2} * \mathrm{SEM} \tag{10}$$

## 2.2. Study 2: Differences in morphological and mechanical properties of the gastrocnemius medialis and Achilles tendon in children with unilateral or bilateral spastic cerebral palsy

### 2.2.1. Study design

In this retrospective study, 33 datasets of children and adolescents diagnosed with unilateral or bilateral SCP, which were included from two clinical studies that had been previously conducted (clinical trial identifier: NCT04570358 (study I) and NCT05269745 (study II), respectively), were analysed (2). The analysis included a total of 23 datasets from study I and 10 datasets from the second study (2). Both studies followed the identical methodology and received positive approval from the Ethics Committee of the Medical University of Graz (registration numbers: 31-130 ex 18/19 for study I and 32-115 ex 19/20 for study II) (2). In each study, the parents of the participants gave written informed consent prior to their involvement (2).

### 2.2.2. Participants

As mentioned above, datasets from 33 children and adolescents diagnosed with SCP were analysed, of which 15 had unilateral SCP, and 18 had bilateral SCP (2). The participants of the study were recruited exclusively from the orthopaedic department of the Medical University hospital (2). All children and adolescents involved in the study were ambulatory, capable of understanding and following verbal instructions (2). Exclusion criteria compromised of conditions other than SCP (e.g., ataxic, dyskinetic, athetoid, etc.) (2). Additionally, individuals, who had previously undergone muscle-relaxing or oral antispastic medication, received applications of botulinum toxin within the last six months, had undergone any prior surgery on the plantar flexors within the previous 12 months, or had any other disorders affecting the lower limb, were also excluded (2). The characteristics of the participants are displayed in Table 3. The individual characteristics of the participants can be found in the Supplementary Table 1. The evaluation of the selective voluntary motor control was carried out using the “Selective Control Assessment of the Lower Extremity” (SCALE, (149)) (2). In individuals with unilateral SCP, the assessment focused on the affected leg, for children and adolescents with bilateral SCP, the evaluation targeted the more affected leg (2).

**Table 3.** Participant characteristics of the children and adolescents with unilateral spastic cerebral palsy (USCP) and those with bilateral spastic cerebral palsy (BSCP). Mean (SD) [range]. Table and adapted caption reproduced from (2) with permission of the publisher (Elsevier).

| **Anthropometric** | USCP | BSCP |
|---|---|---|
| Number | 15 | 18 |
| Gender (female/male) | 7/8 | 7/11 |
| Age (years) | 10.2 (2.4) [6-15] | 10.8 (2.5) [7-15] |
| Body mass (kg) | 41.2 (16.3) | 41.6 (16.2) |
| Body height (cm) | 144.0 (15.1) | 144.1 (16.0) |
| Lower leg length (cm) | 34.5 (4.1) | 34.0 (4.3) |
| **Clinical characteristics** | | |
| GMFCS Level I/II/III | 13/2/0 | 11/4/3 |
| SCALE (points: 2/1/0) | 0/12/3 | 3/14/1 |

The grading of the SCALE is presented for the more affected leg or the affected leg in children with BSCP and those with USCP, respectively. Scoring was limited to the ankle joint, with a score of 2 points for normal function, 1 point for impaired function, and 0 points for inability to perform.

### 2.2.3. Data Collection and processing

#### 2.2.3.1. Ankle range of motion and isometric muscle strength

The ankle plantarflexor muscle strength of the lower leg was assessed using an isokinetic dynamometer (CON-TREX MJ, CMV AG, Duebendorf, Switzerland) through isometric maximum voluntary contraction (IMVC) (2). Initially, the participants assumed a seated position with their body upright at a 70° angle, ensuring that their knees did not make contact with the seat (2). Afterwards, the foot was fixed to the adjustable footplate by means of straps, ensuring that the knee is in an extended position and the centre of the ankle joint was aligned with the axis of rotation of the dynamometer (Figure 10) (2). To familiarize the participants with the measurement procedure, they completed submaximal trials, during which they were provided with a live visual display of the applied torque (2). After familiarization, the participants performed IMVCs at an ankle angle, which corresponded to 50% of the individual ankle joint RoM, for a period of 5 seconds (2). This was followed by a two-minute rest period, with the aim of preventing fatigue (2). The trial was discarded and repeated if the participant did not follow instructions or did not apply the maximum force against the footplate (2). The RoM was determined in a passive condition prior to the IMVCs as described elsewhere (188, 189). The

isometric peak torque was used for the further analyses and was additionally normalized to body mass (2).

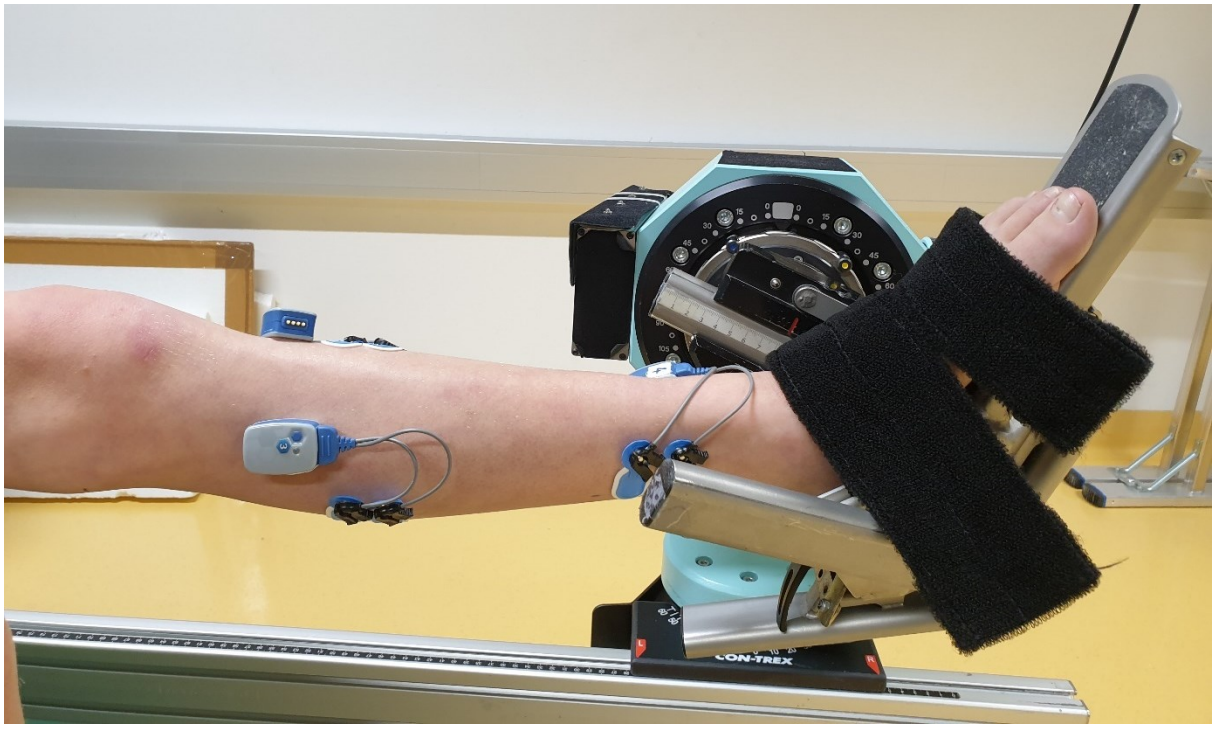


**Figure 10.** Measurement setup for assessing IMVC using an isokinetic dynamometer. The participant is in a seated position with their body upright at an 70° angle. The foot is fixed to the adjustable footplate by means of straps, ensuring that the knee is in an extended position and the centre of the ankle joint is aligned with the axis of rotation of the dynamometer. This figure was created by the author of this thesis.

#### 2.2.3.2. Muscle and tendon properties

##### 2.2.3.2.1. Morphological and architectural muscle-tendon properties

Free-hand 3D US was used to investigate the morphological characteristics of the GM and AT in a passive state at fixed ankle joint positions (2, 92). At first, the participants were asked to lie down on an examination bench in a prone position with their feet hanging over the edge of the bench (2). A custom-made footplate was attached to the foot and fixed with straps to allow ankle movement in the sagittal plane and stabilize the subtalar joint (2, 180, 182). The footplate is also fitted with a connector for attaching a pluggable torque wrench fitted with an inclinometer (2). After the footplate was fixed to the foot, an elevation was placed under the distal end of the lower leg to keep the knee angle at approximately 20° to ensure a comfortable lying position for the subject (2). The initial step involved determining the resting angle of the ankle joint, which corresponded to an ankle joint position with 0 Nm of external torque applied,

and the ankle angle, which corresponded to a dorsiflexion position of 4 Nm of externally applied torque (2). After these two angles were determined, a one-centimetre-thick layer of US gel was applied to cover the entire backside of the lower leg, serving as a buffer for the US measurements to prevent any pressure from the US probe being applied to the skin surface (2). From the knee to the calcaneus, several transverse US scans (i.e., full sweep) were taken, covering the medial and lateral condyles, the entire GM muscle belly and AT (Figure 11A) (2, 92). The scans started medially and overlapped laterally by approximately 1 cm (2). In addition to the full sweep, a single transverse scan was also recorded (2). This scan started from the lateral condyle, covered the medial condyle, and proceeded towards the MTJ and then the calcaneus (Figure 11B) (2). Two complete full sweeps and two single sweeps were performed, with those sweeps with better image clarity being selected for further analysis (2). A B-mode US device (LA523, MyLab60; Esaote S.p.A., Genova, Italy) with a 6 cm linear array transducer was used to capture the 3DfUS data (2). During the US scanning, the position of a rigid four-marker cluster mounted on the US probe was tracked at a frequency of 100 Hz by a 3D motion capture system consisting of 10 calibrated infrared cameras (Miqus M3, Qualisys AB, Gothenburg, Sweden) (2). As it is not possible to place electrodes on the gastrocnemius muscle during the full sweeps due to the US gel covering, EMG signals were recorded from the tibialis anterior (TA) muscle (EMG, Noraxon Ultium, Noraxon U.S.A. Inc, Scottsdale, Arizona, USA) to ensure that the tissue was scanned in a relaxed state (2). The EMG of the GL was measured during each single sweep in addition to the TA muscle (2). The EMG signals were recorded at a frequency of 2000 Hz and checked for muscle activity immediately after each scan (2). Skin preparation and placement of surface electrodes (Blue Sensor N, Ambu A/S, Ballerup, Denmark) were performed according to SENIAM guidelines (179) and additionally verified by US (2).

By combing the 3D coordinate position of the reflective four-marker cluster captured by the 3D motion capture system and the video data from the B-Mode US scans, a 3D reconstruction of the GM MTU was computed by a custom-made software programmed in MATLAB (2, 92).

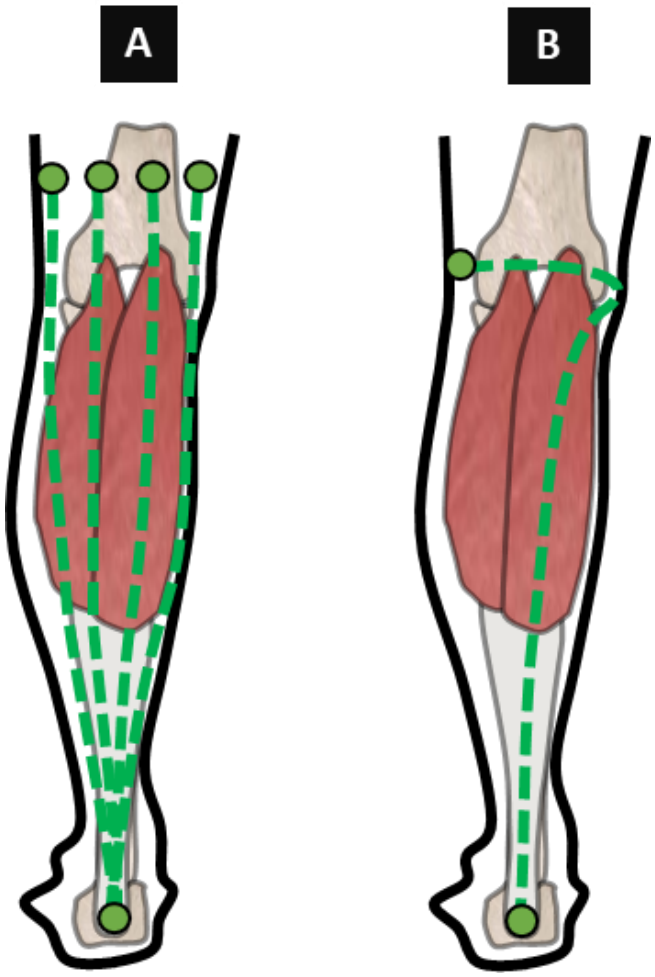


**Figure 11:** A: Green marked pathways of the multiple transverse US scans (i.e., full sweep) from the knee to the calcaneus, starting medially and continuing to the lateral side until the lateral condyle and the entire GM is scanned; B: Green marked pathway of the single sweep starting from the lateral condyle, covering the medial condyle, and proceeding towards the MTJ and the calcaneus. This figure was created by the author of this thesis.

The volume of the GM muscle was assessed by outlining the borders of the GM muscle belly in the transverse planes starting from the origin, which was defined as the plane in which the most superficial landmarks of the lateral and medial condyles were visible, to the MTJ using the Medical Imaging Interaction Toolkit (MITK © German Cancer Research Center) based on 3D reconstructed images of the full sweep (Figure 12) (2). At approximately 2 cm intervals, the boundaries of the GM muscle belly were segmented (2). Next, ITK-SNAP (190) was used to generate a 3D model of the GM muscle by interpolating the space between the segmented cross-sections (see Figure 12B) (2). The calculation of the volume of the GM muscle was performed by adding voxels of the segmented and interpolated 3D GM muscle model (2).

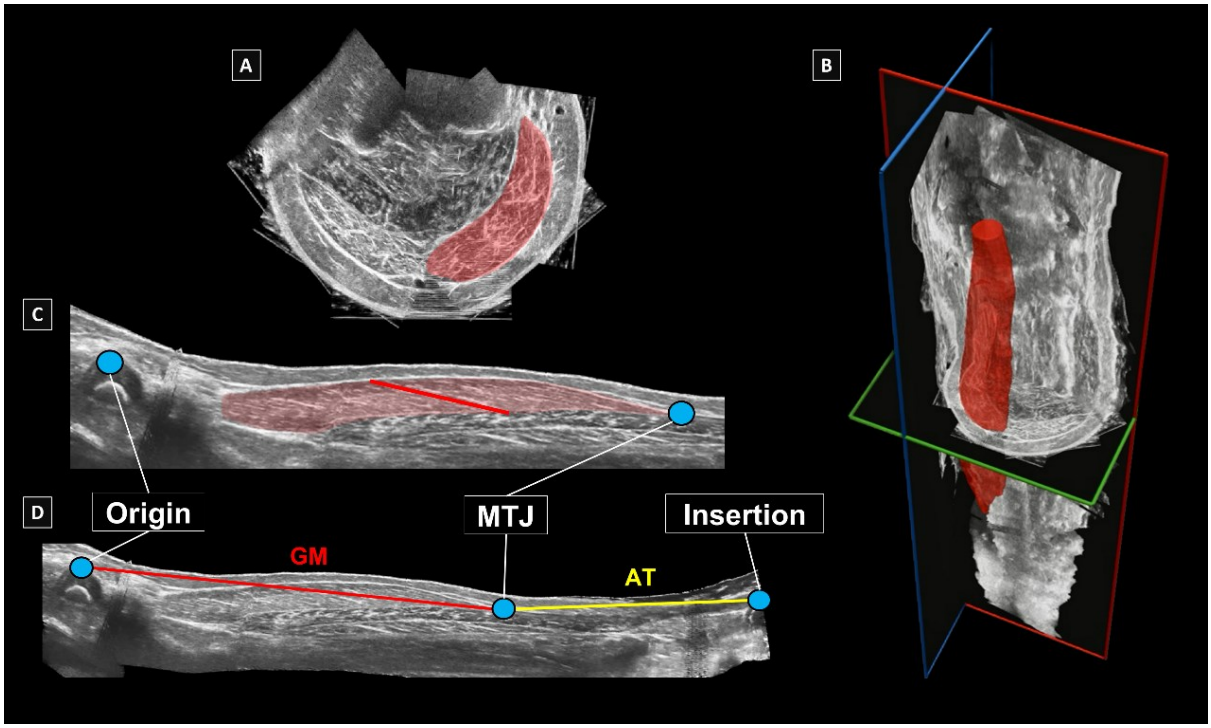


**Figure 12:** Outcomes of the 3DfUS analysis: A) the segmented boundaries of the GM muscle in the transverse plane as displayed in a red mask, B) the reconstructed 3D model of the segmented GM muscle belly (highlighted in red), C) the assessment of the GM fascicle length within the mid-longitudinal muscle plane, and D) the assessment of the length of the GM muscle belly and AT. Figure and adapted caption reproduced from (2) with permission of the publisher (Elsevier).

To examine the individual sweeps, the anatomical landmarks of the origin, MTJ, and insertion were evaluated three times in all three planes using the MITK software (2). The mean of the three determined landmarks were subsequently used for further analysis (2). The architectural and morphological properties of the muscle and tendon were evaluated in the mid-longitudinal muscle plane, which passes through the previous determined origin and MTJ, using a custom analysis routine programmed in MATLAB, which has been described elsewhere in detail (2, 92, 182). By analysing the single sweeps, the length of GM muscle belly, AT, GM MTU, muscle fascicle, and the pennation angle were determined (2). Fascicle length was measured three times for each subject and single sweep at the point that corresponds to two-thirds of the distance from the origin to the MTJ of the GM muscle belly (2), following the method described by Weide et al. (92). For further analysis, the mean of the two lowest deviating fascicle lengths was calculated and used, while the third length was discarded (2).

#### 2.2.3.2.2. Gastrocnemius medialis muscle belly and Achilles tendon lengthening behaviour

The method for calculating the dynamic lengthening behaviour of the GM muscle belly and AT is described in section 2.1 and in the study by Habersack et al (1). Following the 3DfUS measurements, which has been described in the previous chapter, reflective markers were positioned over the origin and insertion of the GM MTU (2). In addition to these markers, a 59-mm linear array US transducer (LogicScan 128; Telemed, Vilnius, Lithuania) was placed on the lower leg and fixed with straps to visualize the most distal muscular part of the GM muscle belly (2). At a sampling frequency of 60 Hz, the US transducer recorded the MTJ shift (2). To determine the dynamic lengthening behaviour of the GM muscle belly, AT and GM MTU, external torque was applied to the footplate to rotate the ankle joint continuously within the sagittal plane from the individual maximum plantar flexion (as shown in Figure 13A) to maximum dorsal flexion (Figure 13B) at slow velocity (~20°/s) (2).

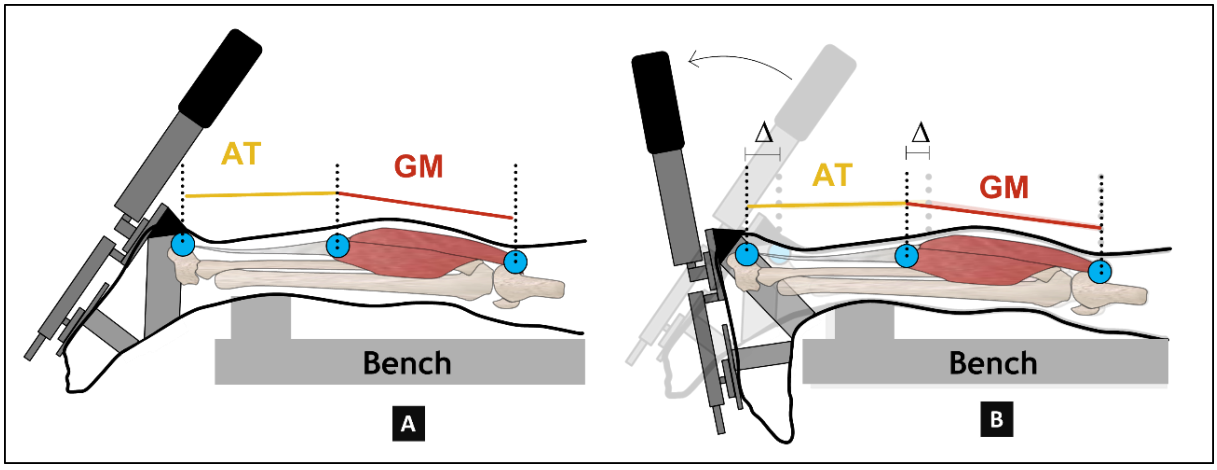


**Figure 13.** Measurement of the dynamic lengthening behaviour of the AT and GM muscle belly during passive ankle movement from maximum plantarflexion (A) to maximum dorsiflexion (B). Figure and adapted caption reproduced with modifications from (2) with permission of the publisher (Elsevier).

During sagittal ankle dorsiflexion rotations, various parameters were measured synchronously, including externally applied torque, US video data, marker positions captured by the 3D motion capture system, and TA and GL EMG activity (2). Two dorsiflexion movements were performed and their mean values have been used for the statistical analysis (2).

In the post-processing phase, the muscle and tendon displacement was determined by manually tracking the movement of the MTJ in the US videos using Tracker software (Tracker, version 4.91) to receive the vertical and horizontal coordinate of the MTJ in the US

video (2, 183). Additionally, the positions of the reflective markers were mathematically corrected to align with the anatomical landmarks in vivo (2), as described in the previous chapter 2.1.5. The length of the muscle belly was calculated as the linear distance between the corrected origin and the MTJ, while the length of the tendon was determined as the distance between the MTJ and the corrected heel marker (2). The MTU length was then calculated by adding the GM muscle and AT lengths (2). The changes in the lengths of the GM muscle belly and the AT were assessed over a standardised torque interval from 0 Nm to 6 Nm (2). All participants were able to reach this torque interval comfortably (2).

### 2.2.4. Statistical analyses

Statistical analyses were conducted by using SPSS (version 26, SPSS Inc., Chicago, Illinois) and the level of significance was set at $\alpha = 0.05$ (2). In a first step, data normality was tested using Q-Q plots, histograms and the Shapiro-Wilk test (2). Group differences were calculated using an independent t-test for normally distributed data or the Mann-Whitney-U-test for non-normally distributed data, respectively (2). In addition, effect sizes (Cohen's d) were also calculated (2), with 0.2 indicating a small effect, 0.5 a medium effect, and 0.8 a large effect (191).

# 3. Results

## 3.1. Study 1: 3D Ultrasound validation and reliability study

**Validity**

Data analysis showed that the proposed 3D US approach systematically yielded shorter tissue lengths compared with MRI (1). Bland-Altman plots (Figure 14) showed mean differences between the methods ranging from -1.42 mm to -5.57 mm (max. error = 1.2%), with the smallest deviation for the length of the muscle belly (≤ − 1.7 mm), followed by the length of AT (≤ − 3.8 mm) (1).

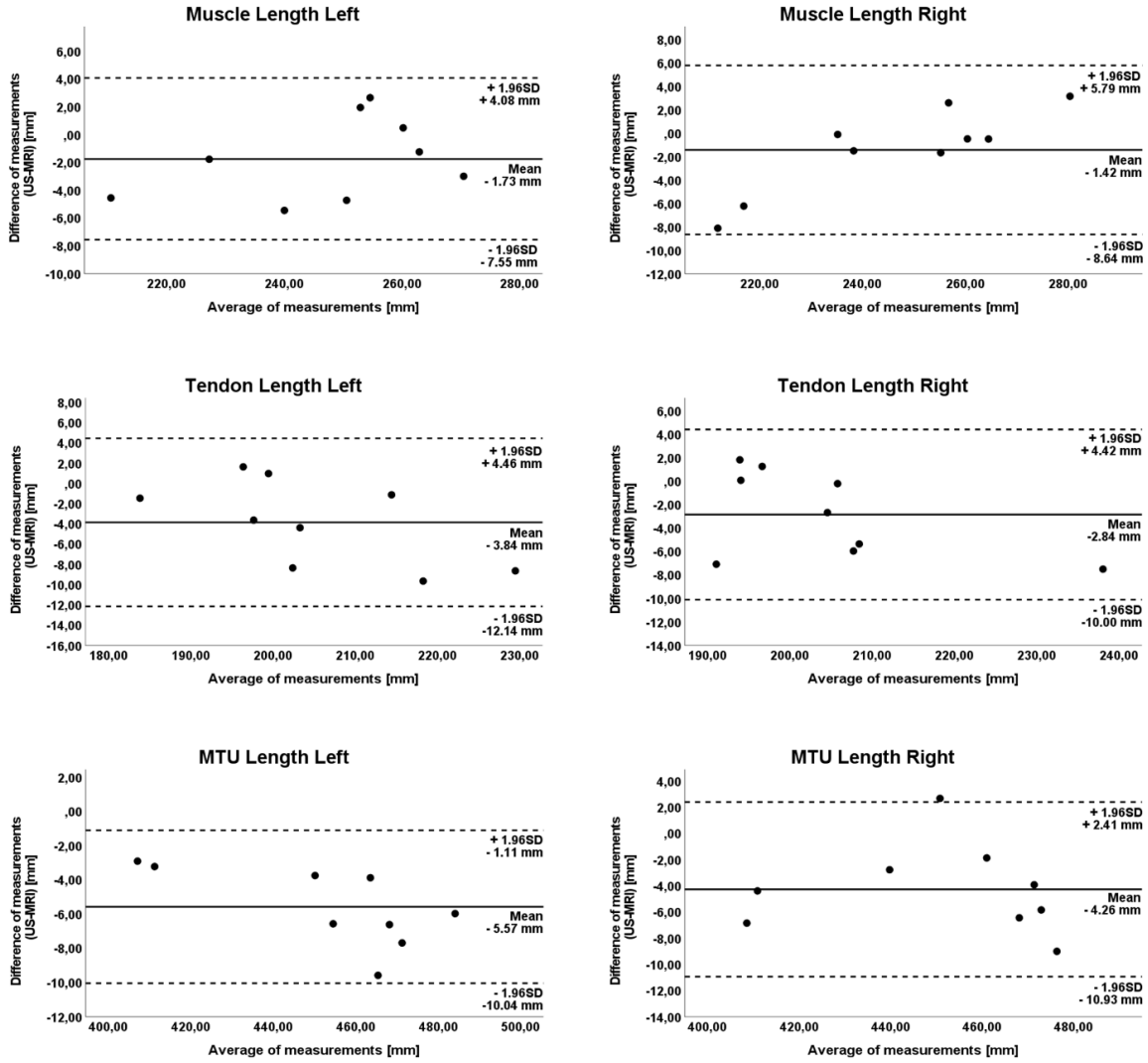


**Figure 14.** Difference of US and MRI assessments of GM MTU length, GM muscle belly length, and AT length. Bland–Altman Plots showing difference of the US and MRI measurements against their mean. SD, standard deviation. Figure and adapted caption reproduced from (1) with permission of the publisher (Springer Nature).

## Reliability

Static length measurements

The mean CVs of the static length assessments using the 3D US approach ranged from 0.1% to 1.6% for muscle belly length, from 0.1% to 1.6% for tendon length, and from 0.02% to 1.0% for MTU length (Table 4) (1).

**Table 4.** Summary of static US assessments showing mean (mm), SD (mm), CV (%) for session 1 and 2 for the left and right leg. Table and adapted caption reproduced from (1) with permission of the publisher (Springer Nature).

| | | Session 1 | | Session 2 | |
|---|---|---|---|---|---|
| **Left side** | | **mean ± SD** | **CV** | **mean ± SD** | **CV** |
| **Muscle belly length** | **Intra-Rater** | | | | |
| | Rater 1 | 244.71 ± 24.45 | 0.12 | 242.18 ± 21.60 | 0.16 |
| | Rater 2 | 246.27 ± 22.22 | 0.12 | 242.34 ± 22.13 | 0.32 |
| | **Inter-Rater** | | | | |
| | Pre | 245.49 ± 23.21 | 1.20 | – | – |
| | Post | – | – | 242.26 ± 21.69 | 1.32 |
| **Tendon length** | **Intra-Rater** | | | | |
| | Rater 1 | 197.34 ± 31.09 | 0.17 | 194.28 ± 30.15 | 0.19 |
| | Rater 2 | 196.98 ± 29.03 | 0.13 | 197.55 ± 30.68 | 0.37 |
| | **Inter-Rater** | | | | |
| | Pre | 197.16 ± 30.00 | 1.18 | – | – |
| | Post | – | – | 195.92 ± 30.35 | 1.58 |
| **MTU length** | **Intra-Rater** | | | | |
| | Rater 1 | 442.05 ± 34.84 | 0.03 | 436.46 ± 34.81 | 0.03 |
| | Rater 2 | 443.24 ± 33.94 | 0.02 | 439.89 ± 33.80 | 0.03 |
| | **Inter-Rater** | | | | |
| | Pre | 442.65 ± 34.34 | 0.49 | – | – |
| | Post | – | – | 438.18 ± 34.24 | 0.71 |
| **Right side** | | | | | |
| **Muscle belly length** | **Intra-Rater** | | | | |
| | Rater 1 | 244.00 ± 23.80 | 0.13 | 240.27 ± 20.62 | 0.18 |
| | Rater 2 | 246.77 ± 21.34 | 0.21 | 243.39 ± 22.30 | 0.15 |
| | **Inter-Rater** | | | | |
| | Pre | 245.39 ± 22.42 | 1.55 | – | – |
| | Post | – | – | 241.83 ± 21.34 | 1.32 |
| **Tendon length** | **Intra-Rater** | | | | |
| | Rater 1 | 195.70 ± 32.77 | 0.20 | 193.26 ± 33.07 | 0.21 |
| | Rater 2 | 194.86 ± 33.92 | 0.25 | 194.81 ± 31.95 | 0.19 |
| | **Inter-Rater** | | | | |
| | Pre | 195.29 ± 33.29 | 1.12 | – | – |
| | Post | – | – | 194.04 ± 32.47 | 1.07 |
| **MTU length** | **Intra-Rater** | | | | |
| | Rater 1 | 439.70 ± 36.61 | 0.02 | 433.53 ± 35.75 | 0.02 |
| | Rater 2 | 441.63 ± 35.76 | 0.02 | 438.20 ± 33.66 | 0.02 |
| | **Inter-Rater** | | | | |
| | Pre | 440.67 ± 36.10 | 0.58 | – | – |
| | Post | – | – | 435.87 ± 34.60 | 1.01 |

Pre, results from session 1; Post, results from session 2.

Excellent intra- and inter-rater reliability was calculated for all tissue lengths and both sides with $ICC_{(2,2)}$ values ≥ 0.97 (Table 5) (1). The values of the SEM ranged from 0.10 mm to 0.63 mm, while the values of the MDC were less than 1.8 mm (1).

**Table 5**. Summary of static US measurements showing intra- and inter-class correlation coefficients ($ICC_{(2,2)}$) and their confidence intervals (95% CI), pooled SD (mm), SEM (mm), and $MDC_{95}$ (mm) for the left and right leg. Table and adapted caption reproduced from (1) with permission of the publisher (Springer Nature).

| | | $ICC_{(2.2)}$ | 95% CI | Pooled SD | SEM | $MDC_{95}$ |
|---|---|---|---|---|---|---|
| **Left side** | | | | | | |
| **Muscle belly length** | **Intra-Rater** | | | | | |
| | Rater 1 | 0.983 | 0.950 – 0.994 | 3.11 | 0.41 | 1.13 |
| | Rater 2 | 0.970 | 0.911 – 0.990 | 3.65 | 0.63 | 1.75 |
| | **Inter-Rater** | | | | | |
| | Pre | 0.987 | 0.963 – 0.995 | 2.88 | 0.33 | 0.91 |
| | Post | 0.984 | 0.953 – 0.995 | 3.06 | 0.39 | 1.07 |
| **Tendon length** | **Intra-Rater** | | | | | |
| | Rater 1 | 0.994 | 0.967 – 0.998 | 3.00 | 0.23 | 0.65 |
| | Rater 2 | 0.996 | 0.988 – 0.999 | 1.95 | 0.12 | 0.34 |
| | **Inter-Rater** | | | | | |
| | Pre | 0.995 | 0.987 – 0.998 | 2.29 | 0.16 | 0.45 |
| | Post | 0.993 | 0.956 – 0.998 | 3.04 | 0.25 | 0.71 |
| **MTU length** | **Intra-Rater** | | | | | |
| | Rater 1 | 0.994 | 0.978 – 0.998 | 2.88 | 0.22 | 0.62 |
| | Rater 2 | 0.994 | 0.983 – 0.998 | 2.85 | 0.22 | 0.61 |
| | **Inter-Rater** | | | | | |
| | Pre | 0.997 | 0.991 – 0.999 | 2.14 | 0.12 | 0.32 |
| | Post | 0.994 | 0.963 – 0.998 | 3.08 | 0.24 | 0.66 |
| **Right side** | | | | | | |
| **Muscle belly length** | **Intra-Rater** | | | | | |
| | Rater 1 | 0.975 | 0.928 – 0.992 | 3.60 | 0.57 | 1.58 |
| | Rater 2 | 0.990 | 0.970 – 0.997 | 2.13 | 0.21 | 0.59 |
| | **Inter-Rater** | | | | | |
| | Pre | 0.981 | 0.941 – 0.994 | 3.74 | 0.52 | 1.43 |
| | Post | 0.982 | 0.929 – 0.995 | 3.15 | 0.42 | 1.17 |
| **Tendon length** | **Intra-Rater** | | | | | |
| | Rater 1 | 0.994 | 0.983 – 0.998 | 2.75 | 0.21 | 0.59 |
| | Rater 2 | 0.996 | 0.988 – 0.999 | 2.16 | 0.14 | 0.38 |
| | **Inter-Rater** | | | | | |
| | Pre | 0.996 | 0.990 – 0.999 | 2.17 | 0.14 | 0.38 |
| | Post | 0.997 | 0.990 – 0.999 | 1.85 | 0.10 | 0.28 |
| **MTU length** | **Intra-Rater** | | | | | |
| | Rater 1 | 0.993 | 0.973 – 0.998 | 3.46 | 0.29 | 0.80 |
| | Rater 2 | 0.996 | 0.988 – 0.999 | 2.25 | 0.14 | 0.40 |
| | **Inter-Rater** | | | | | |
| | Pre | 0.995 | 0.985 – 0.998 | 2.53 | 0.18 | 0.50 |
| | Post | 0.989 | 0.934 – 0.997 | 4.22 | 0.44 | 1.23 |

Pre, results from session 1; Post, results from session 2

Dynamic length measurements

The dynamic length measurements for both raters had mean CV of ≤ 0.9% (1) (Table 6). The inter-rater reliability showed slightly elevated values, with the muscle belly length recording the highest CV of 2.2% (1).

**Table 6.** Summary of dynamic US assessments showing mean values of the common applied torque interval (0 - 5.5 Nm) for absolute length changes (mm) and CV (%) for session 1 and 2. Table and adapted caption reproduced from (1) with permission of the publisher (Springer Nature).

| | | Session 1 | | Session 2 | |
|---|---|---|---|---|---|
| | | **mean ± SD** | **CV** | **mean ± SD** | **CV** |
| **Muscle belly** | **Intra-Rater** | | | | |
| | Rater 1 | 16.91 ± 4.97 | 0.59 | 17.69 ± 5.19 | 0.52 |
| | Rater 2 | 15.53 ± 5.05 | 0.88 | 15.33 ± 6.16 | 0.85 |
| | **Inter-Rater** | | | | |
| | Pre | 16.20 ± 4.97 | 2.24 | – | – |
| | Post | – | – | 16.56 ± 5.69 | 1.74 |
| **Tendon** | **Intra-Rater** | | | | |
| | Rater 1 | 4.06 ± 2.76 | 0.35 | 3.50 ± 2.29 | 0.59 |
| | Rater 2 | 1.90 ± 1.94 | 0.58 | 1.20 ± 1.57 | 0.66 |
| | **Inter-Rater** | | | | |
| | Pre | 2.95 ± 2.58 | 1.82 | – | – |
| | Post | – | – | 2.39 ± 2.27 | 1.38 |
| **MTU** | **Intra-Rater** | | | | |
| | Rater 1 | 20.30 ± 5.51 | 0.24 | 21.20 ± 5.67 | 0.22 |
| | Rater 2 | 16.85 ± 4.36 | 0.29 | 16.53 ± 5.26 | 0.27 |
| | **Inter-Rater** | | | | |
| | Pre | 18.51 ± 5.16 | 1.40 | – | – |
| | Post | – | – | 18.95 ± 5.87 | 1.26 |

Pre, results from session 1; Post, results from session 2

Values for the ICC of ≥ 0.94 demonstrated excellent reliability for both intra- as well as inter-rater assessments of length changes (refer to Table 7) (1). However, the inter-rater comparison resulted in a wider range of CI, while the SEM, ranging from 0.2 to 1.3 mm, was minimal for both intra- and inter-rater reliability (1). For all tissue length changes, the MDC values for intra-rater reliability were less than 1.4 mm (1). The inter-rater comparison revealed that the MDC values were consistently below 3.6 mm (1).

**Table 7.** Summary of dynamic US measurements showing mean values of the common applied torque interval (0 - 5.5 Nm) for intra- and inter-class correlation coefficients ($ICC_{(2,2)}$) and their 95% CI, pooled SD (mm), SEM (mm), $MDC_{95}$ (mm). Table and adapted caption reproduced from (1) with permission of the publisher (Springer Nature).

| | | $ICC_{(2,2)}$ | 95% CI | Pooled SD | SEM | $MDC_{95}$ |
|---|---|---|---|---|---|---|
| **Muscle belly** | **Intra-Rater** | | | | | |
| | Rater 1 | 0.983 | 0.946 – 0.994 | 2.73 | 0.36 | 0.99 |
| | Rater 2 | 0.977 | 0.928 – 0.993 | 3.22 | 0.49 | 1.35 |
| | **Inter-Rater** | | | | | |
| | Pre | 0.938 | 0.448 – 0.985 | 5.17 | 1.29 | 3.57 |
| | Post | 0.958 | 0.430 – 0.990 | 4.01 | 0.82 | 2.28 |
| **Tendon** | **Intra-Rater** | | | | | |
| | Rater 1 | 0.995 | 0.986 – 0.998 | 2.63 | 0.19 | 0.52 |
| | Rater 2 | 0.992 | 0.976 – 0.997 | 2.93 | 0.26 | 0.73 |
| | **Inter-Rater** | | | | | |
| | Pre | 0.988 | 0.964 – 0.996 | 3.73 | 0.41 | 1.13 |
| | Post | 0.994 | 0.981 – 0.998 | 2.75 | 0.21 | 0.59 |
| **MTU** | **Intra-Rater** | | | | | |
| | Rater 1 | 0.990 | 0.970 – 0.997 | 3.83 | 0.38 | 1.06 |
| | Rater 2 | 0.995 | 0.982 – 0.998 | 2.77 | 0.20 | 0.54 |
| | **Inter-Rater** | | | | | |
| | Pre | 0.974 | 0.770 – 0.994 | 6.01 | 0.97 | 2.69 |
| | Post | 0.982 | 0.376 – 0.997 | 5.41 | 0.73 | 2.01 |

Pre, results from session 1; Post, results from session 2

## 3.2. Study 2: Differences in morphological and mechanical properties of the gastrocnemius medialis and Achilles tendon in children with unilateral or bilateral spastic cerebral palsy.

Children and adolescents with bilateral SCP and those with unilateral SCP did not differ significantly ($p \geq 0.05$) in anthropometric characteristics (2). Thus, possible differences in muscle architecture and function cannot be attributed to anthropometric group differences (2). All data sets (15 for unilateral and 18 for bilateral SCP) were included in the analysis of ankle joint function and isometric muscle strength (2). Nevertheless, there were no significant differences ($p \geq 0.38$) between children and adolescents with bilateral SCP and those with unilateral SCP in isometric muscle strength and ankle joint variables (Table 8) (2).

**Table 8.** Isometric muscle strength and ankle joint function in children and adolescents with USCP or BSCP. Negative ankle values in maximum plantarflexion and maximum dorsiflexion correspond to a plantar flexed position. In addition, isometric strength is normalized to body mass. Data are presented as mean (SD). Table and adapted caption reproduced from (2) with permission of the publisher (Elsevier).

| Parameter | USCP | BSCP | Mean difference (%) | p-value | Cohen's d |
|---|---|---|---|---|---|
| Max. DF [°] | −7.86 (11.91) | −6.83 (8.35) | −13.06 | 0.77 | −0.10 |
| Max. PF [°] | −45.49 (4.49) | −44.40 (3.38) | −2.40 | 0.43 | −0.28 |
| RoM [°] | 37.61 (11.43) | 37.57 (8.47) | −0.12 | 0.99 | 0.01 |
| Isometric strength [Nm] | 18.94 (12.62) | 24.24 (20.71) | 28.01 | 0.99 | −0.30 |
| Norm. isometric strength [Nm/kg] | 0.48 (0.27) | 0.59 (0.46) | 24.07 | 0.38 | −0.30 |

Max. DF: maximum dorsiflexion; Max. PF: maximum plantarflexion; RoM: range of motion; Norm: normalized.

Due to technical issues, certain data sets pertaining to the mechano-morphological muscle-tendon properties and the GM muscle architecture were unable to be included and analysed (Supplementary Table 2 & 3) (2). The analysis of the GM muscle architecture and the static lengths of the muscle-tendon morphological properties, including GM muscle length, AT length and MTU length and their respective ratios, was based on 15 datasets for unilateral SCP and 10 for bilateral SCP (2). 15 datasets for unilateral SCP and 14 for bilateral SCP were included to examine the dynamic lengthening behaviour of the GM muscle, AT and MTU (2).

No significant differences ($p \geq 0.25$) were observed in either the mechano-morphological muscle-tendon properties or the GM muscle architecture between the groups (Table 9) (2).

**Table 9.** Morphological muscle-tendon and architectural GM muscle properties in children and adolescents with USCP or BSCP. Muscle volume is normalized to body mass. The lengths of the GM muscle, AT and MTU as well as their respective length changes are normalized to the length of the lower leg, which is measured from the lateral tibial plateau to the lateral malleolus (mm). Data are presented as mean (SD). Table and adapted caption reproduced from (2) with permission of the publisher (Elsevier).

| Parameter | USCP | BSCP | Mean difference (%) | p-value | Cohen's d |
|---|---|---|---|---|---|
| **Muscle-tendon morphological properties** | | | | | |
| GM muscle length [mm] | 189.57 (26.64) | 184.12 (30.96) | −2.87 | 0.64 | 0.19 |
| Norm. GM muscle length | 0.55 (0.06) | 0.54 (0.06) | −1.87 | 0.66 | 0.18 |
| AT tendon length [mm] | 155.72 (32.72) | 162.61 (32.72) | 4.42 | 0.61 | −0.21 |
| Norm. AT tendon length | 0.45 (0.06) | 0.48 (0.06) | 5.78 | 0.29 | −0.45 |
| MTU length [mm] | 345.29 (47.24) | 346.73 (53.81) | 0.42 | 0.94 | −0.03 |
| Norm. MTU length | 1.00 (0.04) | 1.02 (0.05) | 1.90 | 0.31 | −0.43 |
| Ratio GM - MTU length [%] | 55.12 (5.38) | 53.20 (4.83) | −3.47 | 0.35 | 0.37 |
| Ratio AT - MTU length [%] | 44.88 (5.38) | 46.80 (4.83) | 4.27 | 0.35 | −0.37 |
| GM muscle lengthening [mm] | 12.71 (4.28) | 12.93 (5.06) | 1.71 | 0.90 | −0.05 |
| Norm. GM muscle lengthening | 0.04 (0.01) | 0.04 (0.02) | 5.36 | 0.72 | −0.13 |
| AT lengthening [mm] | 6.40 (4.02) | 5.15 (2.57) | −19.47 | 0.38 | 0.38 |
| Norm. AT lengthening | 0.02 (0.02) | 0.01 (0.01) | −27.50 | 0.58 | 0.37 |
| MTU lengthening [mm] | 17.95 (3.98) | 16.77 (5.31) | −6.55 | 0.55 | 0.25 |
| Norm. MTU lengthening | 0.06 (0.02) | 0.05 (0.01) | −14.99 | 0.25 | 0.56 |
| **Muscle architectural properties** | | | | | |
| Fascicle length [mm] | 36.31 (10.50) | 39.28 (10.78) | 8.15 | 0.50 | −0.28 |
| Norm. fascicle length | 0.11 (0.04) | 0.12 (0.02) | 7.41 | 0.59 | −0.23 |
| Muscle thickness [mm] | 11.97 (2.67) | 13.16 (3.47) | 9.95 | 0.34 | −0.40 |
| Norm. muscle thickness | 0.04 (0.01) | 0.04 (0.01) | 10.48 | 0.29 | −0.46 |
| Pennation angle [°] | 18.85 (4.96) | 18.20 (4.26) | −3.41 | 0.74 | 0.14 |
| GM volume [ml] | 66.36 (23.31) | 58.16 (39.39) | −12.35 | 0.34 | 0.25 |
| Norm. GM volume [ml/kg] | 1.73 (0.46) | 1.57 (0.72) | −9.06 | 0.52 | 0.26 |

# 4. Discussion

## 4.1. Study 1: 3D Ultrasound validation and reliability study

To investigate the lengthening behaviour of human MTUs, it is crucial to use examination methods that are easily applicable, valid, and reliable (1). The methods should not be limited by prerequisites and should accurately represent the properties of the tissues without oversimplification. Therefore, a 3D US approach was developed and evaluated for its validity in comparison to MRI for assessing the GM muscle belly, AT, and GM MTU length, as well as for the reliability of static and dynamic length measurements (1).

The results demonstrated that the proposed approach had good accuracy (with a mean error of approximately 1.1%) and excellent intra- and inter-rater reliability (1). A comparative analysis with MRI showed a slight underestimation of static lengths by approximately 0.7%, 1.5%, and 1.1% for the muscle belly, AT, and MTU lengths, respectively (1). Excellent intra- and inter-rater reliability was also found with high ICC (≥ 0.94), low SEM (≤ 1.3 mm), and good $MDC_{95}$ (≤ 3.6 mm), especially for the lengths assessed in a static condition (e.g., SEM ≤ 0.6 mm; $MDC_{95}$ ≤ 1.8 mm) (1).

### 4.1.1. Validity

This study presents a novel US approach for measuring the total GM MTU length, including separate evaluations of tendon and muscle belly lengths (1). Prior research has evaluated the reliability of 2D US approaches, but only a minority of studies have compared the validity with a gold standard such as MRI (86, 91) or cadaver measurements (75). Validity was reported for either muscle belly (91) or tendon length (75, 86). For example, Barber et al. (91) found a high level of validity using the 3DfUS approach, although the estimated length of the GM muscle belly was slightly underestimated by 1.3 ± 2.2%, i.e., 3.0 ± 5.4 mm (1). Barfod et al. (86) showed a satisfactory correlation between MRI and their novel US measurement with an underestimation of the AT length by 4 mm (1). In two separate studies, Silbernagel et al. found a high validity of a hybrid motion capture–US method (27) (error of less than 1%) and of EFOV imaging (75) (ICC = 0.895), when compared to anthropometric measurements on cadavers or a lamb shank, respectively (1). In both studies, the AT lengths determined with the respective US method were shorter than those detected via the gold standard (1, 27, 75).

Consistent with previous studies, the proposed 3D US approach resulted in an underestimation of GM muscle belly and AT lengths, albeit only by approximately 1.6 mm (0.7%) and 3.3 mm (1.5%), respectively (results including both legs and raters) (1). Therefore, the proposed 3D US approach exhibits less deviation compared to MRI in relation to previous studies (1). Due

to the underestimated muscle belly and tendon lengths, MTU length was shorter by 4.9 mm (1.1%) when assessed with the 3D US approach (1). The differences observed in tissue lengths as assessed by US and MRI may be attributed to imaging difficulties of crucial anatomical landmarks with B-mode US (1). These sites include the most superficial point of the medial femoral condyle, the MTJ, and the proximal tendon insertion (1). The anatomical sites can be easily identified during post-processing of the MRI images in all three spatial planes (1). However, factors such as handling of the US probe, probe positioning, and pressure applied during the imaging procedure may directly affect the determination and visibility of anatomical landmarks in the US images (1). In particular, when it comes to tendons, loss of contact and anisotropy may also play a significant role (58). Therefore, the use of a gel pad for detecting AT insertion is recommended in addition to the 3D US approach for future assessments (1).

### 4.1.2. Reliability

#### 4.1.2.1. Static length assessments

To assess the length of the AT and GM muscle belly under static conditions, several reliable US methods are available (1). For instance, Silbernagel et al. (27) used a combination of B-mode US and motion capture techniques to evaluate the length of the AT (1). They reported excellent test-retest reliability for their method with an ICC of 0.97, SEM of 4 mm, and MDC of 11 mm (1). Cenni et al. (3, 89) found comparable results when examining the within-session reliability of an US pointer method (US-PaP) and their previously evaluated 3DfUS method (1). The ICC values for determining AT length using the US-PaP method were > 0.97, with SEM ≤ 3.3 mm, and MDC ≤ 9.4 mm after performing two analyses (3). The 3DfUS approach also showed similar reliability (3, 89). For the measurement of GM muscle belly length, both the US-PaP method and the 3DfUS approach produced similar results with an ICC of 0.98, SEM of no more than 3.6 mm, and MDC of no more than 10.0 mm (3, 89). The reliability of the measurement of GM MTU length was slightly better, with an ICC of 0.99, SEM of no more than 2.5 mm, and MDC of no more than 6.0 mm (3, 89).

Compared to previous studies, the proposed 3D US approach demonstrated superior reliability for static length assessments (1). The CVs were ≤ 1.2%, the SEM was ≤ 0.6 mm, and the MDC values were ≤ 1.8 mm for intra- and inter-rater reliability of AT and GM muscle belly lengths (1). Values for the ICC (≥ 0.975) were also excellent (1). Moreover, the length assessment of the GM MTU was even more reliable, with CV ≤ 0.7%, SEM ≤ 0.3 mm, MDC ≤ 0.8 mm, and ICC ≥ 0.993 (1). Comparable reliability outcomes have only been documented for assessing the AT, either utilizing the 3DfUS (90) or the Copenhagen AT length

measure (83). From a clinical perspective, this MDC values of the 3D US approach suggest that changes of approximately 2 mm are required for changes in length to be considered as real changes due to treatments (1, 187). This outcome is significant for investigating training effects and therapeutic treatments on the MTU (1). Furthermore, the proposed 3D US approach has the potential to identify muscle and tendon changes associated with specific disorders or diseases, such as CP (1).

Other measurement approaches, such as those combining US and tape measurements (25, 81, 86) or US and skin markings (72), have also mostly reported excellent intra- and/or inter-rater reliability (1). However, their results are slightly less reliable than those presented for the proposed 3D US approach or 3DfUS (1). Brouwer et al. (72) examined the reliability of the methodology outlined by Barfod et al. (86) in comparison to AT length assessments conducted with EFOV measurements (1). The study found that the US tape measure approach had better intra- and inter-rater reliability compared to EFOV (1, 72). Additionally, Ryan et al. (74) evaluated the test-retest reliability of the measurement of the AT length by using panoramic US (1). Although they reported an excellent ICC value of 0.954, the SEM of 4.4 mm and MDC of 12.3 mm were relatively high compared to other study results reported above (1). Conversely, Silbernagel et al. (75) demonstrated high test-retest reliability for tendon length assessments using EFOV imaging following the protocol of Ryan et al. (74). They reported an SEM of 0.7 mm, ICC of 0.944 (95% CI: 0.852 – 0.979), and MDC of 1.83 mm (1). Ryan et al. (74) concluded that the panoramic US tendon length assessment reliably detects length changes as observed in various clinical settings (1). However, their reliability results suggest that experience with EFOV/panoramic US needs to be gained (1). Therefore, a potential explanation for the discrepancies between the two studies could be the difference in sonographer experience (1). However, the first study (Ryan et al. (74)) did not report the years of experience of the sonographer, while the second study (Silbernagel et al. (75)) used a sonographer with 3 years of experience. Therefore, it is recommended to use a simple and straightforward length assessment method, such as the one presented in this thesis (1).

#### 4.1.2.2. Dynamic lengthening assessments

While several 2D US approaches mentioned earlier appear reliable for assessing muscle-tendon tissue lengths at rest or in specific static positions, they may not be the best option for evaluating tissue behaviour during dynamic tasks (e.g., 3DfUS and EFOV imaging) (1). Since mechanical tissue behaviour can be affected by length adaptations or interventions, it is also essential to assess tissue lengthening behaviour (1). Previous studies have used a

combination of 2D B-mode US and 3D motion capture to assess muscle and tendon length changes during training (88) as well as clinical studies (192), however, the reliability of these approaches in measuring lengthening behaviour or length changes has rarely been investigated (1). Nakamura et al. (193) investigated the test-retest reliability of the displacement of GM MTJ within a range of 0° to 30° ankle dorsiflexion and demonstrated high reliability using their combined approach (ICC = 0.985, pre-post difference = 0.83%). However, it must be noted that that the MTJ location was determined solely in 2D (1). Further, other studies have rather focused on active conditions (194) or static lengths (88, 192), but did not provide reliability measures specifically for muscle-tendon tissue displacement during passive conditions (1). The proposed 3D US approach demonstrated high intra-rater reliability in assessing the length changes of the whole MTU and its components, including the GM muscle belly and AT (1). Hence, the 3D US approach can be reliably and effectively utilized by a single rater in training or clinical studies to accurately assess length changes, thereby providing a basis for subsequent stiffness calculations (1). Furthermore, excellent inter-rater reliability was found for the AT and also for MTU length changes with CV values ≤ 1.8%, SEM ≤ 1.0 mm, and MDC ≤ 2.7 mm (1). Reliability values for changes in GM muscle belly length were slightly decreased, with a CV of ≤ 2.2%, SEM of ≤ 1.3 mm, and MDC of ≤ 3.6 mm (1). Variations in CI values were more pronounced for MTU and muscle belly length changes (1). This variability could be attributed to discrepancies among investigators in the handling of the measuring devices, potentially influenced by variations in anthropometric factors such as body height and hand size, which might have impacted the results (1). The taller person with larger hands might have had a more stable positioning in front of the examination table, therefore, an advantage to adequately move the inclino-dynamometer steadily guiding the foot sole into greater dorsiflexion within the sagittal plane. However, the shorter person with smaller hands may have unknowingly experienced difficulties in moving the joint, therefore, addressing the GM muscle belly differently. However, also other factors (e.g., movement velocity) should be considered. Further research is therefore required.

The present study has some limitations. The position of subjects in supine or prone positions could have affected passive forces exerted on the GM muscle belly, despite maintaining the same configuration of the joint (91), and thus influenced the results (1). Nevertheless, given the minimal disparities noted between the 3D US approach and MRI in this investigation, both factors might be negligible (1). Additionally, it is important to note that the assessment of the approach was solely conducted for the GM MTU (1). Validation for other muscles of the lower leg and/or different muscle groups could be explored in subsequent studies (1). Nonetheless, the findings demonstrate the potential of the 3D US concept (1).

## 4.2. Study 2: Differences in morphological and mechanical properties of the gastrocnemius medialis and Achilles tendon in children with unilateral or bilateral spastic cerebral palsy

This study is the first to have a comprehensive collection of information on the function of the ankle joint, isometric muscle strength, and morphological muscle-tendon properties in children with unilateral SCP and compare it with children with bilateral SCP (2). Despite indications of possible deviations between groups at the muscle-tendon level due to skeletal and functional impairments, no significant differences were found in any of the parameters studied (2).

Individuals with unilateral SCP present a different aetiology compared to those affected bilaterally, resulting in deviant pathogenesis and differing symptoms between the two groups (2). In summary, individuals with unilateral CP typically experience mild functional impairments without cognitive impairments or comorbidities (107, 109). On the other hand, bilaterally affected individuals have a higher risk of mobility loss with aging compared to their unilaterally affected peers (142). Furthermore, differences in lower limb strength, walking patterns, and foot abnormalities between the groups are likely to result in variations in the utilization and impact on the movement-generating MTUs of their lower limbs (2). Alterations in MTU ratios can hinder the efficient transmission of force, resulting in difficulties in generating force for activities such as standing up from a seated position, walking, or climbing stairs (2). For example, research by Schranz et al. (195) demonstrated a correlation between ankle power during gait and the morphology of both the GM muscle belly and the AT (2). Consequently, alterations in MTU length and ratios can result in various abnormal gait patterns (2). It is crucial to comprehend these implications to customize interventions that meet the distinct needs of people with CP (2). Considering the finding of decreased growth rate of GM muscle in young children with unilateral CP (167), the study in this thesis aimed to identify differences in muscle strength, ankle joint function, and muscle-tendon properties between children with unilateral or bilateral SCP (2). However, the results of this study do not support this hypothesis as no significant differences were found in any of the investigated parameters between groups of unilateral or bilateral CP (2). Moreover, the results contradict the assumption that lower growth rates of the GM muscle in children with unilateral CP, when compared with those with bilateral CP, would result in reduced calf muscle size (167) in older children (2). In contrast to the study by Barber et al. (167), which examined the volume of the calf muscle in relatively young children (mean age 5.5 ± 1.5 years for unilaterally affected and 5.3 ± 1.6 years for bilaterally affected children), the participants in the current study were older,

ranging from approximately 8 to 13 years (mean age 10.2 ± 2.4 years for unilaterally affected and 10.8 ± 2.5 years for bilaterally affected children) (2). As both studies only considered chronological age and not biological age, it is possible that the study populations were in different stages of development and growth (2). These different stages of growth may have influenced the group differences observed in the current study (2). Furthermore, it is important to consider that the proposed study exclusively included individuals with SCP, while the study by Barber et al. (167) did not specify the type of CP in their participants (2). Additionally, variations in treatment history among participants could have influenced the results (2). Finally, it is important to note that both studies used a cross-sectional design, which limits their ability to provide insights into longitudinal growth-related developments between individuals with unilateral or bilateral CP (2).

The study found no significant differences in GM MTU, muscle belly, and AT properties, as well as plantar flexor muscle strength between children with bilateral SCP and those with unilateral SCP (2). This lack of difference is likely due to the high level of functionality exhibited by all participants included in the study, as they were all ambulatory (2). Children with unilateral CP appear to be more physically active than their bilaterally affected peers (196, 197), although they may compensate for deficits in muscle activation by relying more on the unaffected limb (2, 167, 198, 199). Consequently, the increased physical activity might provide a similar stimulus to the affected leg as experienced by children with bilateral CP, who equally load both affected legs (2). However, this hypothesis lacks substantial evidence to support it (2).

It is important to consider age and gender factors when assessing physical activity in people with unilateral SPC (2). Studies have shown that younger children and males tend to display higher levels of physical activity compared to females and adolescents (2, 196, 200–203). Moreover, the activity level of individuals with CP typically declines, and symptoms may worsen, with this decline potentially being more pronounced in bilaterally affected individuals (2, 142). Therefore, it is possible that differences in joint function, muscle strength, and muscle-tendon pathology between the groups may be more noticeable in adolescents and young adults than in children (2). The results of the study suggest that pre-pubertal groups may experience similar loading stimuli on their muscles and tendons, even if there is varying muscle growth (2). It is recommended to analyse gait kinetics, kinematics, and joint contact forces to investigate the loading stimuli during gait in both groups (2). Although the study found no significant differences between children with bilateral or unilateral SCP in terms of muscle-tendon properties and lengthening behaviour of the GM MTU and its components, it is important to note that the small sample size may have limited the statistical power to detect subtle differences (2). For instance, the results suggest a possible decrease in the normalised

length of the GM MTU (-2%, Cohen's d = -0.43) in children with unilateral SCP (2). Additionally, there was an increased thickness of GM muscle (+10.5%, d = 0.46), greater normalised MTU lengthening (+15%, d = 0.56), and higher normalised muscle volume (+9.1%, d = 0.26) (2). Therefore, further studies with larger sample sizes are necessary to investigate potential differences in muscle-tendon properties between individuals with unilateral or bilateral SCP (2). Longitudinal studies, which take into account biological age, are also crucial for a comprehensive understanding of these differences, even though assessing biological age in children with CP may be challenging (2).

## 4.3. Strengths and weaknesses of the thesis

The results of the validation and reliability study (study 1) indicate that the US approach can accurately and reliably assess the lengths and lengthening behaviour of the GM MTU, GM muscle belly, and AT (1). Previous studies have frequently used the cadaveric regression model proposed by Grieve et al. (204) to determine the length changes of the MTU during passive measurements (183, 205, 206). This model allows for the calculation of the MTU length change based on the ankle joint angle (183, 205, 206). When combined with US data on muscle length change, this method allows for the estimation of the AT length change (183). It is important to note that the equation used in this model was derived from measurements taken from eight cadavers who passed away before the age of 60 (204). It is widely acknowledged that both the aging process (207, 208) and SCP (153, 189) can significantly alter the properties of muscle and tendon tissues. This raises the question of whether this model is still appropriate for estimating MTU length changes in children, particularly those with SCP. Therefore, the first study (1) presented in this thesis introduced a new 3D US approach to measure length changes directly. The tissue length values obtained from this approach can be used as an accurate estimation of the true muscle belly and tendon lengths. This is considered as a strength of the approach due to the excellent validity and reliability results. The validity check revealed that the approach slightly underestimated the static tissue lengths when compared to MRI (1). The cause of this underestimation is unclear, as it is likely due to a combination of factors rather than a single measure or action. For instance, the localization of landmarks using US and the manual placement of markers on the skin may introduce some inaccuracy. Ultrasound provides a cross-sectional image, while MRI can precisely determine localization in all three spatial directions. Magnetic resonance imaging is better than US at visualising cartilage, which may affect the localization of the origin and insertion. However, it should be noted that the 1% underestimation corresponds to approximately 1-2 mm of the entire muscle

or tendon length, which might be not clinically relevant and is still highly accurate for a low-cost alternative to MRI.

Another advantage of this measurement methodology is its versatility. It can be used to determine both the static lengths of the GM MTU and its components at specific foot angles, as well as the lengthening behaviour throughout the entire RoM of the ankle joint. Both static and dynamic measurements can be performed using the same measurement method and equipment, which is advantageous compared to 3DfUS and EFOV imaging. Additionally, by synchronously recording the applied torque to the footplate, an estimation of the stiffness of the individual tissue types (e.g., entire MTU, muscle belly, and tendon) can be made.

Another advantage of this approach is that the foot does not need to be positioned in a specific way, and there are no specific requirements for the placement of the US device. The anatomical points in vivo can be calculated mathematically, regardless of the location of the foot. One important advantage is that the lengths are calculated in three dimensions, allowing for the measurement of real lengths rather than just the projection of tissue lengths onto the skin, as it is the case with tape measurements.

Moreover, the presented approach only requires a short training and practice period. Unlike 3DfUS and EFOV, where the skills and experience of the examiner are crucial, long-term experience does not seem to play a significant role in this approach. There are no special considerations to be made during the measurement, such as uniform pressure, as it is the case with 3DfUS. Therefore, this measurement method is applicable following a short training period.

Furthermore, only a short time is required to measure tissue lengths. Subject preparation is the most time-consuming aspect, taking only a few minutes, which includes locating the origin, MTJ, and insertion points, placing markers, and positioning the US probe. The recording itself only takes a few milliseconds under static conditions. Therefore, this method is particularly suitable for individuals who may have difficulty remaining still due to age or disability. However, this method has the disadvantage of not providing real-time results and requiring post-processing of the data. Nonetheless, with the installation of a simple and user-friendly data processing routine and an associated interface, this can be completed in just a few minutes. The delayed receipt of information about the outcome parameters makes this approach less suitable for daily clinical use. Furthermore, clinics often do not have the necessary 3D motion analysis system due to its high cost. As a result, this measurement methodology is primarily suitable for biomechanical laboratories and studies that require precise and dependable length data.

Moreover, a limitation of this approach is that it only allows for investigating the passive lengthening behaviour of the GM MTU and its components (1). Furthermore, the measurement methodology cannot be directly applied to other muscle groups or extremities. To adapt this approach for the use with other muscle groups or extremities, it is important to detect the origin and insertion of the respective MTU using US. Therefore, this approach can be easily adapted for superficial muscles such as the GL. The origin and insertion of the muscle are easily visible by US, and markers can be placed over the defined anatomical landmarks. However, for deeper muscles such as the soleus, defining the origin reliably is more challenging due to its wide-ranging shape. Furthermore, it is recommended to adapt the mathematical calculations for other muscle groups and follow the same procedures as described above. If any alterations are made to the placement of markers or mathematical calculations, it is crucial to carry out new tests regarding reliability and validity.

Furthermore, the proposed methodology is currently not adjusted to accurately quantify the dynamic expansions of the GM MTU during activities such as walking or jumping. This is because these movements do not only involve flexing and extending the ankle joint, but the knee joints also undergo a degree of flexion and extension during walking, which introduces a higher level of complexity. As a result, marker placement and calculation methods must be modified accordingly. During the development of this application, it is important to consider various factors and difficulties that may arise. For example, marker shifts caused by skin movement, particularly in the knee joint, must be taken into account. Additionally, the influence of gravity and inertia due to mass and movement should not be overlooked. It is worth noting that the size of the resulting error will depend on the direction of the shift if slipping occurs. When the US transducer is moved distally, it might have little effect on the calculation of tissue length. This is because the MTJ is only moving in the US video and is being tracked frame by frame. However, moving the transducer in a medial-lateral direction has a greater effect as it alters the plane in which the MTJ is defined. To mitigate this issue, it is essential to use a custom-made probe holder and fixation with straps and tapes. However, it may not be possible to completely eradicate this issue, especially when increasing the cadence.

In addition to the proposed 3D US approach, tissue length changes can also be computed by musculoskeletal simulations, for example OpenSim, a widely recognized biomechanical modelling software (209, 210). While both the 3D US approach and musculoskeletal simulations offer valuable insights into MTU length dynamics, each method possesses its own set of advantages, limitations, and potential biases. Musculoskeletal simulations provide a platform for biomechanical modelling, allowing for intricate simulations and analysis, especially during gait and movement (211). Its widespread usage within the biomechanics community

speaks to its versatility and standardized approach, allowing for comparison of results across various studies (209). Moreover, the user-friendly interface and extensive library of musculoskeletal models make it accessible to researchers with diverse backgrounds and expertise levels. However, with regard to MTU length assessments, the reliance on generalized muscle properties and assumptions derived from cadaveric studies or literature data may result inaccuracies when applied to individualized anatomical variations or specific conditions, such as CP, potentially leading to inaccuracies in simulated MTU behaviour (209). Another challenge with OpenSim lies in validating its simulations against in vivo data, which can be complex due to the limitations of available measurement techniques (209). In contrast, the 3D US approach proposed in this thesis offers a more direct and patient-specific approach, thereby capturing muscle and tendon behaviour with high accuracy (1). However, this method may be limited by factors such as image resolution and operator variability, which might impact the accuracy and reliability of the measurements (1). Furthermore, the proposed 3D US approach is not yet adapted for dynamic length measurements during gait (1). Therefore, it is essential to have a comprehensive understanding of the strengths, weaknesses, and applicability of each approach in order to interpret and contextualise the study results.

In summary, the study concludes that the proposed 3D US approach is a reliable and valid method for assessing the length and lengthening behaviour of the GM MTU, muscle belly, and AT under both static and dynamic conditions. The assessment of MTU plasticity is crucial in understanding the effects of (neuro-)muscular diseases or disorders, whereby measuring individual muscle belly and tendon length is a helpful technique.

In the second study of this thesis, the 3D US approach was employed to investigate the morphological and mechanical properties of the plantar flexor MTU in children with SCP. Although the study employs a broad measurement methodology to accurately and reliably measure morphologic muscle properties, it does not take into account all biomechanical parameters (2). To further elucidate the morphological properties of the plantar flexor MTU, future studies could incorporate additional biomechanical parameters such as muscle stiffness (2). In the current study, the muscle stiffness can only be estimated by combining the lengthening behaviour and the applied torque to the ankle joint (2). However, promising techniques such as shear wave elastography or tensiomyography offer a non-invasive assessment of muscle stiffness (212, 213). By measuring the speed of shear waves propagating through the muscle tissue, shear wave elastography offers insights into muscle quality and function in SCP (212, 214).

In interpreting the findings of this study, it is essential to consider the limitations of a focused examination solely on the GM MTU and ankle joint (2). While these components represent significant contributors to lower limb function, they represent only a fraction of the intricate musculoskeletal system involved in movement (2). Therefore, to gain a more comprehensive understanding of the biomechanical adaptations in individuals with CP, future studies should adopt a broader approach (2). The incorporation of additional muscles into the analysis such as the TA, soleus, GL, and hamstrings would provide a more nuanced perspective on the complexities of motor function in CP (2). By additionally investigating possible adaptations of these muscles, the holistic nature of musculoskeletal adaptations and their implications for functional outcomes in SCP can be better evaluated (2).

The absence of data on the physical activity levels of children with USCP or BSCP is a notable gap in the methodology, which could have provided valuable context for interpreting the results (2). Physical activity plays a pivotal role in the shaping of musculoskeletal adaptation, influencing muscle-tendon properties, and ultimately impacting functional outcomes (2, 196, 197). By integrating assessments of physical activity, future research can elucidate the relationship between activity levels and musculoskeletal properties in individuals with USCP or BSCP (2).

Furthermore, the sample size of the study may have constrained its ability to detect subtle differences between groups, thereby limiting the generalisability of the findings (2). A larger cohort would offer a more robust foundation for drawing meaningful conclusions and informing clinical practice effectively (2).

Notwithstanding these constraints, the findings of the proposed study represent a significant advance in the understanding of the complexities of musculoskeletal adaptations in USCP and BSCP (2). Building upon the findings of this study, future studies can pursue on more comprehensive research questions aimed at investigating the intricate mechanisms underlying musculoskeletal adaptation in USCP and BSCP (2).

## 4.4. Future directions

Shear wave elastography is a promising US-based technique that offers the potential for quantitative, in vivo measurement of tissue material properties (213). This modality may find widespread application in clinical settings and has already been used to evaluate stiffness in various muscles, such as the gastrocnemius, TA, and hamstrings (215). Researchers have used this technique to investigate muscle stiffness in children with CP, revealing increased stiffness compared to their TD peers (216). Shear wave elastography could be a useful tool for

evaluating the biomechanical properties of muscles and tendons in children with CP, particularly when assessing the impact of new interventions.

To gain a comprehensive understanding of all levels of the ICF (217), it is necessary to extend the investigations by including assessments of active tissue dynamics. The study in this thesis only included the passive dynamic lengthening behaviour of the GM MTU using the 3D US approach, as previously mentioned. In children with CP, a disruption in the interaction of muscle and tendon length changes during walking may limit the effective generation and transfer of force to the joints required for movement due to the neurological control of the muscle being affected. Therefore, future studies should investigate whether individuals with unilateral or bilateral SCP differ in terms of active length changes during walking.

An additional aspect that should be investigated in future studies is the use of clinical 3D gait analysis, which is a well-established method to describe and analyse the gait pattern from a kinematic (joint angles) and kinetic (joint moments) point of view, which further serves as an input data for musculoskeletal simulations. These simulations can be used to improve the understanding of the biomechanical pathomechanisms associated with CP and to estimate internal joint forces and cartilage loading, which cannot yet be measured non-invasively (218, 219). The second study in this thesis showed that there are no differences at the muscle-tendon level between individuals with unilateral or bilateral SCP, but there are functional deviations found in previous studies (2, 107, 109, 139–147). These deviations may affect the loading and joint forces during gait, which can have an impact on the tibiofemoral and patellofemoral joint contact forces, potentially leading to degenerative joint wear.

In addition to the musculoskeletal differences between unilaterally affected and bilaterally affected individuals, there may be differences in cardiovascular parameters and metabolic factors that may limit the activity levels and also affect muscle growth. In addition, exercise limitations and altered muscle metabolism may cause differences in metabolic factors such as energy expenditure and nutrient supply. These factors may affect musculoskeletal function and muscle growth. Further research is needed to investigate these potential differences and to better understand their influence on the health and well-being of individuals with CP.

## 4.5. Conclusion

The 3D US approach proposed in this study demonstrated excellent validity in assessing the GM MTU, muscle belly, and AT length separately (1). Although it slightly underestimated tissue lengths compared to MRI, the difference between the two methods was minimal (≤ 1.5%) (1). Additionally, the US approach showed high reliability in assessing tissue lengths and

lengthening behaviour under both static and dynamic conditions (1). The results of the study suggest that the presented 3D US approach can be used to assess the effects of treatments or short and long-term training interventions (1).

Therefore, this approach was used in combination with other methodological approaches to firstly investigate potential differences in isometric muscle strength, mechano-morphological properties of the GM MTU, and ankle joint function in children with bilateral SCP compared to those with unilateral SCP (2). The results of the study revealed no significant differences in any outcome measures between the two groups (2). Based on this finding, it seems that study designs and treatment approaches for muscle-tendon pathology do not need to be modified based on the subtype of CP involvement (2). However, future studies should include kinematic and kinetic gait parameters and investigate associated tissue and joint dynamics, such as MTU elongation during gait and muscle forces, in order to gain a full understanding and draw valid conclusions (2).

# 5. References

1. Habersack A, Zussner T, Thaller S, Tilp M, Svehlik M, Kruse A. Validity and reliability of a novel 3D ultrasound approach to assess static lengths and the lengthening behavior of the gastrocnemius medialis muscle and the Achilles tendon in vivo. Knee Surg Sports Traumatol Arthrosc 2022; 30(12):4203–13. Available from: URL: https://link.springer.com/article/10.1007/s00167-022-07076-2.

2. Habersack A, Svehlik M, Guggenberger B, Tilp M, Kruse A. Gastrocnemius medialis and Achilles tendon properties do not differ between children with unilateral or bilateral spastic cerebral palsy. J Biomech 2024; 166:112041. Available from: URL: https://www.sciencedirect.com/science/article/pii/S0021929024001180.

3. Cenni F, Schless S-H, Bar-On L, Molenaers G, van Campenhout A, Aertbeliën E et al. Can in Vivo Medial Gastrocnemius Muscle-Tendon Unit Lengths be Reliably Estimated by Two Ultrasonography Methods? A Within-Session Analysis. Ultrasound Med Biol 2018; 44(1):110–8.

4. Avancini C, Oliveira LF de, Menegaldo LL, Vieira TM. Variations in the spatial distribution of the amplitude of surface electromyograms are unlikely explained by changes in the length of medial gastrocnemius fibres with knee joint angle. PLoS One 2015; 10(5):e0126888.

5. Bressel E, McNair PJ. Biomechanical behavior of the plantar flexor muscle-tendon unit after an Achilles tendon rupture. Am J Sports Med 2001; 29(3):321–6.

6. Schmidt RF, Lang F, Heckmann M. Physiologie des Menschen: Mit Pathophysiologie: mit herausnehmbaren Repetitorium. 31., überarb. und aktualisierte Aufl. Heidelberg: Springer Medizin; 2010. (Springer-Lehrbuch).

7. Trovato F, Imbesi R, Conway N, Castrogiovanni P. Morphological and Functional Aspects of Human Skeletal Muscle. JFMK 2016; 1(3):289–302. Available from: URL: https://www.mdpi.com/2411-5142/1/3/289.

8. Howard JJ, Herzog W. Skeletal Muscle in Cerebral Palsy: From Belly to Myofibril. Front Neurol 2021; 12:620852.

9. Moreau NG, Simpson KN, Teefey SA, Damiano DL. Muscle Architecture Predicts Maximum Strength and Is Related to Activity Levels in Cerebral Palsy. Phys Ther 2010; 90(11):1619–30.

10. Lieber RL, Smith LR. 6 - Skeletal muscle changes due to cerebral palsy. In: Shepherd RB, editor. Cerebral Palsy in Infancy : Targeted activity to optimize early growth and development.

Oxford: Churchill Livingstone; 2014. p. 135–55 Available from: URL: https://www.sciencedirect.com/science/article/pii/B9780702050992000066.

11. Handsfield GG, Williams S, Khuu S, Lichtwark G, Stott NS. Muscle architecture, growth, and biological Remodelling in cerebral palsy: a narrative review. BMC Musculoskelet Disord 2022; 23(1):233. Available from: URL: https://www.ncbi.nlm.nih.gov/pmc/articles/PMC8908685/.

12. Engelhardt S, Menche N, editors. Biologie, Anatomie, Physiologie: Kompaktes Lehrbuch für Pflegeberufe. 6., überarb. Aufl., [Nachdr.]. München: Elsevier, Urban & Fischer; 2010. (Pflege heute).

13. Gadeberg P, Andersen H, Jakobsen J. Volume of ankle dorsiflexors and plantar flexors determined with stereological techniques. J Appl Physiol (1985) 1999; 86(5):1670–5.

14. Kaya Keles CS, Ates F. How mechanics of individual muscle-tendon units define knee and ankle joint function in health and cerebral palsy-a narrative review. Front Bioeng Biotechnol 2023; 11:1287385.

15. Lieber RL. Skeletal muscle structure, function, and plasticity: The physiological basis of rehabilitation. 3rd ed. Baltimore: Lippincott Williams & Wilkins; 2010. (Health). Available from: URL: http://www.loc.gov/catdir/enhancements/fy1009/2009019057-d.html.

16. Maganaris CN, Narici MV, Maffulli N. Biomechanics of the Achilles tendon. Disabil Rehabil 2008; 30(20-22):1542–7.

17. Kruse A, Rivares C, Weide G, Tilp M, Jaspers RT. Stimuli for Adaptations in Muscle Length and the Length Range of Active Force Exertion-A Narrative Review. Front. Physiol. 2021; 12:742034.

18. Rodrigues V, Rao MK, Nayak S. Multiple Heads of Gastrocnemius with Bipennate Fiber Arrangement- A Clinically Significant Variation. J Clin Diagn Res 2016; 10(8):AD01-2.

19. Barber L, Carty C, Modenese L, Walsh J, Boyd R, Lichtwark G. Medial gastrocnemius and soleus muscle-tendon unit, fascicle, and tendon interaction during walking in children with cerebral palsy. Developmental Medicine & Child Neurology 2017; 59(8):843–51.

20. Perry J, Burnfield JM. Gait analysis: Normal and pathological function. Second edition. Thorofare: Slack; 1992. Available from: URL: https://ebookcentral.proquest.com/lib/kxp/detail.action?docID=6178052.

21. Rubenson J, Pires NJ, Loi HO, Pinniger GJ, Shannon DG. On the ascent: the soleus operating length is conserved to the ascending limb of the force-length curve across gait mechanics in humans. J Exp Biol 2012; 215(Pt 20):3539–51.

22. Lichtwark GA, Wilson AM. Interactions between the human gastrocnemius muscle and the Achilles tendon during incline, level and decline locomotion. J Exp Biol 2006; 209(Pt 21):4379–88.

23. Fukunaga T, Kubo K, Kawakami Y, Fukashiro S, Kanehisa H, Maganaris CN. In vivo behaviour of human muscle tendon during walking. Proc Biol Sci 2001; 268(1464):229–33.

24. Cronin NJ, Avela J, Finni T, Peltonen J. Differences in contractile behaviour between the soleus and medial gastrocnemius muscles during human walking. J Exp Biol 2013; 216(Pt 5):909–14.

25. Barber L, Barrett R, Lichtwark G. Validity and reliability of a simple ultrasound approach to measure medial gastrocnemius muscle length. J Anat 2011; 218(6):637–42.

26. Fry NR, Childs CR, Eve LC, Gough M, Robinson RO, Shortland AP. Accurate measurement of muscle belly length in the motion analysis laboratory: potential for the assessment of contracture. Gait Posture 2003; 17(2):119–24.

27. Silbernagel KG, Steele R, Manal K. Deficits in heel-rise height and achilles tendon elongation occur in patients recovering from an Achilles tendon rupture. Am J Sports Med 2012; 40(7):1564–71.

28. Barfod KW. Achilles tendon rupture; assessment of nonoperative treatment. Dan Med J 2014; 61(4):B4837.

29. Pillen S, Arts IMP, Zwarts MJ. Muscle ultrasound in neuromuscular disorders. Muscle & Nerve 2008; 37(6):679–93. Available from: URL: https://onlinelibrary.wiley.com/doi/10.1002/mus.21015.

30. Alanen AM, Falck B, Kalimo H, Komu ME, Sonninen VH. Ultrasound, computed tomography and magnetic resonance imaging in myopathies: correlations with electromyography and histopathology. Acta Neurol Scand 1994; 89(5):336–46.

31. Yousaf T, Dervenoulas G, Politis M. Chapter Two - Advances in MRI Methodology. In: Politis M, editor. International Review of Neurobiology: Imaging in Movement Disorders: Imaging Methodology and Applications in Parkinson's Disease. Academic Press; 2018. p. 31–76 Available from: URL: https://www.sciencedirect.com/science/article/pii/S0074774218300758.

32. van Geuns RJ, Wielopolski PA, Bruin HG de, Rensing BJ, van Ooijen PM, Hulshoff M et al. Basic principles of magnetic resonance imaging. Progress in Cardiovascular Diseases 1999; 42(2):149–56. Available from: URL: https://www.sciencedirect.com/science/article/pii/S0033062099700149.

33. Rajan SS. MRI: A conceptual overview. New York: Springer; 1998.

34. Politis M, editor. International Review of Neurobiology: Imaging in Movement Disorders: Imaging Methodology and Applications in Parkinson's Disease. Academic Press; 2018.

35. Heiken JP, Glazer HS, Lee JK, Murphy WA, Gado M. Manual of clinical magnetic resonance imaging. Raven Press,New York, NY; 1986. Available from: URL: https://www.osti.gov/biblio/5560200.

36. Williams SA, Stott NS, Valentine J, Elliott C, Reid SL. Measuring skeletal muscle morphology and architecture with imaging modalities in children with cerebral palsy: a scoping review. Developmental Medicine & Child Neurology 2021; 63(3):263–73.

37. Budzik J-F, Balbi V, Verclytte S, Pansini V, Le Thuc V, Cotten A. Diffusion tensor imaging in musculoskeletal disorders. Radiographics 2014; 34(3):E56-72.

38. Heymsfield SB, Adamek M, Gonzalez MC, Jia G, Thomas DM. Assessing skeletal muscle mass: historical overview and state of the art. J Cachexia Sarcopenia Muscle 2014; 5(1):9–18.

39. Khalil C, Budzik JF, Kermarrec E, Balbi V, Le Thuc V, Cotten A. Tractography of peripheral nerves and skeletal muscles. European journal of radiology 2010; 76(3):391–7.

40. Koltzenburg M, Yousry T. Magnetic resonance imaging of skeletal muscle. Curr Opin Neurol 2007; 20(5):595–9.

41. Kim HK, Lindquist DM, Serai SD, Mariappan YK, Wang LL, Merrow AC et al. Magnetic resonance imaging of pediatric muscular disorders: recent advances and clinical applications. Radiol Clin North Am 2013; 51(4):721–42.

42. Kuo GP, Carrino JA. Skeletal muscle imaging and inflammatory myopathies. Curr Opin Rheumatol 2007; 19(6):530–5.

43. Le Bihan D, Breton E, Lallemand D, Grenier P, Cabanis E, Laval-Jeantet M. MR imaging of intravoxel incoherent motions: application to diffusion and perfusion in neurologic disorders. Radiology 1986; 161(2):401–7.

44. Longwei X. Clinical application of diffusion tensor magnetic resonance imaging in skeletal muscle. Muscles Ligaments Tendons J 2012; 2(1):19–24. Available from: URL: https://pubmed.ncbi.nlm.nih.gov/23738269/.

45. Napadow VJ, Kamm RD, Gilbert RJ. A biomechanical model of sagittal tongue bending. J Biomech Eng 2002; 124(5):547–56.

46. Noseworthy MD, Davis AD, Elzibak AH. Advanced MR imaging techniques for skeletal muscle evaluation. Semin Musculoskelet Radiol 2010; 14(2):257–68.

47. Oudeman J, Nederveen AJ, Strijkers GJ, Maas M, Luijten PR, Froeling M. Techniques and applications of skeletal muscle diffusion tensor imaging: A review. J Magn Reson Imaging 2016; 43(4):773–88.

48. Pierpaoli C, Basser PJ. Toward a quantitative assessment of diffusion anisotropy. Magn Reson Med 1996; 36(6):893–906.

49. Pradat P-F, Dib M. Biomarkers in amyotrophic lateral sclerosis: facts and future horizons. Mol Diagn Ther 2009; 13(2):115–25.

50. van DONKELAAR CC, Kretzers LJ, Bovendeerd PH, Lataster LM, NICOLAY K, JANSSEN JD et al. Diffusion tensor imaging in biomechanical studies of skeletal muscle function. J Anat 1999; 194 (Pt 1)(Pt 1):79–88.

51. Rasmussen OS. Sonography of tendons. Scand J Med Sci Sports 2000; 10(6):360–4.

52. O'Connor PJ, Grainger AJ, Morgan SR, Smith KL, Waterton JC, Nash AFP. Ultrasound assessment of tendons in asymptomatic volunteers: a study of reproducibility. Eur Radiol 2004; 14(11):1968–73.

53. Ozçakar L, Tok F, Muynck M de, Vanderstraeten G. Musculoskeletal ultrasonography in physical and rehabilitation medicine. J Rehabil Med 2012; 44(4):310–8.

54. Barkovich MJ, Xu D, Desikan RS, Williams C, Barkovich AJ. Pediatric neuro MRI: tricks to minimize sedation. Pediatr Radiol 2018; 48(1):50–5. Available from: URL: https://link.springer.com/article/10.1007/s00247-017-3785-1.

55. Yousif A. Al-Naser, Dawood Tafti. CT Instrumentation and Physics. In: Al-Naser YA, Tafti D, editors. StatPearls [Internet]. StatPearls Publishing; 2023 Available from: URL: https://www.ncbi.nlm.nih.gov/books/NBK597347/.

56. Goldman LW. Principles of CT and CT technology. Journal of Nuclear Medicine Technology 2007; 35(3):115-28; quiz 129-30. Available from: URL: https://tech.snmjournals.org/content/35/3/115.long.

57. Mazonakis M, Damilakis J. Computed tomography: What and how does it measure? European journal of radiology 2016; 85(8):1499–504. Available from: URL: https://pubmed.ncbi.nlm.nih.gov/26995675/.

58. Jacobson JA. Musculoskeletal ultrasound and MRI: which do I choose? Semin Musculoskelet Radiol 2005; 9(2):135–49.

59. Ashir A, Jerban S, Barrère V, Wu Y, Shah SB, Andre MP et al. Skeletal Muscle Assessment Using Quantitative Ultrasound: A Narrative Review. Sensors (Basel) 2023; 23(10).

60. Morakkabati-Spitz N, Gieseke J, Kuhl C, Lutterbey G, Falkenhausen M von, Träber F et al. MRI of the pelvis at 3 T: very high spatial resolution with sensitivity encoding and flip-angle sweep technique in clinically acceptable scan time. Eur Radiol 2006; 16(3):634–41.

61. Lin EC, Middleton WD, Teefey SA. Extended field of view sonography in musculoskeletal imaging. J Ultrasound Med 1999; 18(2):147–52.

62. Fish P. Physics and instrumentation of diagnostic medical ultrasound. Wiley; 1990.

63. Shirley IM. A User's guide to diagnostic ultrasound. Tunbridge Wells: Kent Pitman Medical; 1978.

64. Ying M, Sin M-H. Comparison of extended field of view and dual image ultrasound techniques: accuracy and reliability of distance measurements in phantom study. Ultrasound Med Biol 2005; 31(1):79–83.

65. Weng L. Method and apparatus for generating large compound ultrasound image. J. Acoust. Soc. Am. 1997; 101(6):3239.

66. Brown LG. A survey of image registration techniques. ACM Comput. Surv. 1992; 24(4):325–76.

67. Cotter AM, Jacques EG, Izquierdo LA. Extended field of view sonography: a useful tool in the diagnosis and management of abdominal pregnancy. J Clin Ultrasound 2004; 32(4):207–10.

68. Huang Q, Zeng Z, Li X. 2.5-D Extended Field-of-View Ultrasound. IEEE Trans Med Imaging 2018; 37(4):851–9.

69. Sauerbrei EE. Extended field-of-view sonography: utility in clinical practice. J Ultrasound Med 1999; 18(5):335–41.

70. Weng L, Tirumalai AP, Lowery CM, Nock LF, Gustafson DE, Behren PL von et al. US extended-field-of-view imaging technology. Radiology 1997; 203(3):877–80.

71. Weng L. Method and apparatus for generating and displaying panoramic ultrasound images. J. Acoust. Soc. Am. 1999; 105(1):28.

72. Brouwer EF, Myhrvold SB, Benth JŠ, Hoelsbrekken SE. Ultrasound measurements of Achilles tendon length using skin markings are more reliable than extended-field-of-view imaging. Knee Surg Sports Traumatol Arthrosc 2018; 26(7):2088–94.

73. Franchi MV, Fitze DP, Hanimann J, Sarto F, Spörri J. Panoramic ultrasound vs. MRI for the assessment of hamstrings cross-sectional area and volume in a large athletic cohort. Sci Rep 2020; 10(1):14144.

74. Ryan ED, Rosenberg JG, Scharville MJ, Sobolewski EJ, Thompson BJ, King GE. Test-retest reliability and the minimal detectable change for achilles tendon length: a panoramic ultrasound assessment. Ultrasound Med Biol 2013; 39(12):2488–91.

75. Silbernagel KG, Shelley K, Powell S, Varrecchia S. Extended field of view ultrasound imaging to evaluate Achilles tendon length and thickness: a reliability and validity study. Muscles Ligaments Tendons J 2016; 6(1):104–10.

76. Stokes OM, Theobald PS, Pugh ND, Nokes LDM. Panoramic ultrasound to measure in vivo tendo Achilles strain. Foot Ankle Int 2010; 31(10):905–9.

77. Weng L, Tirumalai AP, Lowery CM, Nock LF, Gustafson DE, Behren PL von et al. US extended-field-of-view imaging technology. Radiology 1997; 203(3):877–80.

78. Skypala J, Jandacka D, Hamill J. Reliability of a measurement technique for achilles tendon length. J Sports Sci 2019; 37(20):2389–95.

79. Enhanced Extended-Field-of-View Ultrasound for Musculoskeletal Tissues Using Parallel Computing. Bentham Science Publishers. Available from: URL: https://www.ingentaconnect.com/content/ben/cmir/2014/00000010/00000004/art00003.

80. Zheng S, Huang Q, Jin L, Wei G. Real-time extended-field-of-view ultrasound based on a standard PC. Applied Acoustics 2012; 73(4):423–32.

81. Intziegianni K, Cassel M, König N, Müller S, Fröhlich K, Mayer F. Ultrasonography for the assessment of the structural properties of the Achilles tendon in asymptomatic individuals: An intra-rater reproducibility study. IES 2015; 23(4):263–70.

82. Kruse A, Schranz C, Tilp M, Svehlik M. Muscle and tendon morphology alterations in children and adolescents with mild forms of spastic cerebral palsy. BMC Pediatr 2018; 18(1):156.

83. Hansen MS, Kristensen MT, Budolfsen T, Ellegaard K, Hölmich P, Barfod KW. Reliability of the Copenhagen Achilles length measure (CALM) on patients with an Achilles tendon rupture. Knee Surg Sports Traumatol Arthrosc 2020; 28(1):281–90.

84. Matsukiyo A, Goh A-C, Asagai Y. Relationship between muscle-tendon length, range of motion, and resistance to passive movement in children with normal and increased tone. Journal of physical therapy science 2017; 29(2):349–55.

85. Barfod KW, Riecke AF, Boesen A, Hansen P, Maier JF, Doessing S et al. Validity and reliability of an ultrasound measurement of the free length of the Achilles tendon. Dan Med J 2018; 65(3).

86. Barfod KW, Riecke AF, Boesen A, Hansen P, Maier JF, Døssing S et al. Validation of a novel ultrasound measurement of achilles tendon length. Knee Surg Sports Traumatol Arthrosc 2015; 23(11):3398–406.

87. Cenni F, Bar-On L, Schless S-H, Kalkman B, Aertbelien E, Bruyninckx H et al. Medial Gastrocnemius Muscle-Tendon Junction and Fascicle Lengthening across the Range of Motion Analyzed in 2-D and 3-D Ultrasound Images. Ultrasound Med Biol 2018; 44(12):2505–18.

88. Kay AD, Blazevich AJ. Moderate-duration static stretch reduces active and passive plantar flexor moment but not Achilles tendon stiffness or active muscle length. J Appl Physiol (1985) 2009; 106(4):1249–56.

89. Cenni F, Monari D, Desloovere K, Aertbeliën E, Schless S-H, Bruyninckx H. The reliability and validity of a clinical 3D freehand ultrasound system. Comput Methods Programs Biomed 2016; 136:179–87.

90. Merza E, Pearson S, Lichtwark G, Garofolini A, Malliaras P. Reliability of Human Achilles Tendon Stiffness Measures Using Freehand 3-D Ultrasound. Ultrasound Med Biol 2021; 47(4):973–81.

91. Barber L, Barrett R, Lichtwark G. Validation of a freehand 3D ultrasound system for morphological measures of the medial gastrocnemius muscle. J Biomech 2009; 42(9):1313–9.

92. Weide G, van der Zwaard S, Huijing PA, Jaspers RT, Harlaar J. 3D Ultrasound Imaging: Fast and Cost-effective Morphometry of Musculoskeletal Tissue. J Vis Exp 2017; (129).

93. Passmore E, Sangeux M. Defining the medial-lateral axis of an anatomical femur coordinate system using freehand 3D ultrasound imaging. Gait Posture 2016; 45:211–6. Available from: URL: https://www.sciencedirect.com/science/article/pii/S0966636216000473.

94. Surveillance of Cerebral Palsy in Europe. Surveillance of cerebral palsy in Europe: a collaboration of cerebral palsy surveys and registers. Dev Med Child Neurol 2000; 42(12):816–24.

95. Oskoui M, Coutinho F, Dykeman J, Jetté N, Pringsheim T. An update on the prevalence of cerebral palsy: a systematic review and meta-analysis. Developmental Medicine & Child Neurology 2013; 55(6):509–19. Available from: URL: https://onlinelibrary.wiley.com/doi/10.1111/dmcn.12080.

96. Koman LA, Smith BP, Shilt JS. Cerebral palsy. Lancet 2004; 363(9421):1619–31.

97. McIntyre S, Goldsmith S, Webb A, Ehlinger V, Hollung SJ, McConnell K et al. Global prevalence of cerebral palsy: A systematic analysis. Developmental Medicine & Child Neurology 2022; 64(12):1494–506. Available from: URL: https://www.ncbi.nlm.nih.gov/pmc/articles/PMC9804547/.

98. Graham HK, Rosenbaum P, Paneth N, Dan B, Lin J-P, Damiano DL et al. Cerebral palsy. Nat Rev Dis Primers 2016; 2(1):15082. Available from: URL: https://www.nature.com/articles/nrdp201582.

99. Touyama M, Touyama J, Toyokawa S, Kobayashi Y. Trends in the prevalence of cerebral palsy in children born between 1988 and 2007 in Okinawa, Japan. Brain Dev 2016; 38(9):792–9.

100. Sellier E, Platt MJ, Andersen GL, Krägeloh-Mann I, La Cruz J de, Cans C. Decreasing prevalence in cerebral palsy: a multi-site European population-based study, 1980 to 2003. Developmental Medicine & Child Neurology 2016; 58(1):85–92.

101. Reid SM, Meehan E, McIntyre S, Goldsmith S, Badawi N, Reddihough DS. Temporal trends in cerebral palsy by impairment severity and birth gestation. Developmental Medicine & Child Neurology 2016; 58 Suppl 2:25–35.

102. Galea C, McIntyre S, Smithers-Sheedy H, Reid SM, Gibson C, Delacy M et al. Cerebral palsy trends in Australia (1995-2009): a population-based observational study. Developmental Medicine & Child Neurology 2019; 61(2):186–93.

103. YANG S, XIA J, GAO J, WANG L. Increasing prevalence of cerebral palsy among children and adolescents in China 1988-2020: A systematic review and meta-analysis. J Rehabil Med 2021; 53(5):jrm00195.

104. Sankar C, Mundkur N. Cerebral palsy-definition, classification, etiology and early diagnosis. Indian J Pediatr 2005; 72(10):865–8.

105. Rosenbaum P, Paneth N, Leviton A, Goldstein M, Bax M, Damiano D et al. A report: the definition and classification of cerebral palsy April 2006. Dev Med Child Neurol Suppl 2007; 109:8–14.

106. McIntyre S, Morgan C, Walker K, Novak I. Cerebral palsy—don't delay. Developmental disabilities research reviews 2011; 17(2):114–29. Available from: URL: https://pubmed.ncbi.nlm.nih.gov/23362031/.

107. Graham HK, Rosenbaum P, Paneth N, Dan B, Lin J-P, Damiano DL et al. Cerebral palsy. Nat Rev Dis Primers 2016; 2:15082.

108. Bax M, Tydeman C, Flodmark O. Clinical and MRI correlates of cerebral palsy: the European Cerebral Palsy Study. JAMA 2006; 296(13):1602–8. Available from: URL: https://pubmed.ncbi.nlm.nih.gov/17018805/.

109. Patel DR, Neelakantan M, Pandher K, Merrick J. Cerebral palsy in children: a clinical overview. Transl Pediatr 2020; 9(Suppl 1):S125-S135.

110. Rodda JM, Graham HK, Nattrass GR, Galea MP, Baker R, Wolfe R. Correction of severe crouch gait in patients with spastic diplegia with use of multilevel orthopaedic surgery. J Bone Joint Surg Am 2006; 88(12):2653–64.

111. Sharan D. Orthopedic surgery in cerebral palsy: Instructional course lecture. Indian J Orthop 2017; 51(3):240–55.

112. Hanna SE, Rosenbaum PL, Bartlett DJ, Palisano RJ, Walter SD, Avery L et al. Stability and decline in gross motor function among children and youth with cerebral palsy aged 2 to 21 years. Developmental Medicine & Child Neurology 2009; 51(4):295–302.

113. Bell KJ, Ounpuu S, DeLuca PA, Romness MJ. Natural progression of gait in children with cerebral palsy. J Pediatr Orthop 2002; 22(5):677–82.

114. Shortland A. Muscle deficits in cerebral palsy and early loss of mobility: can we learn something from our elders? Developmental Medicine & Child Neurology 2009; 51 Suppl 4:59–63.

115. Scholtes VA, Becher JG, Comuth A, Dekkers H, van Dijk L, Dallmeijer AJ. Effectiveness of functional progressive resistance exercise strength training on muscle strength and mobility in children with cerebral palsy: a randomized controlled trial. Developmental Medicine & Child Neurology 2010; 52(6):e107-13. Available from: URL: https://pubmed.ncbi.nlm.nih.gov/20132136/.

116. Colver A, Fairhurst C, Pharoah POD. Cerebral palsy. Lancet 2014; 383(9924):1240–9.

117. Rethlefsen SA, Ryan DD, Kay RM. Classification systems in cerebral palsy. Orthop Clin North Am 2010; 41(4):457–67. Available from: URL: https://www.sciencedirect.com/science/article/pii/S0030589810000593.

118. Krägeloh-Mann I, Cans C. Cerebral palsy update. Brain Dev 2009; 31(7):537–44.

119. Bar-On L, Molenaers G, Aertbeliën E, van Campenhout A, Feys H, Nuttin B et al. Spasticity and its contribution to hypertonia in cerebral palsy. Biomed Res Int 2015; 2015:317047.

120. Pidgeon TS, Ramirez JM, Schiller JR. Orthopaedic Management of Spasticity. Rhode Island medical journal (2013) 2015; 98(12):26–31. Available from: URL: https://pubmed.ncbi.nlm.nih.gov/26623452/.

121. Pathophysiology of spasticity and clinical experience with baclofen. Spasticity: disordered motor control; 1980.

122. Sakzewski L, Ziviani J, Boyd R. Systematic review and meta-analysis of therapeutic management of upper-limb dysfunction in children with congenital hemiplegia. Pediatrics 2009; 123(6):e1111-22. Available from: URL: https://pubmed.ncbi.nlm.nih.gov/19451190/.

123. Klingels K, Demeyere I, Jaspers E, Cock P de, Molenaers G, Boyd R et al. Upper limb impairments and their impact on activity measures in children with unilateral cerebral palsy. Eur J Paediatr Neurol 2012; 16(5):475–84.

124. Morrell DS, Pearson JM, Sauser DD. Progressive bone and joint abnormalities of the spine and lower extremities in cerebral palsy. Radiographics 2002; 22(2):257–68.

125. Gage JR, Schwartz MH, Koop SE. The identification and treatment of gait problems in cerebral palsy. 2nd ed., repr. London: Mac Keith Press; 2014. (Clinics in Developmental MedicineNo 180-181).

126. Zonta MB, Bruck I, Puppi M, Muzzolon S, Neto AdC, Coutinho dos Santos LH. Effects of early spasticity treatment on children with hemiplegic cerebral palsy: a preliminary study. Arq Neuropsiquiatr 2013; 71(7):453–61.

127. Shamsoddini A, Amirsalari S, Hollisaz M-T, Rahimnia A, Khatibi-Aghda A. Management of spasticity in children with cerebral palsy. Iran J Pediatr 2014; 24(4):345–51.

128. Campbell ML, Hoon AH, Johnston MV. Cerebral Palsy. In: Haith MM, Benson JB, editors. Encyclopedia of infant and early childhood development. Amsterdam, Boston: Elsevier Academic Press; 2008. p. 260–8 Available from: URL: https://www.sciencedirect.com/science/article/pii/B9780123708779000323.

129. Basoya S, Kumar S, Wanjari A. Cerebral Palsy: A Narrative Review on Childhood Disorder. Cureus 2023; 15(11):e49050.

130. Surveillance of cerebral palsy in Europe: a collaboration of cerebral palsy surveys and registers. Surveillance of Cerebral Palsy in Europe (SCPE). Dev Med Child Neurol 2000; 42(12):816–24. Available from: URL: https://pubmed.ncbi.nlm.nih.gov/11132255/.

131. Molnar GE. Rehabilitation in cerebral palsy. West J Med 1991; 154(5):569–72.

132. Paul S, Nahar A, Bhagawati M, Kunwar AJ. A Review on Recent Advances of Cerebral Palsy. Oxid Med Cell Longev 2022; 2022:2622310.

133. Fogel BL. Childhood cerebellar ataxia. J Child Neurol 2012; 27(9):1138–45.

134. Eggink H, Kremer D, Brouwer OF, Contarino MF, van Egmond ME, Elema A et al. Spasticity, dyskinesia and ataxia in cerebral palsy: Are we sure we can differentiate them? Eur J Paediatr Neurol 2017; 21(5):703–6.

135. Cerebral Palsy. New York: Scholars Portal; 2005.

136. Rosenbaum P. Cerebral palsy: what parents and doctors want to know. BMJ 2003; 326(7396):970–4.

137. Palisano R, Rosenbaum P, Walter S, Russell D, Wood E, Galuppi B. Development and reliability of a system to classify gross motor function in children with cerebral palsy. Dev Med Child Neurol 1997; 39(4):214–23.

138. Reid SM, Carlin JB, Reddihough DS. Using the Gross Motor Function Classification System to describe patterns of motor severity in cerebral palsy. Developmental Medicine & Child Neurology 2011; 53(11):1007–12.

139. Ruiz Brunner MdlM, Cuestas E, Heinen F, Schroeder AS. Growth in infants, children and adolescents with unilateral and bilateral cerebral palsy. Sci Rep 2022; 12(1):1879.

140. Stanek JL, Emerson JA, Murdock FA, Petroski GF. Growth characteristics in cerebral palsy subtypes: a comparative assessment. Developmental Medicine & Child Neurology 2016; 58(9):931–5.

141. MINCIU I. Clinical correlations in cerebral palsy. Maedica (Bucur) 2012; 7(4):319–24.

142. Morgan P, McGinley J. Gait function and decline in adults with cerebral palsy: a systematic review. Disabil Rehabil 2014; 36(1):1–9.

143. Root L. Tendon surgery on the feet of children with cerebral palsy. Dev Med Child Neurol 1976; 18(5):671–4. Available from: URL: https://onlinelibrary.wiley.com/doi/epdf/10.1111/j.1469-8749.1976.tb04217.x.

144. Wren TAL, Rethlefsen S, Kay RM. Prevalence of specific gait abnormalities in children with cerebral palsy: influence of cerebral palsy subtype, age, and previous surgery. J Pediatr Orthop 2005; 25(1):79–83.

145. Frost HM. Cerebral palsy. The spastic crouch. Clin Orthop Relat Res 1971; 80:2–8.

146. Bennet GC, Rang M, Jones D. Varus and valgus deformities of the foot in cerebral palsy. Dev Med Child Neurol 1982; 24(4):499–503.

147. Wiley ME, Damiano DL. Lower-extremity strength profiles in spastic cerebral palsy. Dev Med Child Neurol 1998; 40(2):100–7.

148. Cenni F, Alexander N, Sukanen M, Mustafaoglu A, Wang Z, Wang R et al. ISB clinical biomechanics award winner 2023: Medial gastrocnemius muscle and Achilles tendon interplay during gait in cerebral palsy. Clin Biomech (Bristol, Avon) 2024; 111:106158.

149. Trappe SW, Trappe TA, Lee GA, Costill DL. Calf muscle strength in humans. Int J Sports Med 2001; 22(3):186–91.

150. Massaad A, Assi A, Bakouny Z, Bizdikian AJ, Skalli W, Ghanem I. Alterations of treatment-naïve pelvis and thigh muscle morphology in children with cerebral palsy. J Biomech 2019; 82:178–85.

151. Pitcher CA, Elliott CM, Panizzolo FA, Valentine JP, Stannage K, Reid SL. Ultrasound characterization of medial gastrocnemius tissue composition in children with spastic cerebral palsy. Muscle & Nerve 2015; 52(3):397–403.

152. Handsfield GG, Meyer CH, Abel MF, Blemker SS. Heterogeneity of muscle sizes in the lower limbs of children with cerebral palsy. Muscle & Nerve 2016; 53(6):933–45.

153. Barrett RS, Lichtwark GA. Gross muscle morphology and structure in spastic cerebral palsy: a systematic review. Developmental Medicine & Child Neurology 2010; 52(9):794–804.

154. Sahrmann AS, Stott NS, Besier TF, Fernandez JW, Handsfield GG. Soleus muscle weakness in cerebral palsy: Muscle architecture revealed with Diffusion Tensor Imaging. PLoS One 2019; 14(2):e0205944.

155. Shortland AP, Fry NR, Eve LC, Gough M. Changes to medial gastrocnemius architecture after surgical intervention in spastic diplegia. Developmental Medicine & Child Neurology 2004; 46(10):667–73.

156. Moreau NG, Teefey SA, Damiano DL. In vivo muscle architecture and size of the rectus femoris and vastus lateralis in children and adolescents with cerebral palsy. Developmental Medicine & Child Neurology 2009; 51(10):800–6.

157. Mohagheghi AA, Khan T, Meadows TH, Giannikas K, Baltzopoulos V, Maganaris CN. In vivo gastrocnemius muscle fascicle length in children with and without diplegic cerebral palsy. Dev Med Child Neurol 2008; 50(1):44–50.

158. Chen Y, He L, Xu K, Li J, Guan B, Tang H. Comparison of calf muscle architecture between Asian children with spastic cerebral palsy and typically developing peers. PLoS One 2018; 13(1):e0190642.

159. Kruse A, Schranz C, Tilp M, Svehlik M. Correction to: Muscle and tendon morphology alterations in children and adolescents with mild forms of spastic cerebral palsy. BMC Pediatr 2018; 18(1):273.

160. Shortland AP, Harris CA, Gough M, Robinson RO. Architecture of the medial gastrocnemius in children with spastic diplegia. Developmental Medicine & Child Neurology 2002; 44(3):158–63.

161. D'Souza A, Bolsterlee B, Lancaster A, Herbert RD. Muscle architecture in children with cerebral palsy and ankle contractures: an investigation using diffusion tensor imaging. Clin Biomech (Bristol, Avon) 2019; 68:205–11.

162. Gao F, Zhao H, Gaebler-Spira D, Zhang L-Q. In vivo evaluations of morphologic changes of gastrocnemius muscle fascicles and achilles tendon in children with cerebral palsy. Am J Phys Med Rehabil 2011; 90(5):364–71.

163. Barber L, Hastings-Ison T, Baker R, Barrett R, Lichtwark G. Medial gastrocnemius muscle volume and fascicle length in children aged 2 to 5 years with cerebral palsy. Developmental Medicine & Child Neurology 2011; 53(6):543–8.

164. Smith LR, Lee KS, Ward SR, Chambers HG, Lieber RL. Hamstring contractures in children with spastic cerebral palsy result from a stiffer extracellular matrix and increased in vivo sarcomere length. The Journal of Physiology 2011; 589(Pt 10):2625–39.

165. Mathewson MA, Ward SR, Chambers HG, Lieber RL. High resolution muscle measurements provide insights into equinus contractures in patients with cerebral palsy. J Orthop Res 2015; 33(1):33–9.

166. Lieber RL, Fridén J. Spasticity causes a fundamental rearrangement of muscle-joint interaction. Muscle & Nerve 2002; 25(2):265–70.

167. Barber LA, Read F, Lovatt Stern J, Lichtwark G, Boyd RN. Medial gastrocnemius muscle volume in ambulant children with unilateral and bilateral cerebral palsy aged 2 to 9 years. Developmental Medicine & Child Neurology 2016; 58(11):1146–52.

168. Willerslev-Olsen M, Choe Lund M, Lorentzen J, Barber L, Kofoed-Hansen M, Nielsen JB. Impaired muscle growth precedes development of increased stiffness of the triceps surae musculotendinous unit in children with cerebral palsy. Developmental Medicine & Child Neurology 2018; 60(7):672–9.

169. Valera-Calero JA, Ojedo-Martín C, Fernández-de-Las-Peñas C, Cleland JA, Arias-Buría JL, Hervás-Pérez JP. Reliability and Validity of Panoramic Ultrasound Imaging for Evaluating Muscular Quality and Morphology: A Systematic Review. Ultrasound Med Biol 2021; 47(2):185–200.

170. Booth CM, Cortina-Borja MJF, Theologis TN. Collagen accumulation in muscles of children with cerebral palsy and correlation with severity of spasticity. Developmental Medicine & Child Neurology 2001; 43(5):314–20.

171. Wren TAL, Cheatwood AP, Rethlefsen SA, Hara R, Perez FJ, Kay RM. Achilles tendon length and medial gastrocnemius architecture in children with cerebral palsy and equinus gait. J Pediatr Orthop 2010; 30(5):479–84.

172. Herskind A, Ritterband-Rosenbaum A, Willerslev-Olsen M, Lorentzen J, Hanson L, Lichtwark G et al. Muscle growth is reduced in 15-month-old children with cerebral palsy. Developmental Medicine & Child Neurology 2016; 58(5):485–91.

173. Walden F von, Gantelius S, Liu C, Borgström H, Björk L, Gremark O et al. Muscle contractures in patients with cerebral palsy and acquired brain injury are associated with extracellular matrix expansion, pro-inflammatory gene expression, and reduced rRNA synthesis. Muscle & Nerve 2018; 58(2):277–85.

174. Lieber RL, Fridén J. Muscle contracture and passive mechanics in cerebral palsy. J Appl Physiol (1985) 2019; 126(5):1492–501. Available from: URL: https://journals.physiology.org/doi/full/10.1152/japplphysiol.00278.2018?rfr_dat=cr_pub%20%200pubmed&url_ver=z39.88-2003&rfr_id=ori%3arid%3acrossref.org&utm_source=trendmd&utm_medium=cpc&utm_campaign=journal_of_applied_physiology_trendmd_1.

175. Weide G, Huijing PA, Bar-On L, Sloot L, Buizer AI, Becher JG et al. Gastrocnemius Medialis Muscle Geometry and Extensibility in Typically Developing Children and Children With Spastic Paresis Aged 6-13 Years. Front. Physiol. 2020; 11:528522. Available from: URL: https://www.frontiersin.org/articles/10.3389/fphys.2020.528522/full.

176. Haberfehlner H, Jaspers RT, Rutz E, Becher JG, Harlaar J, van der Sluijs JA et al. Knee Moment-Angle Characteristics and Semitendinosus Muscle Morphology in Children with Spastic Paresis Selected for Medial Hamstring Lengthening. PLoS One 2016; 11(11):e0166401. Available from: URL: https://journals.plos.org/plosone/article?id=10.1371/journal.pone.0166401.

177. Walter SD, Eliasziw M, Donner A. Sample size and optimal designs for reliability studies. Statist. Med. 1998; 17(1):101–10.

178. Kruse A, Stafilidis S, Tilp M. Ultrasound and magnetic resonance imaging are not interchangeable to assess the Achilles tendon cross-sectional-area. Eur J Appl Physiol 2017; 117(1):73–82.

179. Hermens HJ, Freriks B, Disselhorst-Klug C, Rau G. Development of recommendations for SEMG sensors and sensor placement procedures. Journal of Electromyography and Kinesiology 2000; 10(5):361–74. Available from: URL: https://www.sciencedirect.com/science/article/pii/s1050641100000274.

180. Huijing PA, Bénard MR, Harlaar J, Jaspers RT, Becher JG. Movement within foot and ankle joint in children with spastic cerebral palsy: a 3-dimensional ultrasound analysis of medial gastrocnemius length with correction for effects of foot deformation. BMC Musculoskelet Disord 2013; 14:365.

181. Bénard MR, Jaspers RT, Huijing PA, Becher JG, Harlaar J. Reproducibility of hand-held ankle dynamometry to measure altered ankle moment-angle characteristics in children with

spastic cerebral palsy. Clin Biomech (Bristol, Avon) 2010; 25(8):802–8. Available from: URL: https://www.sciencedirect.com/science/article/pii/s0268003310001191.

182. Weide G, Huijing PA, Becher JG, Jaspers RT, Harlaar J. Foot flexibility confounds the assessment of triceps surae extensibility in children with spastic paresis during typical physical examinations. J Biomech 2020; 99:109532.

183. Kruse A, Schranz C, Svehlik M, Tilp M. Mechanical muscle and tendon properties of the plantar flexors are altered even in highly functional children with spastic cerebral palsy. Clin Biomech (Bristol, Avon) 2017; 50:139–44. Available from: URL: https://www.sciencedirect.com/science/article/pii/s0268003317302723.

184. Koo TK, Li MY. A Guideline of Selecting and Reporting Intraclass Correlation Coefficients for Reliability Research. Journal of Chiropractic Medicine 2016; 15(2):155–63. Available from: URL: https://www.sciencedirect.com/science/article/pii/S1556370716000158.

185. Shrout PE, Fleiss JL. Intraclass correlations: uses in assessing rater reliability. Psychol Bull 1979; 86(2):420–8.

186. Atkinson G, Nevill AM. Statistical methods for assessing measurement error (reliability) in variables relevant to sports medicine. Sports Med 1998; 26(4):217–38.

187. Hars M, Herrmann FR, Trombetti A. Reliability and minimal detectable change of gait variables in community-dwelling and hospitalized older fallers. Gait Posture 2013; 38(4):1010–4.

188. Kruse A, Habersack A, Weide G, Jaspers RT, Svehlik M, Tilp M. Eight weeks of proprioceptive neuromuscular facilitation stretching and static stretching do not affect muscle-tendon properties, muscle strength, and joint function in children with spastic cerebral palsy. Clin Biomech (Bristol, Avon) 2023; 107:106011.

189. Barber L, Barrett R, Lichtwark G. Medial gastrocnemius muscle fascicle active torque-length and Achilles tendon properties in young adults with spastic cerebral palsy. J Biomech 2012; 45(15):2526–30.

190. Yushkevich PA, Piven J, Hazlett HC, Smith RG, Ho S, Gee JC et al. User-guided 3D active contour segmentation of anatomical structures: significantly improved efficiency and reliability. Neuroimage 2006; 31(3):1116–28.

191. Cohen J. Statistical Power Analysis for the Behavioral Sciences. Burlington: Elsevier Science; 2013.

192. Theis N, Korff T, Kairon H, Mohagheghi AA. Does acute passive stretching increase muscle length in children with cerebral palsy? Clin Biomech (Bristol, Avon) 2013; 28(9-10):1061–7.

193. Nakamura M, Ikezoe T, Takeno Y, Ichihashi N. Acute and prolonged effect of static stretching on the passive stiffness of the human gastrocnemius muscle tendon unit in vivo. J Orthop Res 2011; 29(11):1759–63.

194. Kubo K, Kanehisa H, Fukunaga T. Effects of resistance and stretching training programmes on the viscoelastic properties of human tendon structures in vivo. The Journal of Physiology 2002; 538(1):219–26.

195. Schranz C, Kruse A, Tilp M, Svehlik M. Is there a relationship between muscle-tendon properties and a variety of functional tasks in children with spastic cerebral palsy? Gait Posture 2021; 85:14–9. Available from: URL: https://www.sciencedirect.com/science/article/pii/S0966636221000114.

196. van Wely L, Becher JG, Balemans ACJ, Dallmeijer AJ. Ambulatory activity of children with cerebral palsy: which characteristics are important? Developmental Medicine & Child Neurology 2012; 54(5):436–42.

197. Nieuwenhuijsen C, van der Slot WMA, Beelen A, Arendzen JH, Roebroeck ME, Stam HJ et al. Inactive lifestyle in adults with bilateral spastic cerebral palsy. J Rehabil Med 2009; 41(5):375–81.

198. Lamontagne A, Richards CL, Malouin F. Coactivation during gait as an adaptive behavior after stroke. Journal of Electromyography and Kinesiology 2000; 10(6):407–15.

199. Gross R, Leboeuf F, Hardouin JB, Lempereur M, Perrouin-Verbe B, Remy-Neris O et al. The influence of gait speed on co-activation in unilateral spastic cerebral palsy children. Clin Biomech (Bristol, Avon) 2013; 28(3):312–7.

200. Mitchell LE, Ziviani J, Boyd RN. Characteristics associated with physical activity among independently ambulant children and adolescents with unilateral cerebral palsy. Dev Med Child Neurol 2015; 57(2):167–74.

201. Lauruschkus K, Westbom L, Hallström I, Wagner P, Nordmark E. Physical activity in a total population of children and adolescents with cerebral palsy. Res Dev Disabil 2013; 34(1):157–67.

202. Stevens SL, Holbrook EA, Fuller DK, Morgan DW. Influence of age on step activity patterns in children with cerebral palsy and typically developing children. Arch Phys Med Rehabil 2010; 91(12):1891–6.

203. Trost SG, Pate RR, Sallis JF, Freedson PS, Taylor WC, Dowda M et al. Age and gender differences in objectively measured physical activity in youth. Med Sci Sports Exerc 2002; 34(2):350–5.

204. Grieve DW, DW G, PHEASANT S, PR C. Biomechanics. Prediction of gastrocnemius length from knee and ankle joint posture; 1978.

205. Kato E, Kanehisa H, Fukunaga T, Kawakami Y. Changes in ankle joint stiffness due to stretching: The role of tendon elongation of the gastrocnemius muscle. European Journal of Sport Science 2010; 10(2):111–9.

206. Morse CI, Degens H, Seynnes OR, Maganaris CN, Jones DA. The acute effect of stretching on the passive stiffness of the human gastrocnemius muscle tendon unit. The Journal of Physiology 2008; 586(1):97–106.

207. Narici MV, Maffulli N, Maganaris CN. Ageing of human muscles and tendons. Disabil Rehabil 2008; 30(20-22):1548–54.

208. Onambele GL, Narici MV, Maganaris CN. Calf muscle-tendon properties and postural balance in old age. J Appl Physiol (1985) 2006; 100(6):2048–56.

209. Kainz H, Schwartz MH. The importance of a consistent workflow to estimate muscle-tendon lengths based on joint angles from the conventional gait model. Gait Posture 2021; 88:1–9. Available from: URL: https://www.sciencedirect.com/science/article/pii/S0966636221001703.

210. Arnold AS, Liu MQ, Schwartz MH, Ounpuu S, Delp SL. The role of estimating muscle-tendon lengths and velocities of the hamstrings in the evaluation and treatment of crouch gait. Gait Posture 2006; 23(3):273–81. Available from: URL: https://www.sciencedirect.com/science/article/pii/S0966636205000627.

211. Delp SL, Anderson FC, Arnold AS, Loan P, Habib A, John CT et al. OpenSim: open-source software to create and analyze dynamic simulations of movement. IEEE Trans Biomed Eng 2007; 54(11):1940–50.

212. Gennisson J-L, Catheline S, Chaffaï S, Fink M. Transient elastography in anisotropic medium: application to the measurement of slow and fast shear wave speeds in muscles. J. Acoust. Soc. Am. 2003; 114(1):536–41.

213. Bercoff J, Tanter M, Fink M. Supersonic shear imaging: a new technique for soft tissue elasticity mapping. IEEE Trans Ultrason Ferroelectr Freq Control 2004; 51(4):396–409.

214. Lee SSM, Gaebler-Spira D, Zhang L-Q, Rymer WZ, Steele KM. Use of shear wave ultrasound elastography to quantify muscle properties in cerebral palsy. Clin Biomech (Bristol, Avon) 2016; 31:20–8.

215. Ryu J, Jeong WK. Current status of musculoskeletal application of shear wave elastography. Ultrasonography 2017; 36(3):185–97.

216. Brandenburg JE, Eby SF, Song P, Kingsley-Berg S, Bamlet W, Sieck GC et al. Quantifying passive muscle stiffness in children with and without cerebral palsy using ultrasound shear wave elastography. Developmental Medicine & Child Neurology 2016; 58(12):1288–94.

217. Kostanjsek N. Use of The International Classification of Functioning, Disability and Health (ICF) as a conceptual framework and common language for disability statistics and health information systems. BMC Public Health 2011; 11 Suppl 4(Suppl 4):S3.

218. Smith CR, Choi KW, Negrut D, Thelen DG. Efficient Computation of Cartilage Contact Pressures within Dynamic Simulations of Movement. Comput Methods Biomech Biomed Eng Imaging Vis 2018; 6(5):491–8.

219. Seth A, Hicks JL, Uchida TK, Habib A, Dembia CL, Dunne JJ et al. OpenSim: Simulating musculoskeletal dynamics and neuromuscular control to study human and animal movement. PLoS Comput Biol 2018; 14(7):e1006223.

# 6. Appendix

**Supplementary Table 1**. Individual characteristics of the children with USCP and BSCP. Table and adapted caption reproduced from (1) with permission of the publisher (Springer Nature).

| Number | Study | Paresis | Sex | Age (y) | GMFCS | SCALE | Body mass (kg) | Height (cm) | Lower leg length (mm) |
|---|---|---|---|---|---|---|---|---|---|
| 1 | 1 | USCP | f | 9 | I | 1 | 29.0 | 129.0 | 315 |
| 2 | 1 | USCP | f | 9 | II | 0 | 41.0 | 142.0 | 335 |
| 3 | 1 | USCP | m | 10 | I | 1 | 38.0 | 155.0 | 370 |
| 4 | 1 | USCP | f | 12 | I | 1 | 62.0 | 151.0 | 360 |
| 5 | 1 | USCP | m | 12 | I | 1 | 50.0 | 163.0 | 415 |
| 6 | 1 | USCP | f | 11 | I | 1 | 36.0 | 142.0 | 335 |
| 7 | 1 | USCP | f | 15 | I | 1 | 50.0 | 162.0 | 380 |
| 8 | 1 | USCP | m | 9 | I | 0 | 28.0 | 138.5 | 350 |
| 9 | 1 | USCP | f | 11 | I | 1 | 43.0 | 147.5 | 360 |
| 10 | 1 | USCP | m | 12 | I | 1 | 56.0 | 151.0 | 380 |
| 11 | 2 | USCP | m | 9 | I | 1 | 31.5 | 138.0 | 320 |
| 12 | 2 | USCP | m | 8 | I | 1 | 34.0 | 138.0 | 320 |
| 13 | 2 | USCP | f | 6 | II | 1 | 18.0 | 113.0 | 250 |
| 14 | 2 | USCP | m | 7 | I | 1 | 22.0 | 123.0 | 300 |
| 15 | 2 | USCP | m | 13 | I | 0 | 80.0 | 167.0 | 380 |
| 16 | 1 | BSCP | m | 10 | I | 2 | 48.0 | 150.0 | 380 |
| 17 | 1 | BSCP | m | 9 | I | 2 | 42.0 | 147.0 | 355 |
| 18 | 1 | BSCP | m | 13 | III | 1 | 73.0 | 168.0 | 380 |
| 19 | 1 | BSCP | m | 12 | III | 0 | 49.0 | 140.0 | 325 |
| 20 | 1 | BSCP | f | 7 | III | 1 | 19.0 | 117.0 | 275 |
| 21 | 1 | BSCP | m | 11 | II | 1 | 35.0 | 136.5 | 320 |
| 22 | 1 | BSCP | f | 14 | I | 1 | 60.0 | 163.0 | 420 |
| 23 | 1 | BSCP | f | 13 | I | 1 | 55.0 | 160.0 | 385 |
| 24 | 1 | BSCP | f | 13 | I | 1 | 59.0 | 156.0 | 370 |
| 25 | 1 | BSCP | m | 9 | I | 1 | 28.0 | 137.0 | 325 |
| 26 | 1 | BSCP | f | 10 | I | 1 | 31.0 | 137.5 | 335 |
| 27 | 1 | BSCP | f | 7 | I | 1 | 25.0 | 121.0 | 270 |
| 28 | 1 | BSCP | m | 11 | I | 2 | 66.0 | 162.0 | 380 |
| 29 | 2 | BSCP | m | 15 | I | 1 | 46.0 | 162.0 | 375 |
| 30 | 2 | BSCP | m | 7 | II | 1 | 32.0 | 128.0 | 300 |
| 31 | 2 | BSCP | m | 13 | II | 1 | 33.0 | 151.0 | 340 |
| 32 | 2 | BSCP | f | 8 | II | 1 | 24.0 | 121.0 | 290 |
| 33 | 2 | BSCP | m | 12 | I | 1 | 23.0 | 136.0 | 300 |

Abbreviations: SCALE: Selective Control Assessment of the Lower Extremity; USCP: unilateral spastic cerebral palsy; BSCP: bilateral spastic cerebral palsy; GMFCS: Gross Motor Function Classification System; m: male; f: female; Study 1: Data from clinical trial NCT04570358; Study 2: Data from clinical trial NCT05269745.

**Supplementary Table 2**. Individual morphological muscle-tendon properties of the children with USCP and BSCP. Table and adapted caption reproduced from (1) with permission of the publisher (Springer Nature).

| ID | USCP/ BSCP | GM muscle length [mm] | AT tendon length [mm] | MTU length [mm] | Ratio GM - MTU length [%] | Ratio AT - MTU length [%] | GM muscle lengthening [mm] | AT lengthening [mm] | MTU lengthening [mm] |
|---|---|---|---|---|---|---|---|---|---|
| 1 | USCP | 169.52 | 134.04 | 303.56 | 55.84 | 44.16 | 15.69 | 6.09 | 21.77 |
| 2 | USCP | 184.75 | 134.07 | 318.82 | 57.95 | 42.05 | 16.24 | - | - |
| 3 | USCP | 182.26 | 193.28 | 375.54 | 48.53 | 51.47 | 10.33 | 10.64 | 20.97 |
| 4 | USCP | 229.11 | 135.29 | 364.41 | 62.87 | 37.13 | 12.79 | 8.08 | 20.86 |
| 5 | USCP | 222.45 | 207.10 | 429.55 | 51.79 | 48.21 | 15.12 | 2.27 | 17.38 |
| 6 | USCP | 170.96 | 186.95 | 357.90 | 47.77 | 52.23 | 11.37 | 5.02 | 16.38 |
| 7 | USCP | 199.32 | 195.28 | 394.60 | 50.51 | 49.49 | 10.66 | 11.33 | 22.00 |
| 8 | USCP | 173.33 | 164.63 | 337.96 | 51.29 | 48.71 | 8.58 | 9.32 | 17.90 |
| 9 | USCP | 220.50 | 132.01 | 352.51 | 62.55 | 37.45 | 18.04 | 2.39 | 20.43 |
| 10 | USCP | 191.74 | 178.08 | 369.82 | 51.85 | 48.15 | 12.12 | 8.97 | 21.10 |
| 11 | USCP | 199.46 | 125.80 | 325.25 | 61.32 | 38.68 | 15.10 | - | - |
| 12 | USCP | 207.57 | 125.96 | 333.52 | 62.23 | 37.77 | 11.05 | 0.84 | 11.89 |
| 13 | USCP | 144.73 | 101.85 | 246.58 | 58.70 | 41.30 | 9.53 | 0.89 | 10.42 |
| 14 | USCP | 140.57 | 136.58 | 277.15 | 50.72 | 49.28 | 20.74 | - | - |
| 15 | USCP | 207.22 | 184.92 | 392.15 | 52.84 | 47.16 | 3.32 | 10.97 | 14.30 |
| 16 | BSCP | 187.75 | 180.70 | 368.45 | 50.96 | 49.04 | 13.36 | 7.60 | 20.95 |
| 17 | BSCP | - | - | - | - | - | 19.56 | - | - |
| 18 | BSCP | - | - | - | - | - | - | - | - |
| 19 | BSCP | - | - | - | - | - | 9.86 | 9.25 | 19.11 |
| 20 | BSCP | 143.74 | 113.45 | 257.19 | 55.89 | 44.11 | - | - | - |
| 21 | BSCP | - | - | - | - | - | 12.40 | 4.50 | 16.90 |
| 22 | BSCP | - | - | - | - | - | 15.14 | 8.73 | 23.87 |
| 23 | BSCP | 192.66 | 194.90 | 387.56 | 49.71 | 50.29 | - | - | - |
| 24 | BSCP | 205.21 | 164.12 | 369.33 | 55.56 | 44.44 | 21.34 | 2.68 | 24.03 |
| 25 | BSCP | - | - | - | - | - | 9.23 | 6.28 | 15.50 |
| 26 | BSCP | - | - | - | - | - | 15.15 | 3.12 | 18.27 |
| 27 | BSCP | - | - | - | - | - | - | - | - |
| 28 | BSCP | 199.63 | 217.37 | 417.00 | 47.87 | 52.13 | 12.68 | 4.23 | 16.91 |
| 29 | BSCP | 220.64 | 186.13 | 406.77 | 54.24 | 45.76 | 14.90 | - | - |
| 30 | BSCP | 145.26 | 155.75 | 301.01 | 48.26 | 51.74 | 3.96 | 5.20 | 9.16 |
| 31 | BSCP | 229.37 | 130.77 | 360.14 | 63.69 | 36.31 | 18.73 | - | - |
| 32 | BSCP | 161.56 | 128.45 | 290.00 | 55.71 | 44.29 | 5.79 | 4.00 | 9.79 |
| 33 | BSCP | 155.36 | 154.49 | 309.85 | 50.14 | 49.86 | 8.91 | 1.11 | 10.03 |

Abbreviations: GM: gastrocnemius medialis; AT: Achilles tendon; MTU: muscle-tendon unit; USCP, unilateral spastic cerebral palsy; BSCP, bilateral spastic cerebral palsy

**Supplementary Table 3**. Individual architectural muscle-tendon properties, ankle joint function and isometric muscle strength of the children with USCP and BSCP. Negative ankle values correspond to a plantar flexed position. Table and adapted caption reproduced from (1) with permission of the publisher (Springer Nature).

| ID | USCP/ BSCP | Fascicle length [mm] | Muscle thickness [mm] | Pennation angle [°] | GM muscle volume [ml] | Max. DF [°] | Max. PF [°] | RoM [°] | Isometric strength [Nm] |
|---|---|---|---|---|---|---|---|---|---|
| 1 | USCP | 25.22 | 8.40 | 18.22 | 37.81 | 3 | -42.4 | 45.4 | 10.62 |
| 2 | USCP | 39.43 | 12.09 | 17.33 | - | -18.4 | -47.5 | 29.1 | 14.11 |
| 3 | USCP | 31.89 | 11.46 | 19.71 | 81.91 | -1.9 | -46.7 | 44.8 | 35.86 |
| 4 | USCP | 41.14 | 17.28 | 23.18 | - | -5.3 | -46.4 | 41.1 | 37.18 |
| 5 | USCP | 34.14 | 11.18 | 17.38 | 85.70 | -7.8 | -46.1 | 38.3 | 22.76 |
| 6 | USCP | 20.21 | 9.14 | 25.78 | 53.78 | 11.8 | -42.9 | 54.7 | 12.39 |
| 7 | USCP | 30.63 | 11.26 | 20.09 | 82.77 | 5.4 | -46.8 | 52.2 | 46.89 |
| 8 | USCP | 21.65 | 8.18 | 19.35 | 47.13 | -14.6 | -44.7 | 30.1 | 10.69 |
| 9 | USCP | 35.62 | 11.21 | 17.36 | 76.63 | -15.4 | -48.7 | 33.3 | 9.87 |
| 10 | USCP | 25.40 | 12.40 | 29.06 | 71.59 | -8.5 | -41.4 | 32.6 | 6.13 |
| 11 | USCP | 41.60 | 13.00 | 16.23 | 76.64 | 8.9 | -50.2 | 59.1 | 13.83 |
| 12 | USCP | 45.96 | 14.05 | 16.96 | 93.08 | -11.4 | -37.8 | 26.4 | 30.54 |
| 13 | USCP | 51.91 | 10.81 | 9.61 | 31.26 | -12.4 | -41.1 | 28.7 | 10.31 |
| 14 | USCP | 49.44 | 11.90 | 11.04 | 29.97 | -18.5 | -43.1 | 24.6 | 8.39 |
| 15 | USCP | 50.47 | 17.20 | 21.41 | 94.39 | -32.8 | -56.6 | 23.8 | 14.51 |
| 16 | BSCP | 40.33 | 19.20 | 23.36 | - | -13 | -49 | 36 | 45.72 |
| 17 | BSCP | - | - | - | - | -9.3 | -46.4 | 37.1 | 33.08 |
| 18 | BSCP | - | - | - | - | -14.6 | -37.8 | 23.2 | 5.71 |
| 19 | BSCP | - | - | - | 36.18 | 0.4 | -47.1 | 47.5 | 6.57 |
| 20 | BSCP | 27.41 | 6.96 | 13.77 | 24.70 | -13.3 | -46.3 | 33 | 1.29 |
| 21 | BSCP | - | - | - | 33.17 | -9.5 | -40.9 | 31.4 | 11.63 |
| 22 | BSCP | - | - | - | - | -13.9 | -43.9 | 30 | 29.19 |
| 23 | BSCP | 38.33 | 12.33 | 15.90 | 88.62 | -6.9 | -44.1 | 37.2 | 36.78 |
| 24 | BSCP | 45.16 | 15.41 | 20.50 | - | -21.7 | -50.9 | 29.2 | 2.98 |
| 25 | BSCP | - | - | - | 19.98 | -0.9 | -41.3 | 40.4 | 8.88 |
| 26 | BSCP | - | - | - | 39.37 | -3 | -45.8 | 42.8 | 8.36 |
| 27 | BSCP | - | - | - | 26.32 | -2.5 | -42 | 39.5 | 11.15 |
| 28 | BSCP | 38.41 | 14.22 | 20.07 | 113.61 | 11.2 | -46.6 | 57.8 | 77.22 |
| 29 | BSCP | 60.43 | 17.01 | 15.31 | 148.20 | -1 | -46.3 | 45.3 | 45.76 |
| 30 | BSCP | 26.04 | 12.51 | 24.80 | 55.73 | -7.9 | -41.9 | 34 | 26.42 |
| 31 | BSCP | 49.76 | 11.90 | 14.50 | 87.19 | 6.1 | -42.5 | 48.6 | 41.74 |
| 32 | BSCP | 27.62 | 11.67 | 21.03 | 46.66 | -5.8 | -39.9 | 34.1 | 38.15 |
| 33 | BSCP | 39.26 | 10.41 | 12.80 | 36.40 | -17.4 | -46.5 | 29.1 | 5.75 |

Abbreviations: GM: gastrocnemius medialis; AT: Achilles tendon; MTU: muscle-tendon unit; Max. DF: maximum dorsiflexion; Max. PF: maximum plantarflexion; RoM: range of motion; Norm: normalized; USCP, unilateral spastic cerebral palsy; BSCP, bilateral spastic cerebral palsy.